NTNU – Trondheim
Norwegian University of
Science and Technology

Path Following of Underactuated Marine Vessels in the Presence of Ocean Currents

Signe Moe

Master of Science in Engineering Cybernetics
Submission date: June 2013
Supervisor: Kristin Ytterstad Pettersen, ITK

Norwegian University of Science and Technology
Department of Engineering Cybernetics

Preface

These past six months have been exciting, educational and exhausting; I could not have asked for a better last semester at NTNU. I would like to thank my supervisors Ingrid Schjølberg, Kristin Pettersen and Walter Caharija for great feedback and support during my work on this thesis. I am very grateful for all the help and advice you've given me, and I am looking forward to working with you in the years ahead.

Furthermore, I would like to acknowledge my family for always encouraging and believing in me no matter what I want to do. Your support means the world to me! Finally, I want to thank all the wonderful friends I've made in Trondheim, especially Hilde, Marianne, Ylva, Hedvik, Øystein and Kristian. You guys are amazing!

Abstract

The use of marine vessels, especially underwater vehicles, is rapidly increasing. Autonomous marine vehicles are a huge focus area within the oil and gas industry, and can also be utilized for scientific, environmental and military use. There are still many challenges related to making such marine vessels autonomous. A basic task of an autonomous marine vessel is to follow a general path in the presence of unknown ocean currents. This is the key challenge addressed in this thesis.

In this thesis, two theorems that ensure path following given that certain assumptions are satisfied are presented. Theorem 1 applies to surface vessels and Theorem 2 to underwater vehicles. The developed theorems are based on the work of Even Børhaug regarding path following of space curves when no ocean currents are present, and introduce a virtual Serret-Frenet reference frame that is anchored in and propagates along the desired path. The theorems describe a closed-loop system with an ocean current observer, a guidance law, a controller and an update law to drive the Serret-Frenet frame alone the path.

The developed theorems have been implemented and simulated using a model for a supply surface ship and the Hugin AUV by Kongsberg Maritime AS for several different desired paths. In all simulations, the marine craft is able to converge to and track the desired path. Future work includes expanding simulations to include more realistic elements such as state observers and measurement noise, as well as testing the developed theorems on an actual ship/AUV.

The preliminary goal of this thesis was to develop a method to ensure path following in the presence of unknown ocean currents. This has been successfully done, and this thesis will be the basis for an article that will be submitted to the 2014 American Control Conference.

Sammendrag

Bruken av marine fartøy, særlig undervannsfartøy, er raskt økende. Autonome marine farkoster utgjør et stort satsningsområde i olje- og gassindustrien, og kan benyttes for vitenskapelige, miljømessige og millitære formål. Det er fortsatt mange utfordringer knyttet til å gjøre slike fartøy autonome. En grunnleggende oppgave for et autonomt marinefartøy er å følge en generell bane under innflytelse av ukjente havstrømmer. Denne masteroppgaven tar for seg nettopp denne problemstillingen.

I denne avhandlingen blir to teoremer som garanterer følging av en ønsket bane (gitt at enkelte antakelser er oppfylt) presentert. Teorem 1 gjelder for overfatefartøy og Teorem 2 for undervannsfarkoster. Disse teoremene er utviklet med utgangspunkt i arbeidet til Even Børhaug angående følging av en generell bane når ingen havstrøm påvirker fartøyet, og introduserer et virituelt Serret-Frenet referansesystem som er forankret i og propagerer langs den ønskede banen. Teoremene beskriver et system i lukket sløyfe og inkluderer en strøm-estimator, en guidance-lov, en regulator og en oppdateringslov som driver Serret-Frenet referansesystemet fremover.

De dynamiske modellene for et overflateskip og Hugin AUVen til Kongsberg maritime har blitt implementert og de utviklede teoremene har blitt simulert for flere ulike baner. Alle simuleringer viser at det aktuelle fartøyet konvergerer til og følger den ønskede banen. Fremtidig arbeid inkluderer å utvide simuleringene til mer realistiske forhold ved å inkludere en tilstandsobserver og legge til målestøy, samt å teste teoremene på et faktisk skip/AUV.

Hovedformålet med denne oppgaven var å utvikle en metode for å sikre baneføling av et marint fartøy under innflytelse av ukjente havstrømmer. Dette har blitt utfort, og denne masteroppgaven vil være utgangspunktet for en artikkel som skal sendes inn til 2014 American Control Conference.

Nomenclature

AUV	Autonomous Underwater Vehicle
CB	Center of Buoyancy
CG	Center of Gravity
DOF	Degrees of Freedom
DVL	Doppler Velocity Log
EOM	Equations of Motion
GNC	Guidance, Navigation and Control
GNSS	Global Navigation Satellite System
IMU	Inertial Measurement Unit
LOS	Line of Sight
ROV	Remotely Operated Vehicle
UES	Uniformly Exponentially Stable
UGAS	Uniform Global Asymptotic Stability
UGES	Uniformly Globally Exponentially Stable
ULES	Uniformly Local Exponentially Stable
UUV	Unmanned Underwater Vehicles

Contents

List of Figures

List of Tables

Chapter 1

Introduction

The guidance and control of marine vessels is an area of focus within the research community. The use of marine vehicles is increasing rapidly within several fields, such as marine biology, seafloor mapping, oceanography, military use and in oil and gas industry, and the autonomy of such vehicles are increasing rapidly. A basic and highly applicable task for such marine vessels, both surface and underwater, is to follow a general path to perform some mission. There are still challenges related to autonomous path following and tracking tasks, and as such the preliminary goal of this thesis is to develop a method that allows a marine vessel to follow a general path in the presence of unknown ocean currents. This is a very relevant issue for real-life applications.

This thesis presents two theorems as the solution to the addressed problem: Theorem 1 (chapter 6.1) applies to surface vessels and Theorem 2 (chapter 6.2) applies to underwater vehicles. These theorems introduce a virtual Serret-Frenet reference frame that propagates along the desired path and utilize an ocean current observer to estimate the unknown current. Furhermore, the closed loop system includes a guidance law to calculate references for the controlled states, a controller to compute and impose the necessary thruster force and rudder angle(s) to reach said references and an update law to drive the Serret-Frenet frame forward. This is illustrated in figure 1.1. Since the Serret-Frenet frame is anchored in the desired path, the control objectives is to drive the position of the marine vessel to the origin of this frame. Both theorems guarantee that this is achieved given that a number of assumptions are satisfied. Furhermore, Theorem 1 guarantee that the control objectives are achieved with uniform global asymptotic stability (UGAS).

The model for a supply surface ship and the Hugin AUV by Kongsberg Maritime have been implemented in Simulink along with the controllers, guidance law, update law and ocean current observer given by Theorem 1 and 2, and several desired paths have been simulated: A straight line, a circle and a piecewise straight and circular path in the shape of an athletics track for the supply ship, and a straight line, a circle and a helix for Hugin.

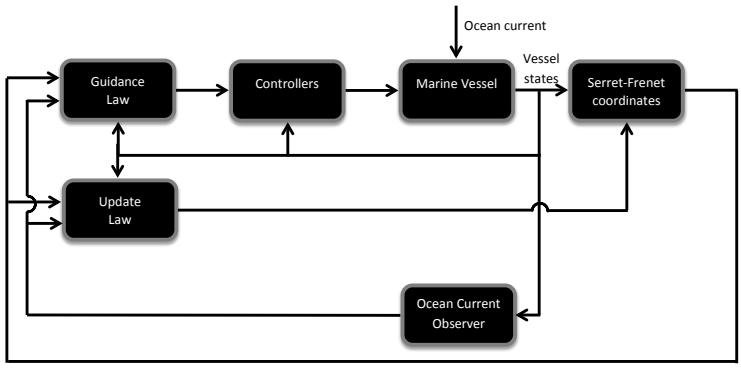

Figure 1.1: Structure of developed closed-loop system for path following.

This thesis is outlined as follows. Chapter 2 of this thesis introduce some relevant background theory. This shortly describes the notation used in this thesis and the general marine craft model. Chapter 3 contains a literature review. Here, a method of transforming the marine vehicle model to simplify the control problems is presented. Different controller types are discussed and a method for ocean current estimation is described. Finally, several established guidance laws for path following are presented. Chapter 4 contains the problem formulation on which this thesis is based, and chapter 5 presents the simulation models and controllers for the supply ship and Hugin. The developed theorems are presented in chapter 6 and the simulation results in chapter 7. Chapter 8 and 9 hold the discussion and conclusion. Finally, appendix A contains some of the formulas and stability theorems that are used in the stability proofs of Theorem 1 and 2. These are shown in detail in appendix B. Throughout this thesis, figures, tables and equations are numbered according to chapter.

Chapter 2

Background Theory

This chapter contains some of the background theory and notation used throughout this thesis. The notation and reference frames are consistent with Fossen [12]. All material in this chapter from [2, 12].

2.1 Reference frames

The reference frames are illustrated in figure 2.1 and 2.2.

2.1.1 Earth-Centered Reference Frames

ECI Intertial (nonaccelerating) frame $\{i\}$ in which Newton's laws apply.

ECEF Earth-centered frame $\{e\}$. The axes rotate relative to the ECI frame along with the Earth. The x-axis intersects the sphere of the Earth at 0° latitude (Equator) and 0° longitude (Greenwich).

2.1.2 Geographic Reference Frames

NED Tangent plane on the surface of the Earth with axes north, east, down. This frame, denoted $\{n\}$, is related to $\{e\}$ through the angles for longitude (l) and latitude (μ). *For a flat Earth navigation one can assume that $\{n\}$ is inertial and that Newton's laws still apply.*

BODY The body reference frame $\{b\}$ is anchored in the vehicle. The position and orientation of the craft should be expressed in the inertial reference frame, approximated by $\{e\}$ or $\{n\}$ for marine vessels, and the linear and angular velocities are described relative the body coordinate system, see table 2.1. The axes coincide with the principle axes of inertia. The normal definition is x_b (from act to fore), y_b (to starboard) and z_b (from top to bottom). This is illustrated in figure 2.2.

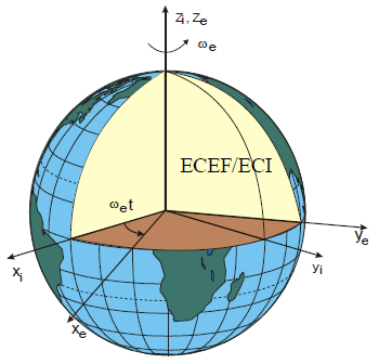

Figure 2.1: Illustration of earth-centered reference frames [12].

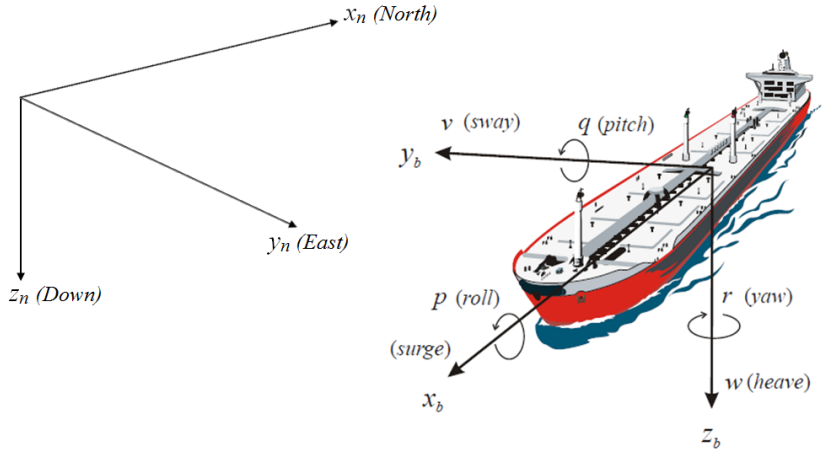

Figure 2.2: Illustration of NED and BODY reference frames [12].

2.2 Notation and Definitions

For a marine vessel, the NED reference frame can be assumed inertial. As such, the following notation is used. Vectors are **bold**, and sub- and superscripts are used as follows: $\boldsymbol{\omega}^b_{b/n}$ is the vector containing angular velocity of $\{b\}$ with respect to $\{n\}$ (subscript b/n) expressed in $\{b\}$ (superscript b) and $\boldsymbol{\Theta}_{nb}$ contains the Euler angles between $\{n\}$ and $\{b\}$.

Vector	Vector	Variable	Name	Definition
$\boldsymbol{\eta}\left(\boldsymbol{\eta}_{b/n}^{n}\right)$	$\boldsymbol{p}_{b/n}^{n}$	x	Surge	Position in x-direction in NED
		y	Sway	Position in y-direction in NED
		z	Heave	Position in z-direction in NED
	$\boldsymbol{\Theta}_{nb}$	ϕ	Roll	Rotation about x-axis in NED
		θ	Pitch	Rotation about y-axis in NED
		ψ	Yaw	Rotation about z-axis in NED
$\boldsymbol{\nu}\left(\boldsymbol{\nu}_{b/n}^{b}\right)$	$\boldsymbol{v}_{b/n}^{b}$	u	Surge velocity	Linear velocity in x-direction in BODY
		v	Sway velocity	Linear velocity in y-direction in BODY
		w	Heave velocity	Linear velocity in z-direction in BODY
	$\boldsymbol{\omega}_{b/n}^{b}$	p	Roll rate	Angular velocity about x-axis in BODY
		q	Pitch rate	Angular velocity about y-axis in BODY
		r	Yaw rate	Angular velocity about z-axis in BODY

Table 2.1: Table containing the states of an underwater vehicle ($\boldsymbol{\eta}$ and $\boldsymbol{\nu}$) and a description of these.

The actual velocity of a marine vessel is not necessarily aligned with the x_b-axis. For instance, the vehicle may experience sideways drifting due to current or waves. In principle, the velocity vector $\boldsymbol{U} = u\boldsymbol{x_b} + v\boldsymbol{y_b} + w\boldsymbol{z_b}$ can have any direction. The following definitions are important for a surface ship or an underwater vehicle operating in a plane (illustration in figure 2.3):

Heading Angle ψ is the angle from the x-axis of $\{n\}$ to the x-axis of $\{b\}$. Positive rotation about the z-axis of $\{n\}$ by right-hand convention. This is the angle that is directly controlled by the rudder.

Sideslip angle β is the angle from the x-axis of $\{b\}$ to the velocity vector $\boldsymbol{U}$ of the vehicle. Positive rotation about the z-axis of $\{b\}$ by right-hand convention.

Course Angle χ is the angle from the x-axis of $\{n\}$ to the velocity vector $\boldsymbol{U}$ of the craft. Positive rotation about the z-axis of $\{n\}$ by right-hand convention. $\chi = \psi + \beta$

For an underwater vehicle operating in 3D space, there exists an angle α (angle of attack) in addition to the sideslip angle β. These angles relate the body coordinate system b to the flow coordinate system f, which is often used to express hydrodynamic data. The connection is given by $\boldsymbol{R}_f^b(\boldsymbol{\Theta_{bf}})$, where $\boldsymbol{\Theta}_{bf} = [0, \alpha, -\beta]^T$ and $\boldsymbol{R}$ is defined in equation (2.7).

$$\begin{aligned} \beta &\triangleq \arcsin\left(\frac{v}{|\boldsymbol{U}|}\right) \\ \alpha &\triangleq \arctan\left(\frac{w}{u}\right) \end{aligned} \tag{2.1}$$

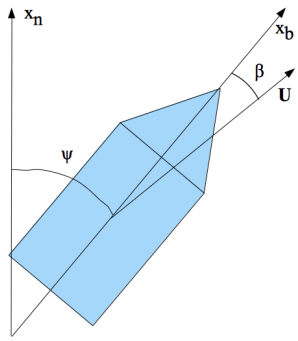

Figure 2.3: Illustration of heading ψ and side-slip β angle. The course angle χ is the sum of heading and side-slip.

2.3 Transformation between Reference Frames

Transformations between BODY and NED The 6 DOF kinematic equation can be expressed in vector form as

$$\begin{aligned} \dot{\boldsymbol{p}}^n_{b/n} &= \boldsymbol{v}^n_{b/n} = \boldsymbol{R}^n_b(\boldsymbol{\Theta}_{nb})\boldsymbol{v}^b_{b/n} \\ \dot{\boldsymbol{\Theta}}_{nb} &= \boldsymbol{\omega}^n_{b/n} = \boldsymbol{T}_\Theta(\boldsymbol{\Theta}_{nb})\boldsymbol{\omega}^b_{b/n} \\ &\Downarrow \\ \dot{\boldsymbol{\eta}} &= \boldsymbol{J}_\Theta(\boldsymbol{\eta})\boldsymbol{\nu} \end{aligned} \tag{2.2}$$

$$\boldsymbol{J}_\Theta(\boldsymbol{\eta}) = \begin{bmatrix} \boldsymbol{R}^n_b(\boldsymbol{\Theta}_{nb}) & \boldsymbol{0}_{3\times 3} \\ \boldsymbol{0}_{3\times 3} & \boldsymbol{T}_\Theta(\boldsymbol{\Theta}_{nb}) \end{bmatrix} \tag{2.3}$$

By considering a rotation about a single axis one can define *the principal rotation matrices*:

$$\boldsymbol{R}_{x,\phi} = \begin{bmatrix} 1 & 0 & 0 \\ 0 & \cos(\phi) & -\sin(\phi) \\ 0 & \sin(\phi) & \cos(\phi) \end{bmatrix} \tag{2.4}$$

$$\boldsymbol{R}_{y,\theta} = \begin{bmatrix} \cos(\theta) & 0 & \sin(\theta) \\ 0 & 1 & 0 \\ -\sin(\theta) & 0 & \cos(\theta) \end{bmatrix} \tag{2.5}$$

$$\boldsymbol{R}_{z,\psi} = \begin{bmatrix} \cos(\psi) & -\sin(\psi) & 0 \\ \sin(\psi) & \cos(\psi) & 0 \\ 0 & 0 & 1 \end{bmatrix} \tag{2.6}$$

Together, these three matrices can describe any rotation about all three axes. The matrix

$$\begin{aligned}\boldsymbol{R}_b^n(\boldsymbol{\Theta}_{nb}) &\triangleq \boldsymbol{R}_{z,\psi}\boldsymbol{R}_{y,\theta}\boldsymbol{R}_{x,\phi} \\ &= \begin{bmatrix} c(\psi)c(\theta) & -s(\psi)c(\phi)+c(\psi)s(\theta)s(\phi) & s(\psi)s(\phi)+c(\psi)s(\theta)c(\phi) \\ s(\psi)c(\theta) & c(\psi)c(\phi)+s(\psi)s(\theta)s(\phi) & -c(\psi)s(\phi)+s(\psi)s(\theta)c(\phi) \\ -s(\theta) & c(\theta)s(\phi) & c(\theta)c(\phi) \end{bmatrix} \\ c(\cdot) &= \cos(\cdot), s(\cdot) = \sin(\cdot), t(\cdot) = \tan(\cdot)\end{aligned} \tag{2.7}$$

describes a rotation of ψ degrees about the z-axis, θ degrees about the y-axis and ϕ degrees about the x-axis.

$$\boldsymbol{R}_n^b(\boldsymbol{\Theta}_{nb}) = \boldsymbol{R}_b^n(\boldsymbol{\Theta}_{nb})^{-1} = \boldsymbol{R}_b^n(\boldsymbol{\Theta}_{nb})^T = \boldsymbol{R}_{x,\phi}^T\boldsymbol{R}_{y,\theta}^T\boldsymbol{R}_{z,\psi}^T$$

The transformation matrix $\boldsymbol{T}_\Theta(\boldsymbol{\Theta}_{nb})$ relates $\dot{\boldsymbol{\Theta}}_{b/n}^n$ to $\boldsymbol{\omega}_{b/n}^b$.

$$\boldsymbol{\omega}_{b/n}^b = \begin{bmatrix}\dot\phi\\0\\0\end{bmatrix} + \boldsymbol{R}_{x,\phi}^T\begin{bmatrix}0\\\dot\theta\\0\end{bmatrix} + \boldsymbol{R}_{x,\phi}^T\boldsymbol{R}_{y,\theta}^T\begin{bmatrix}0\\0\\\dot\psi\end{bmatrix} \triangleq \boldsymbol{T}_\Theta^{-1}(\boldsymbol{\Theta}_{nb})\dot{\boldsymbol{\Theta}}_{bm} \tag{2.8}$$

$$\boldsymbol{T}_\Theta^{-1}(\boldsymbol{\Theta}_{nb}) = \begin{bmatrix}1 & 0 & -s(\theta)\\ 0 & c(\phi) & c(\theta)s(\phi)\\ 0 & -s(\phi) & c(\theta)c(\phi)\end{bmatrix} \tag{2.9}$$

$$\boldsymbol{T}_\Theta(\boldsymbol{\Theta}_{nb}) = \begin{bmatrix}1 & s(\phi)t(\theta) & c(\phi)t(\theta)\\ 0 & c(\phi) & -s(\phi)\\ 0 & \frac{s(\phi)}{c(\theta)} & \frac{c(\phi)}{c(\theta)}\end{bmatrix} \tag{2.10}$$

2.4 Marine Vessel Dynamic Model

The general maneuvering equations of motion (EOMs) for a marine vessel can be represented by the kinematics (2.11) and kinetics (2.12). The kinematics describe geometrical aspects of motion, whereas the kinetics consider the forces causing the motion.

$$\dot{\boldsymbol{\eta}} = \boldsymbol{J}_\Theta(\boldsymbol{\eta})\boldsymbol{\nu} \tag{2.11}$$

$$\begin{aligned}\boldsymbol{M}\dot{\boldsymbol{\nu}} + \boldsymbol{C}(\boldsymbol{\nu})\boldsymbol{\nu} + \boldsymbol{D}(\boldsymbol{\nu})\boldsymbol{\nu} + \boldsymbol{g}(\boldsymbol{\eta}) + \boldsymbol{g}_0 &= \boldsymbol{\tau} + \boldsymbol{\tau}_{wind} + \boldsymbol{\tau}_{wave} \\ \boldsymbol{M}\dot{\boldsymbol{\nu}} + \boldsymbol{C}(\boldsymbol{\nu})\boldsymbol{\nu} + \boldsymbol{D}(\boldsymbol{\nu})\boldsymbol{\nu} + \boldsymbol{g}(\boldsymbol{\eta}) + \boldsymbol{g}_0 &= \boldsymbol{B}\boldsymbol{f} + \boldsymbol{\tau}_{wind} + \boldsymbol{\tau}_{wave}\end{aligned} \tag{2.12}$$

$\boldsymbol{J}_\Theta(\boldsymbol{\eta})$ is the Jacobian matrix defined in equation (2.3). $\boldsymbol{M}$ is the system inertia matrix, $\boldsymbol{C}$ is the Coriolis-centripetal matrix and $\boldsymbol{D}$ is the damping matrix. $\boldsymbol{g}$ is a vector containing gravitational and/or buoyancy forces and moments and $\boldsymbol{g}_0$ is a vector used for pretrimming (ballast control). $\boldsymbol{\tau}$ is a vector containing the control inputs, and $\boldsymbol{\tau}_{wind}$ and $\boldsymbol{\tau}_{wave}$ contains wind and wave forces respectively. $\boldsymbol{\tau}$ is often modeled as $\boldsymbol{B}\boldsymbol{f}$, where $\boldsymbol{f}$ is a vector containing the thruster force(s)

and rudder angle(s), and $\boldsymbol{B}$ is a matrix that maps these angles into corresponding forces affecting the dynamics. Typically, $\boldsymbol{B}$ has the following structure for a 3-DOF surface vessel. T is the thruster force and δ_r is the rudder angle.

$$\boldsymbol{\tau} = \boldsymbol{B}\boldsymbol{f} = \begin{bmatrix} b_{11} & 0 \\ 0 & b_{22} \\ 0 & b_{32} \end{bmatrix} \begin{bmatrix} T \\ \delta_r \end{bmatrix} \tag{2.13}$$

2.5 Ocean Current

Ocean currents are circulation systems of ocean waters that are a result of gravity, wind, salinity change, heat exchange at the sea surface and variation in water density [12]. These can have both horizontal and vertical components and are affected by the Coriolis force and tides. The ocean current is often assumed irrotational and constant (or slowly varying) in the NED/inertial reference frame:

$$\boldsymbol{V}_c^n = \begin{bmatrix} V_x \\ V_y \\ V_z \end{bmatrix} \tag{2.14}$$

By expressing the current in the body frame

$$\boldsymbol{V}_c^b = [\boldsymbol{R}_b^n(\boldsymbol{\Theta}_{nb})]^T \boldsymbol{V}_c^n \tag{2.15}$$

the relative velocity $\boldsymbol{\nu}_r$ can be defined as below:

$$\boldsymbol{\nu}_r = \boldsymbol{\nu}_{b/n}^b - \boldsymbol{\nu}_c^b = \begin{bmatrix} \boldsymbol{v}_{b/n}^b - \boldsymbol{V}_c^b \\ \boldsymbol{\omega}_{b/n}^b \end{bmatrix} = [u_r, v_r, w_r, p, q, r]^T \tag{2.16}$$

2.6 Marine Vessel Dynamic Model revisited

The equations of motion kinetics can be rewritten using the relative velocity vector:

$$\underbrace{\boldsymbol{M}_{RB}\dot{\boldsymbol{\nu}} + \boldsymbol{C}_{RB}(\boldsymbol{\nu})\boldsymbol{\nu}}_{\text{rigid-body forces}} + \underbrace{\boldsymbol{M}_A\dot{\boldsymbol{\nu}}_r + \boldsymbol{C}_A(\boldsymbol{\nu}_r)\boldsymbol{\nu}_r + \boldsymbol{D}(\boldsymbol{\nu}_r)\boldsymbol{\nu}_r}_{\text{hydrodynamic terms}} + \underbrace{\boldsymbol{g}(\boldsymbol{\eta}) + \boldsymbol{g}_0}_{\text{hydrostatic terms}} = \boldsymbol{\tau} + \boldsymbol{\tau}_{wind} + \boldsymbol{\tau}_{wave} \tag{2.17}$$

The hydrogynamic terms describe forces related to drag, frontal pressure against the structure, negative pressure in downstream etc., whereas the hydrostatic terms include buoyancy and gravitational forces. The rigid-body forces are related to the shape and mass off the vessel itself.

As equation (2.17) shows, the rigid-body forces are independent of the ocean current, whereas the hydrodynamic terms can be expressed through the relative velocity. However, it has been shown by Fossen that the EOMs can be represented through relative velocities only:

$$\begin{aligned} \dot{\boldsymbol{\eta}} &= \boldsymbol{J}_\Theta(\boldsymbol{\eta}_r)\boldsymbol{\nu}_r + \begin{bmatrix} \boldsymbol{V}_c^n \\ \boldsymbol{0}_{3\times 1} \end{bmatrix} \\ \boldsymbol{M}\dot{\boldsymbol{\nu}}_r + \boldsymbol{C}(\boldsymbol{\nu}_r)\boldsymbol{\nu}_r + \boldsymbol{D}(\boldsymbol{\nu}_r)\boldsymbol{\nu}_r + \boldsymbol{g}(\boldsymbol{\eta}) + \boldsymbol{g}_0 &= \boldsymbol{\tau} + \boldsymbol{\tau}_{wind} + \boldsymbol{\tau}_{wave} \end{aligned} \tag{2.18}$$

$$\begin{aligned} \boldsymbol{M} &= \boldsymbol{M}_{RB} + \boldsymbol{M}_A \\ \boldsymbol{C} &= \boldsymbol{C}_{RB} + \boldsymbol{C}_A \end{aligned} \tag{2.19}$$

2.7 Actuation of Marine Vessels

In general, a surface vessel has 3 Degrees of Freedom (DOFs) ($\boldsymbol{\eta} = [x, y, \psi]^T$ and $\boldsymbol{\nu} = [u, v, r]^T$), and an underwater vessel has 6 DOFs ($\boldsymbol{\eta} = [x, y, z, \phi, \theta, \psi]^T$ and $\boldsymbol{\nu} = [u, v, q, p, q, r]^T$). The vessel is said to be fully actuated if it is equipped with actuators that can produce forces and/or moments in all DOFs. If it does not, the craft is underactuated. This is often the case in marine vessels, and this limits which control objectives the vessel can satisfy. A simple example of an underactuated vehicle is a car. The car is able to drive back and forward, and can turn sideways. However, it is not able to move sideways directly. In spite of this, given a control objective to move 3 meters to the right, the car is able to complete this by driving forward and turning and then backing up again.

2.8 Motion Control of Marine Vessels

To plan and control a motion of a marine vessel, a guidance, navigation and control (GNC) system as illustrated in figure 2.4 is required. This thesis mainly focuses on the guidance and control system.

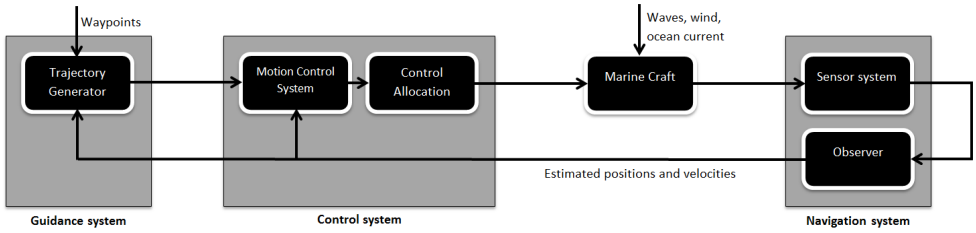

Figure 2.4: GNC system flow. Illustration from [12].

2.8.1 Guidance system

The guidance system computes a reference that is the controller input. This reference can consist of the desired position, velocity, acceleration, heading, depth, etc. of the marine vessel. The complexity of the guidance system depends on the desired behavior of the system. For instance, if the vessel should stay at a stationary position, the desired position is constant and the desired velocity and acceleration are zero. In a more complex system, the guidance system can be used to calculate the optimal trajectory/path for the vessel in question with respect to time, distance, energy-consumption etc. The most common types of motion control objectives are listed below.

Setpoint regulation: The reference is constant.

Trajectory-tracking: The state of the vehicle should track desired position and velocity reference signals that change over time.

Path-following control: The overall goal is to follow a predefined path independent of time. That is, it is not necessary to reach a certain point of the path at a certain time, but to reach, stay on and follow the desired course.

Path-tracking control: A combination of trajectory-tracking and path-following. The vehicle should follow a given path dependent of time.

Target tracking: The goal is to reach a target that may be stationary (setpoint regulation) or in motion with an unknown future path.

2.8.2 Navigation system

The navigation system normally consists of a Global Navigation Satellite System (GNSS) and a set of sensors, e.g. accelerometers, gyroscopes, magnetometers (IMUs), radar/sonar and pressure sensors. These sensors provide data that can be used to estimate the state of the marine vessel through an observer, typically a Kalman filter. Often a low-pass filter is used to remove high-frequency measurement noise from the sensor data.

2.8.3 Control system

The control system receives a reference from the guidance system and must determine the control forces necessary to achieve this based on the reference and the current state of the vessel in question. This system can be subjected to several constraints, such as a saturation on the controlled forces, minimization of energy consumption, exact path/trajectory following etc. The control system depends on feedback from the measured/estimated states of the vessel, and as such it can be vulnerable to measurement noise and inaccurate estimates. A few common controller types are described in chapter 3.3.

Chapter 3

Literature Review

3.1 Underwater Vehicles and Automation

Underwater vehicles have several potential applications within various fields for scientific (seafloor mapping, rapid response to oceanographic and geothermal events, geological sampling), environmental (monitoring of pollution etc.) or military use (water mine search, reconnaissance, surveillance) [20]. In addition, they can be immensely helpful within the oil industry when constructing, inspecting and maintaining undersea structures such as pipelines. As such, underwater vehicles are a very attractive research field with several challenges, such as autonomy, endurance, navigation, sensors/sensor processing, underwater robotic manipulation and communication.

As of today, there are two main types of Unmanned Underwater Vehicles (UUVs). These are ROVs (Remotely Operated Vehicles) and AUVs (Autonomous Underwater Vehicles) . As the name suggests, a ROV is tele-operated, meaning that is requires a human operator to control it, and physically linked via a tether to a submarine or a surface ship [2]. An AUV, on the other hand, is autonomous and can operate without human interaction. Once it is given a command, it can assess the surroundings and make decisions on its own to complete its mission.

An overall goal for unmanned vehicles is to increase the degree of autonomy. The increasing demand for advanced underwater robot technology will eventually lead to completely autonomous underwater robots that will minimize the need for human operators [21]. AUVs have to be reactive, robust, reliable and adaptable in order to work in a changing environment. They have several advantages compared to ROVs and manned underwater vehicles. For instance, operation costs are lower since AUVs don't require a mother vessel with a large crew to operate [2]. In addition, ROVs have limited range due to the tether, which also poses a safety issue. AUVs can operate independent of a link to a surface vessel, and as such they can be used in great depths and/or under ice covered areas. Finally, an AUV can make

its own decisions, and as such the time delay in human-machine interaction that can arise when operating ROVs is irrelevant when working with AUVs.

Obviously, there are different levels of autonomy. For instance, a ROV can have a auto-depth controller that limits the vehicle to a plane in which the operator can control it. Parasuraman et. al. propose a 10-point scale to describe different levels of autonomy [18]. This is shown in table 3.1.

HIGH	10	The computer decides everything and acts autonomously, ignoring the human.
	9	Informs the human only if it, the computer, decides to.
	8	Informs the human only if asked, or
	7	executes automatically, then necessarily informs the human, and
	6	allows the human a restricted time to veto before automatic execution, or
	5	executes the suggestion if the human approves, or
	4	suggest one alternative.
	3	Narrows the selection down to a few, or
	2	the computer offers a complete set of decision/action alternatives, or
LOW	1	the computer offers no assistance: Human must take all decision and actions.

Table 3.1: Levels of autonomy by Parasuraman et. al. [18].

The level of autonomy achieved by underwater vehicles is determined by their performance in three areas [14]: Energy, navigation and decision autonomy. An energy autonomous UUV has reliable power sources and low power consumption, and as such it can operate without interacting with other vessels long-term. Navigation autonomy entails the UUVs ability to navigate and know its position even in unknown areas, and decision autonomy means that the vehicle must be able to perceive its own status and environment, and respond appropriately to unexpected situations without the interference of a human operator.

3.2 Vehicle Model Transformations

The general marine vessel dynamic model (2.18) is given with respect to a certain point on the marine craft. It is common to have models given relative to the Center of Gravity (CG) or Center of Buoyancy (CB). However, the EOMs can be simplified by translating the model to another point p.

For an underactuated surface vessel with a $\boldsymbol{B}$-matrix as equation (2.13), it is easy to see that the rudder angle δ_r affects both the sway and yaw dynamics (v and r). For an underwater vehicle such as in [4], the pitch control δ_q affects both heave

and pitch dynamics (w and q) and the yaw control δ_r affects both yaw and sway dynamics (v and r). This makes the controller design and stability analysis complicated. However, by translating the model, δ_q affects only the pitch dynamics and δ_r affects only the yaw dynamics [4].

The transformation is given below:

$$\begin{aligned}
\bar{u} &= u \\
\bar{v} &= v + \epsilon_1 r \\
\bar{w} &= w + \epsilon_2 q \\
\bar{p} &= p \\
\bar{q} &= q \\
\bar{r} &= r \\
\bar{\boldsymbol{\nu}} &= \underbrace{\begin{bmatrix} 1 & 0 & 0 & 0 & 0 & 0 \\ 0 & 1 & 0 & 0 & 0 & \epsilon_1 \\ 0 & 0 & 1 & 0 & \epsilon_2 & 0 \\ 0 & 0 & 0 & 1 & 0 & 0 \\ 0 & 0 & 0 & 0 & 1 & 0 \\ 0 & 0 & 0 & 0 & 0 & 1 \end{bmatrix}}_{\boldsymbol{T}} \boldsymbol{\nu}
\end{aligned} \tag{3.1}$$

ϵ_1 and ϵ_2 are constant scalars calculated based on the $\boldsymbol{M}$ and $\boldsymbol{B}$ matrices of the vehicle model. If $\epsilon_1 = -\epsilon_2$ the transformation corresponds to a physical translation of the EOMs along the center line of the craft for a distance $\epsilon = \epsilon_1$ [9]. If the vessel in question fulfills certain symmetry demands or has a cylindrical shape, it will result in $\epsilon_1 = -\epsilon_2$.

Examples of this model transformation are given in chapter 5.1 and 5.2.

3.3 Controller types

3.3.1 P, PD, PI and PID Controllers

P, PD and PID controllers calculate a controller input τ based on the deviation between the actual and desired state x and x_d denoted $\tilde{x}$ [3].

P	$\tau = -K_p\tilde{x}$
PD	$\tau = -K_p\tilde{x} - K_d\dot{\tilde{x}}$
PI	$\tau = -K_p\tilde{x} - K_i\int\tilde{x}dt$
PID	$\tau = -K_p\tilde{x} - K_d\dot{\tilde{x}} - K_i\int\tilde{x}dt$

K_p, K_d and K_i are all positive controller gains. A simple P-controller produce an output signal proportional to the current deviation. The derivative term predicts system behavior by examining the slope of error over time and can improve settling

time, whereas the integral term contains the sum of the past error and eliminates the stationary deviation that is a result of a pure P controller. It is important to note that the derivation term is sensitive to measurement noise and a large integrator gain can result in a overshoot response.

These controllers are all simple in the sense that they are completely independent on the system model. As such they are not susceptible to modeling errors. However, they are known to be sensitive to non-linearities, and the tuning of the controller gains can be tricky. In some cases, it may be prudent to adjust these continuously.

3.3.2 Feedback Linearization Controllers

The idea behind feedback linearization controllers is to cancel the non-linearities in the system dynamics [12]. As such, a P, PD, PI or PID controller can be applied to the resulting linear system. However, the drawback of this method is that it requires a known and exact model of the system. For instance, if

$$\dot{x} = -x + F(t, x) + \tau, \tag{3.2}$$

where $F(t, x)$ is a non-linear function,

$$\tau = -F(t, x) + \tau_1 \tag{3.3}$$

reduces the system dynamics to

$$\dot{x} = -x + \tau_1. \tag{3.4}$$

This is a linear system and τ_1 can then be chosen as a PID-controller or another linear system controller to make x converge to x_r. Examples of feedback linearization controllers are given in chapter 5.1.1 and 5.2.1.

3.3.3 Integrator Backstepping Controllers

Integrator backstepping is a technique developed to design stabilizing controls for non-linear systems using control Lyapunov functions [12]. It has a recursive structure. The basic idea is to transform the dynamic model to a new state $\boldsymbol{z}$ with a linear dynamics and a stable equilibrium point in $\boldsymbol{z} = 0$. An example of an integrator backstepping controller is given in chapter 5.2.2. An integrator backstepping controller is a kind of feedback linearization controller since it aims to cancel non-linearities, and as such it is also sensitive to modeling errors. However, it is a more flexible method than pure feedback linearization, as it allows for explotion of stabilizing non-linearities.

3.4 Current Estimation

As mentioned in section 2.5, the current is often assumed constant and irrotational in the inertial (NED) frame. As equation (2.18) shows, the current continuously

affects the kinematics of the system, and as such it would be useful to know the direction and magnitude of this disturbance. There are two approaches to this problem: The current can either be measured or estimated. Direct measurement of ocean current is very difficult. A possible approach is to use a Doppler Velocity Log (DVL) [19]. The DVL uses acoustic measurements to capture the velocity of the marine vessel relative to the bottom and water. As such, it can estimate both absolute and relative velocities, and the current can be estimated as the difference between these two.

A current estimator for a surface ship is given in [1]. It is assumed that both $\boldsymbol{\eta}$ and $\boldsymbol{\nu}_r$ are measured or estimated. Based on the model (2.18), it is known that

$$\begin{aligned} \dot{x} &= \cos(\psi)u_r - \sin(\psi)v_r + V_x \\ \dot{y} &= \sin(\psi)u_r + \cos(\psi)v_r + V_y \end{aligned} \tag{3.5}$$

The current can be estimated by introducing an estimate for x and y that can be compared to the actual, measured position, in addition to estimates of V_x and V_y. The estimates are given below.

$$\begin{aligned} \dot{\hat{x}} &= \cos(\psi)u_r - \sin(\psi)v_r + \hat{V}_x + k_{x1}\tilde{x} \\ \dot{\hat{y}} &= \sin(\psi)u_r + \cos(\psi)v_r + \hat{V}_y + k_{y1}\tilde{y} \\ \dot{\hat{V}}_x &= k_{x2}\tilde{x} \\ \dot{\hat{V}}_y &= k_{y2}\tilde{y} \end{aligned} \tag{3.6}$$

$$\begin{aligned} \tilde{x} &= x - \hat{x} \\ \tilde{y} &= y - \hat{y} \\ \tilde{V}_x &= V_x - \hat{V}_x \\ \tilde{V}_y &= V_y - \hat{V}_y \end{aligned} \tag{3.7}$$

Here, $\tilde{x}$ and $\tilde{y}$ are known because the actual position is measured and the value of the estimates are known.

The system can then be written as equation (3.8). If the constants k_{x1}, k_{x2}, k_{y1} and k_{y2} are larger than zero, the matrices $\boldsymbol{A}$ and $\boldsymbol{B}$ are Hurwitz and the errors $\tilde{x}$, $\tilde{y}$, $\tilde{V}_x$ and $\tilde{V}_y$ will go to zero with global exponential stability (theorem 4.5 in appendix A.3.2).

$$\begin{aligned} \begin{bmatrix} \dot{\tilde{x}} \\ \dot{\tilde{V}}_x \end{bmatrix} &= \underbrace{\begin{bmatrix} -k_{x1} & 1 \\ -k_{x2} & 0 \end{bmatrix}}_{\boldsymbol{A}} \begin{bmatrix} \tilde{x} \\ \tilde{V}_x \end{bmatrix} \\ \begin{bmatrix} \dot{\tilde{y}} \\ \dot{\tilde{V}}_y \end{bmatrix} &= \underbrace{\begin{bmatrix} -k_{y1} & 1 \\ -k_{y2} & 0 \end{bmatrix}}_{\boldsymbol{B}} \begin{bmatrix} \tilde{y} \\ \tilde{V}_y \end{bmatrix} \end{aligned} \tag{3.8}$$

3.5 Path Representation

3.5.1 Waypoints

Straight-line paths are often described using waypoints [12]. In general, a waypoint is given as $\boldsymbol{p}_k = [x_k, y_k, z_k]^T$ ($\boldsymbol{p}_k = [x_k, y_k]^T$ for surface vessels), and a single straight line is given as the line between $\boldsymbol{p}_0$ and $\boldsymbol{p}_1$. In addition, a path can be piecewise linear, in which case it is defined as the path from $\boldsymbol{p}_0$ to $\boldsymbol{p}_n$ via the waypoints $\boldsymbol{p}_i, i \in [1, n-1]$. It is common to represent such paths using straight lines and circular arcs to connect the waypoints. This is illustrated in figure 3.1. One drawback of using this representation is that the desired yaw rate r_d will not be continuous when switching between the straight line ($r_d = 0$) and the circular arc ($r_d = c$, c dependent on the curvature of the circular arc).

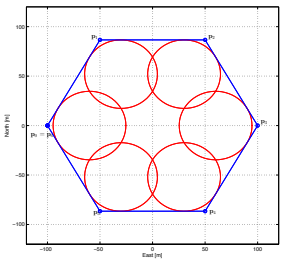

Figure 3.1: Illustration of piecewice straight-line path with circular arcs for waypoint guidance.

3.5.2 Parametrization

A general path, straight or curved, is normally represented through a parametrization which is often assumed known in advance [12]. A general parametrized path in 3D is given as $\boldsymbol{p}_d(\theta) = [x_d(\theta), y_d(\theta), z_d(\theta)]^T$. A simple example of a 2D parametrized curve is a circle.

$$\begin{aligned} \theta &\in [0, 2\pi] \\ x_d(\theta) &= R\cos(\theta) \\ y_d(\theta) &= R\sin(\theta) \end{aligned} \tag{3.9}$$

It is possible, and often useful, to express the path as a function of the traveled distance along the path s. In case of the 2D circle, the parametrization is given below.

$$\begin{aligned} s &\in [0, 2\pi R] \\ x_d(s) &= R\cos\left(\frac{s}{R}\right) \\ y_d(s) &= R\sin\left(\frac{s}{R}\right) \end{aligned} \tag{3.10}$$

3.6 Line of Sight Guidance Laws for Path-Following

Guidance is defined by Shneydor as *"The process for guiding the path of an object towards a given point, which in general may me moving"*. A commonly used method

for path-following is the Line of Sight (LOS) method [12]. In this case, the guidance system is composed of a speed and LOS guidance law, where the LOS law computes a heading reference and the speed law computes a velocity reference. These can be combined in different ways to achieve different motion control objectives.

3.6.1 Line of Sight for Straight Path Following

Line of Sight is a three-point guidance scheme [7] since it is based on three points: A reference point (normally stationary, for instance $\boldsymbol{p}_k$), the position of the marine craft ($\boldsymbol{p}(t)$) and the desired position. LOS can be used to track a moving target, in which case the desired position is time-varying ($\boldsymbol{p}_t(t)$), or to track a certain path, in which case the goal is the next waypoint ($\boldsymbol{p}_{k+1}$). The focus for this thesis is path-following, so LOS as target tracking is disregarded from this point on. Figure 3.2 illustrates the LOS concept for a surface vessel (this is simpler than an underwater vehicle since a ship is limited to a plane). The desired path is the straight line in light blue between $\boldsymbol{p}_k$ and $\boldsymbol{p}_{k+1}$, and the ship is at position $\boldsymbol{p}(t)$, marked i red. In the NED reference frame the x-axis points north and the y-axis points east. However, the path can be specified in a path-fixed reference frame with origin in $\boldsymbol{p}_k$ and x-axis pointing toward $\boldsymbol{p}_{k+1}$. This reference frame is illustrated in dark blue.

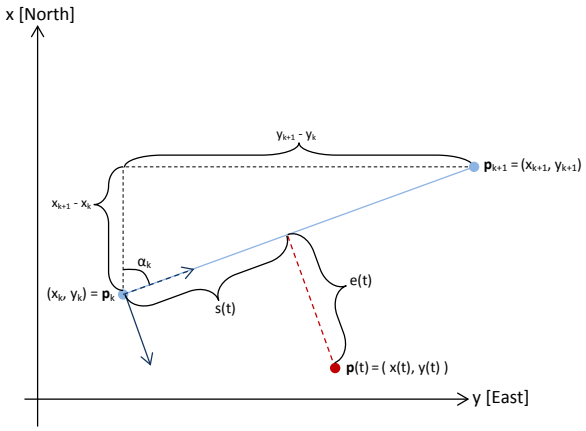

Figure 3.2: Illustration of LOS guidance for surface vessels. The ship is in position $\boldsymbol{p}(t)$ and should navigate towards and converge to the path given as the straight line between $\boldsymbol{p}_k$ and $\boldsymbol{p}_{k+1}$. To simplify the calculations, the NED reference system is translated so the origin is in $\boldsymbol{p}_k$ and rotated so the x-axis points toward $\boldsymbol{p}_{k+1}$. The position of the ship in this reference frame is given as $\boldsymbol{\epsilon}(t) = [s(t), e(t)]^T$

The path fixed coordinate system is defined by rotating the NED coordinate system α_k degrees about the z-axis and then translating the rotated coordinate system so

the origin is placed in $\boldsymbol{p}_k$. As can be seen from figure 3.2, α_k is defined as

$$\alpha_k = \arctan\left(\frac{y_{k+1} - y_k}{x_{k+1} - x_k}\right). \tag{3.11}$$

The transformation from NED to the path-fixed frame is then given as

$$\boldsymbol{\epsilon}(t) = \begin{bmatrix} s(t) \\ e(t) \end{bmatrix} = [\boldsymbol{R}_{z,\alpha_k}(\alpha_k)]^T(\boldsymbol{p}(t) - \boldsymbol{p}_k^n) \tag{3.12}$$

where

$$\boldsymbol{R}_{z,\alpha_k}(\alpha_k) = \begin{bmatrix} \cos(\alpha_k) & -\sin(\alpha_k) \\ \sin(\alpha_k) & \cos(\alpha_k) \end{bmatrix}. \tag{3.13}$$

As shown in figure 3.2, $s(t)$ is the along-track distance and $e(t)$ is the cross-track error. The control objective is to make the ship converge to the straight line and follow it. Mathematically, this corresponds to $e(t)$ becoming 0, so the control objective is given as

$$\lim_{t\to\infty} e(t) = 0. \tag{3.14}$$

There are two approaches to achieve this: Enclosure-based and lookahead-based steering.

Enclosure-Based Steering

In enclosure-based steering a virtual circle with radius R and center in $\boldsymbol{p}(t)$ is considered. The circle will intersect the straight line at two points (provided the radius is large enough). The point $\boldsymbol{p}_{los}$ marked in green is the intersection point closest to the desired direction of travel (towards $\boldsymbol{p}_{k+1}$).

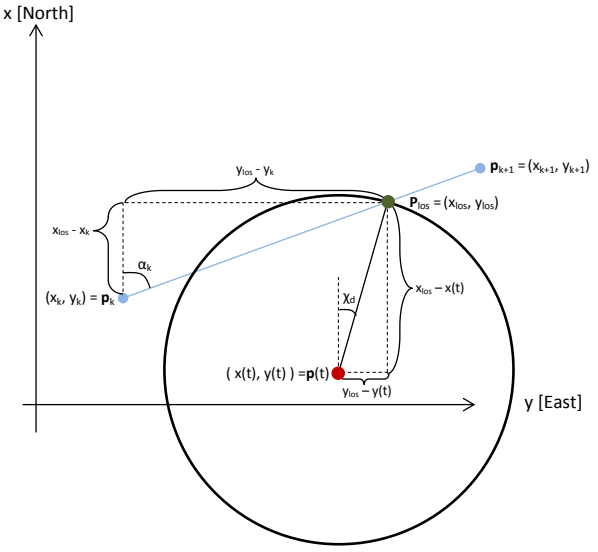

Figure 3.3: Illustration of enclosure-based LOS steering.

The guidance law uses $\boldsymbol{p}_{los}$ to calculate the desired course angle $\chi_d(t)$. As such, it is necessary to compute x_{los} and y_{los}. By geometric considerations, $\boldsymbol{p}_{los}$ can be calculated by solving the equation set below:

$$\begin{aligned} [x_{los} - x(t)]^2 + [y_{los} - y(t)]^2 &= R^2 \\ \tan(\alpha_k) &= \frac{y_{los} - y_k}{x_{los} - x_k} \end{aligned} \tag{3.15}$$

Once $\boldsymbol{p}^n_{los}$ is known, the desired course angle can be decided using equation (3.16).

$$\tan(\chi_d(t)) = \frac{y_{los} - y(t)}{x_{los} - x(t)} \tag{3.16}$$

Lookahead-Based Steering

This method of LoS is computationally easier than enclosure-based guidance. Rather than calculating a point $\boldsymbol{p}_{los}$, it uses a design parameter $\Delta > 0$ referred to as the lookahead distance. In general, Δ may vary as a function of time, e or other parameters. However, it is often chosen to be constant.

In this approach of LOS, the desired course angle is the sum of two angles:

$$\chi_d(e) = \alpha_k + \chi_r(e) \tag{3.17}$$

α_k is defined in equation (3.11), and $\chi_r(e)$ is the path relative angle illustrated in figure 3.4. This angle depends on the cross-track error e and the lookahead distance $\Delta > 0$ and is defined in equation

$$\chi_r(e) = \arctan\left(-\frac{e}{\Delta}\right) \tag{3.18}$$

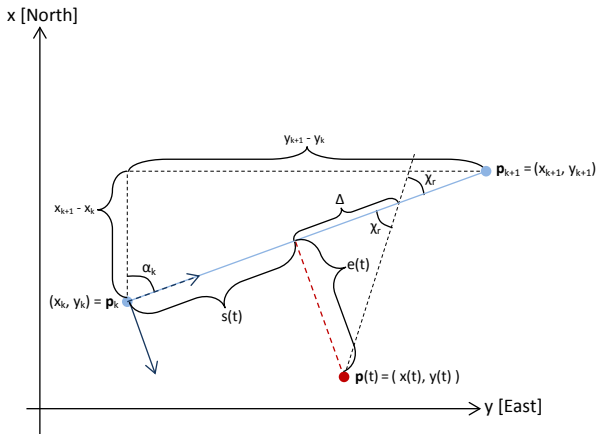

Figure 3.4: Illustration of lookahead-based LOS steering.

Path-Following Controllers

The LOS-methods described above result in a guidance law which provides the desired course angle χ_d (equation (3.16) and (3.17) for enclosure-based and lookahead-based steering respectively). However, this angle is the sum of the desired heading angle ψ_d and the side-slip angle β defined in equation (2.1): $\chi_d = \psi_d + \beta$. The heading ψ is the angle that can be directly affected by turning the rudder of a ship and ψ_d is the reference for any autopilot controller. As such, two control approaches are used to achieve path following.

If velocity measurements are unavailable, the enclosure-based steering law can be applied in such a way that the x-axis of the body reference system is aligned with the LOS-vector. The desired heading angle is then calculated as below.

$$\tan(\psi_d(t)) = \frac{y_{los} - y(t)}{x_{los} - x(t)} \tag{3.19}$$

The side-slip angle β is assumed to be unknown and is omitted from the equations and a heading autopilot can then be used to fulfill the reference heading. However, this approach is faulty when the ship is subjected to environmental forces because the ship will in fact side-slip in the presence of waves, wind and current.

If velocity measurements are available, another approach is to align the velocity vector of the marine vessel with the LoS-vector. In this case, the lookahead-based steering law can be applied with χ_d defined as in equation (3.17). A heading autopilot driven by the error between the desired and actual heading (equation (3.20)) can be applied. In this case, β is computed based on the velocity measurements.

$$\begin{aligned} \tilde{\psi} &= \psi - \psi_d \\ &= \psi - \chi_d + \beta \end{aligned} \tag{3.20}$$

3.6.2 Line of Sight for Circular Path Following

LOS guidance is not limited to straight line paths. In [7], the lookahead-based steering method is explained for circular paths. In general, the desired circular path is fully described by a radius R_c and a center $\boldsymbol{p}_c = [x_c, y_c]^T$ as illustrated in figure 3.5. The ship's position is $\boldsymbol{p}(t) = (x(t), y(t)$, the path-fixed reference frame is shown in blue and the lookahead distance Δ now lies along the tangent of the path.
The desired course angle is very similar to that of the lookahead-based steering for straight paths (3.17):

$$\chi_d(e, t) = \chi_p(t) + \chi_r(e) \tag{3.21}$$

The term $\chi_r(e)$ is defined in equation (3.18) and is identical for straight line and circular path following. The main difference between straight line and circular path following is $\chi_p(t)$. For straight lines, this is a constant angle α_k, whereas the angle

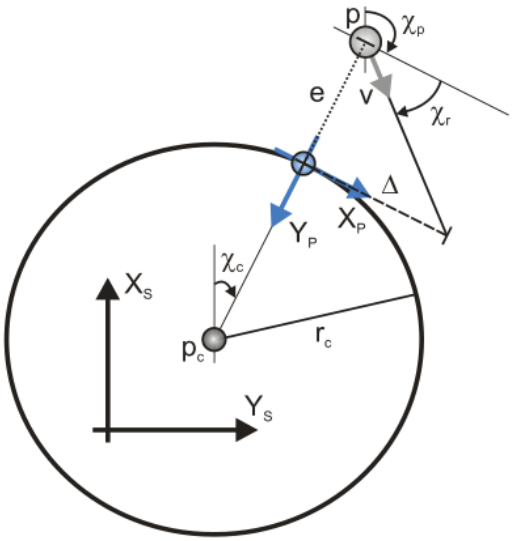

Figure 3.5: Illustration of lookahead-based LoS steering of circular path [7].

changes along the circular path.

$$\begin{aligned} \chi_p(t) &= \chi_c(t) + \lambda \frac{\pi}{2} \\ \tan(\chi_c(t)) &= \frac{y(t) - y_c}{x(t) - x_c} \end{aligned} \tag{3.22}$$

$\lambda = 1$ corresponds to clockwise motion, and $\lambda = -1$ to counter-clockwise motion. As figure 3.5 shows, these equations are purely geometric considerations. The path-fixed coordinate system is anchored in the direct projection of $\boldsymbol{p}(t)$ onto the circular path and the x-axis is parallel to the tangent of the path at this point (shown in blue in figure 3.5). Thus, the cross-track error $e(t)$ is given by equation (3.23).

$$|\boldsymbol{p}(t) - \boldsymbol{p}_c| = R_c - e(t) \tag{3.23}$$

3.6.3 Line of Sight with Integral Effect for Straight Path Following

Traditional LOS is widely used in practice for path following. However, as discussed in chapter 3.6.1, it is susceptible to environmental disturbances unless velocity measurements are available to calculate the side-slip angle β. Another approach is to expand the LOS lookahead-based method and utilize an integral effect to counteract environmental forces by allowing the vessel in question to side-slip [5]. In this article, Børhaug et. al. develop a LOS guidance law with integral effect to

counteract ocean currents for a surface ship with the goal of following a straight line path with a total, constant velocity of U_d. As described in chapter 2.5, the ocean current $\boldsymbol{V}_c$ is assumed constant and irrotational in the inertial frame.

As with traditional LoS, the inertial frame is rotated so that the x-axis is aligned with the straight path that is to be followed. As such, the y-position of the ship corresponds to the cross-track error. If there had been no ocean current, the desired heading angle ψ_d would be zero. This corresponds to the x-axis of the ship being aligned with the velocity vector $U = \sqrt{u^2 + v^2}$ and the side-slip angle β being zero. As such, the ship would be aligned with the desired path. However, if the ocean current has a component acting normally to the path, an underactuated surface vessel is unable to stay identically on the path with zero heading. To cancel out the effects of the ocean current, Børhaug et. al. allow the ship to side-slip such that a component of the surge velocity of the vessel can counteract the current and the resulting velocity vector U is aligned with the desired path. This is illustrated in figure 3.6.

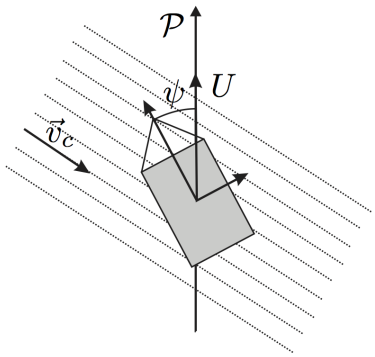

Figure 3.6: Illustration of LoS with integral effect to counteract ocean currents [6]. The total velocity U of the ship is aligned with the path, but the ship itself is rotated slightly with a heading angle of ψ.

As such, the control objectives can be formalized as follows:

$$\begin{aligned} \lim_{t\to\infty} y(t) &= 0 \\ \lim_{t\to\infty} \psi(t) &= \psi_{ss} \\ \lim_{t\to\infty} U(t) &= U_d \end{aligned} \tag{3.24}$$

ψ_{ss} is a constant that the heading $\psi(t)$ should converge to. When the current is constant and the marine vessel is to follow a straight path along the x-axis of the inertial frame, the heading needed to counteract the current is also constant and unique [11]. In [5], Børhaug et. al. show that this steady-state angle is achieved

by using the following guidance law:

$$\begin{aligned} \psi_r(y, y_{int}) &= -\arctan\left(\frac{y + \sigma y_{int}}{\Delta}\right) \\ \dot{y}_{int}(y) &= \frac{\Delta y}{(y + \sigma y_{int})^2 + \Delta^2} \end{aligned} \tag{3.25}$$

Here, σ and Δ are both design parameters (Δ is still the look-ahead distance, and σ is a gain). By adding the integral term, one can se that ψ_r is no longer required to be zero when the cross-track error y is zero, so when the vessel is on the desired path, the integral term will generate the necessary side-slip angle to follow the path in the presence of ocean currents.

Equation (3.25) is a guidance law for the desired heading angle for following a straight line path in an inertial coordinate system with x-axis aligned with the desired path. As with traditional LoS lookahead-based guidance, the total desired heading is calculated by adding ψ_r and the angle between the NED and rotated path-fixed coordinate system α_k (3.17).

$$\psi_d = \alpha_k + \psi_r(e) \tag{3.26}$$

In addition to the guidance law, Børhaug et. al. propose a yaw and a surge controller based on a general 3-DOF model that in combination with the guidance law ensures that the control objectives are achieved. The proposed controllers are adaptive feedback linearization PD- and P-controllers.

In [11], the LoS method with integral effect is expanded to a 6-DOF marine vessel and analyzed at a kinematic level. Similar to [5], the desired equilibrium points is proven to be UGAS (Uniformly Globally Asymptotically Stable) and ULES (Uniformly Locally Exponentially Stable). In addition, the method is simulated using the model for the HUGIN AUV (chapter 5.2) with very good results. In [10], the analysis is expanded to include surge, pitch and yaw controllers. The proposed controllers are feedback linearization P- (surge) and PD-controllers (pitch and yaw). The references for pitch and yaw, $\psi_r(y, y_{int})$ and $\theta_r(z, z_{int})$, are given by the guidance laws in equation (3.27) and (3.28). The method also works for horizontal path following in the presence of a vertical current [9], and can also be used to estimate the direction and magnitude of the current once the steady-state is reached [8].

$$\begin{aligned} \psi_r(y, y_{int}) &= -\arctan\left(\frac{y + \sigma_y y_{int}}{\Delta_y}\right) \\ \dot{y}_{int}(y) &= \frac{\Delta_y y}{(y + \sigma_y y_{int})^2 + \Delta_y^2} \end{aligned} \tag{3.27}$$

$$\begin{aligned} \theta_r(z, z_{int}) &= \arctan\left(\frac{z + \sigma_z z_{int}}{\Delta_z}\right) \\ \dot{z}_{int}(y) &= \frac{\Delta_z z}{(z + \sigma_z z_{int})^2 + \Delta_z^2} \end{aligned} \tag{3.28}$$

3.7 Path Following of Space Curves

In his doctoral thesis [6], Børhaug consider path following of more general paths, and that apply to underwater vehicles as well as surface vessels (that is, the path takes place in 3D space rather than on a plane). The control strategies to follow such paths are based on Serret-Frenet formulas. In general, a continuously differentiable space curve $\mathcal{C}$ in the inertial reference frame can be described using a Serret-Frenet coordinate frame $\{f\}$.

If $\mathcal{C}$ is the curve that is to be followed by a marine vehicle, the Serret-Frenet coordinate system is anchored in $\mathcal{C}$ and propagates along the curve. The coordinate frame has axes along the tangent $\boldsymbol{T}$, the normal $\boldsymbol{N}$ and the binormal $\boldsymbol{B}$ of $\mathcal{C}$. The space curve can be completely described by the initial starting point and direction, the curvature κ and the torsion τ. κ and τ can be parametrized by the arc length s (the distance traveled by a virtual particle propagating the path). As such, $\dot{s}$ gives the instantaneous speed of the particle along the curve. Equation (3.29) shows how the Serret-Frenet reference frame changes as the particle travels along the path.

$$\begin{bmatrix} \dot{\boldsymbol{T}} \\ \dot{\boldsymbol{N}} \\ \dot{\boldsymbol{B}} \end{bmatrix} = \dot{s} \begin{bmatrix} 0 & \kappa(s) & 0 \\ -\kappa(s) & 0 & \tau(s) \\ 0 & -\tau(s) & 0 \end{bmatrix} \begin{bmatrix} \boldsymbol{T} \\ \boldsymbol{N} \\ \boldsymbol{B} \end{bmatrix} \tag{3.29}$$

The linear and angular velocities of the f-frame with respect to the inertial frame also depend on s and $\dot{s}$.

$$\begin{aligned} \boldsymbol{v}_{f/i}^{f} &= [\dot{s}, 0, 0]^T \\ \boldsymbol{\omega}_{f/i}^{f} &= \dot{s} \cdot [\tau(s), 0, \kappa(s)]^T \end{aligned} \tag{3.30}$$

The notation in equation (3.31) is used for the position of the body frame relative to the Serret-Frenet frame and is illustrated for the 2D-case in figure 3.7.

$$\boldsymbol{r}_{b/f}^{f} = x_{b/f}\boldsymbol{T} + y_{b/f}\boldsymbol{N} + z_{b/f}\boldsymbol{B} \tag{3.31}$$

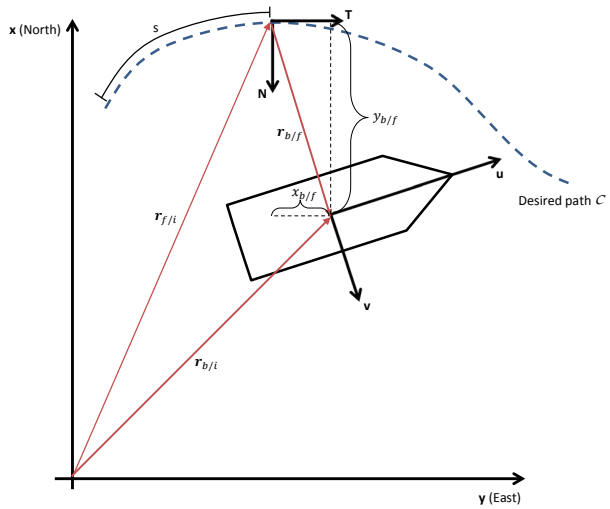

Figure 3.7: Illustration of Serret-Frenet frame for 2D path following. There are 3 coordinate frames: NED (assumed inertial), body (anchored in the marine vehicle) and Serret-Frenet (anchored in the desired path). s is the traveled distance along the path. Furthermore, $\boldsymbol{r}_{b/i} = \boldsymbol{r}_{f/i} + \boldsymbol{r}_{b/f}$ when all vectors are expressed in the same coordinate system. $\boldsymbol{r}^f_{b/f} = x_{b/f}\boldsymbol{T} + y_{b/f}\boldsymbol{N}$.

Denoting the position of the f-frame and b-frame relative to the inertial frame $\boldsymbol{r}_{f/i}$ and $\boldsymbol{r}_{b/i}$ and using equation (A.3), the linear velocity of the b-frame relative to the i-frame can be expressed as

$$\begin{aligned} \boldsymbol{v}_{b/i} &= \frac{{}^i d}{dt}\boldsymbol{r}_{b/i} = \frac{{}^i d}{dt}\left(\boldsymbol{r}_{f/i} + \boldsymbol{r}_{b/f}\right) \\ &= \boldsymbol{v}_{f/i} + \frac{{}^f d}{dt}\boldsymbol{r}_{b/f} + \boldsymbol{\omega}_{f/i} \times \boldsymbol{r}_{b/f}. \end{aligned} \tag{3.32}$$

By expressing all vectors in equation (3.32) in the f-frame, this yields the following result.

$$\begin{aligned} \boldsymbol{v}^f_{b/i} = \boldsymbol{R}^f_b(\boldsymbol{\Theta}_{fb})\boldsymbol{v}^b_{b/i} &= \boldsymbol{v}^f_{f/i} + \frac{{}^f d}{dt}\boldsymbol{r}^f_{b/f} + \boldsymbol{\omega}^f_{f/i} \times \boldsymbol{r}^f_{b/f} \\ &= \begin{bmatrix} \dot{s} \\ 0 \\ 0 \end{bmatrix} + \frac{{}^f d}{dt}\begin{bmatrix} x_{b/f} \\ y_{b/f} \\ z_{b/f} \end{bmatrix} + \dot{s}\begin{bmatrix} \tau(s) \\ 0 \\ \kappa(s) \end{bmatrix} \times \begin{bmatrix} x_{b/f} \\ y_{b/f} \\ z_{b/f} \end{bmatrix} \\ &= \begin{bmatrix} \dot{s} \\ 0 \\ 0 \end{bmatrix} + \begin{bmatrix} \dot{x}_{b/f} \\ \dot{y}_{b/f} \\ \dot{z}_{b/f} \end{bmatrix} + \dot{s}\begin{bmatrix} 0 & -\kappa(s) & 0 \\ \kappa(s) & 0 & \tau(s) \\ 0 & \tau(s) & 0 \end{bmatrix} \begin{bmatrix} x_{b/f} \\ y_{b/f} \\ z_{b/f} \end{bmatrix} \end{aligned} \tag{3.33}$$

3.7.1 Surface vessels

By rearranging the terms in equation (3.33) and applying them to a surface vessel with 3 DOFs, one can express the differential kinematic relationship between the f- and b-frame as below:

$$\begin{bmatrix} \dot{x}_{b/f} \\ \dot{y}_{b/f} \end{bmatrix} = \begin{bmatrix} \cos(\psi_{fb}) & -\sin(\psi_{fb}) \\ \sin(\psi_{fb}) & \cos(\psi_{fb}) \end{bmatrix} \begin{bmatrix} u \\ v \end{bmatrix} - \begin{bmatrix} \dot{s} \\ 0 \end{bmatrix} - \dot{s} \begin{bmatrix} 0 & -\kappa \\ \kappa & 0 \end{bmatrix} \begin{bmatrix} x_{b/f} \\ y_{b/f} \end{bmatrix} \tag{3.34}$$

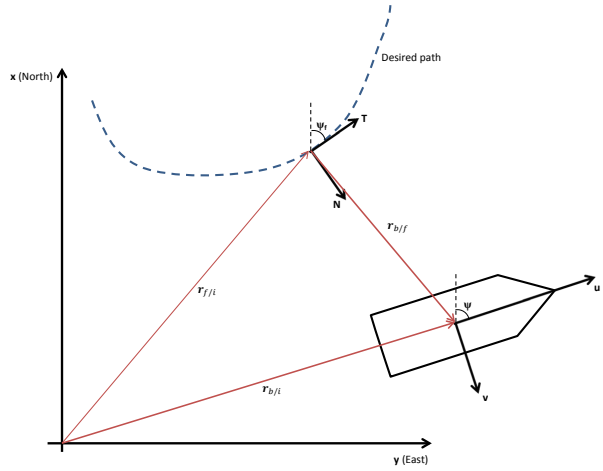

Figure 3.8: Illustration of Serret-Frenet frame for 2D path following. ψ is the yaw angle between the NED and body coordinate system, and ψ_f is the yaw angle between the NED and Serret-Frenet coordinate system. $\psi_{fb} = \psi - \psi_f$.

$\psi_{fb} = \psi - \psi_f$ is the heading of the body frame relative to the heading of the Serret-Frenet frame (illustrated in figure 3.8). ψ is assumed measured and ψ_f depends on the known, desired path.

The control objective is make the marine vessel converge to and track the curve. In addition, one can include a desired speed profile $u_c(t, s(t))$ along the curve as a control objective. Since the Serret-Frenet coordinate frame is anchored in the path at all times, this can be mathematically described as following:

$$\begin{aligned} \lim_{t\to\infty} x_{b/f} &= 0 \\ \lim_{t\to\infty} y_{b/f} &= 0 \\ \lim_{t\to\infty} u(t) - u_c(t, s(t)) &= 0 \end{aligned} \tag{3.35}$$

To accomplish this, Børhaug suggests a guidance law and an update law as below:

$$\psi_d = \psi_f - \arctan\left(\frac{v}{u_c}\right) - \arctan\left(\frac{y_{b/f}}{\sqrt{\Delta^2 + \left(x_{b/f}\right)^2}}\right) \tag{3.36}$$

$$\dot{s} = \underbrace{\sqrt{u_c^2 + v^2}}_{\triangleq U_c} \frac{\sqrt{\Delta^2 + x_{b/f}^2} + x_{b/f}}{\sqrt{\Delta^2 + x_{b/f}^2 + y_{f/b}^2}} \tag{3.37}$$

Δ is a constant design parameter. It is important to note this guidance law actually enables tracking of the Serret-Frenet reference frame: The reference position of the marine vessel is the origin of this reference frame. $\dot{s} = 0$ corresponds to the Serret-Frenet frame being stationary, something that would result in the marine vessel also being stationary in the origin of this frame. By choosing $\dot{s}$ through the update law, the Serret-Frenet frame propagates along the desired path and drives the reference position forward along the desired path. The Serret-Frenet frame is a virtual auxiliary frame, and as such the propagation along this path, $\dot{s}$, can be chosen freely. The desired heading angle in equation (3.36) can be used as a reference for a yaw controller, and u_c as a reference for a surge controller. In his thesis, Børhaug shows that the guidance law and update law ensure exponential achievement the control objectives when used in combination with feedback linearization surge and yaw controllers given that certain assumptions are satisfied. These controllers are specified in chapter 5.1.1.

3.7.2 Underwater vessels

By rearranging the terms in equation (3.33) and applying them to an underwater vehicle with 5 DOFs (roll ϕ is assumed zero[1]), the differential kinematic relationship between the f- and b-frame can be expressed as below:

$$\begin{bmatrix} \dot{x}_{b/f} \\ \dot{y}_{b/f} \\ \dot{y}_{b/f} \end{bmatrix} = \boldsymbol{R}_b^f(\boldsymbol{\Theta}_{fb}) \begin{bmatrix} u \\ v \\ w \end{bmatrix} - \begin{bmatrix} \dot{s} \\ 0 \\ 0 \end{bmatrix} - \dot{s} \begin{bmatrix} 0 & -\kappa & 0 \\ \kappa & 0 & -\tau \\ 0 & \tau & 0 \end{bmatrix} \begin{bmatrix} x_{b/f} \\ y_{b/f} \\ z_{b/f} \end{bmatrix} \tag{3.38}$$

$\boldsymbol{R}_b^f(\boldsymbol{\Theta}_{fb}) = [\boldsymbol{R}_f^i(\boldsymbol{\Theta}_{if})]^T \boldsymbol{R}_b^i(\boldsymbol{\Theta}_{ib})$, where $\boldsymbol{\Theta}_{ib} = [0, \theta, \psi]^T$ is the orientation of the body frame with respect to the inertial frame (NED) and $\boldsymbol{\Theta}_{if} = [\phi_f, \theta_f, \psi_f]^T$ is the orientation of the Serret-Frenet frame with respect to the inertial frame. $\boldsymbol{\Theta}_{ib}$ is assumed measured and $\boldsymbol{\Theta}_{if}$ depends on the desired path. Naturally, the desired path is known, and $\boldsymbol{\Theta}_{if}$ can be parametrized as a function of the traveled distance along the desired path s.

As with surface vessels, the control objective is make the underwater vehicle converge to and track the desired path. The control objectives are shown below. As

[1] Roll is assumed passively stabilized by fins or gravity.

with the surface vessel, a desired surge profile $u_c(t, s(t))$ is defined.

$$\begin{aligned} \lim_{t\to\infty} x_{b/f} &= 0 \\ \lim_{t\to\infty} y_{b/f} &= 0 \\ \lim_{t\to\infty} z_{b/f} &= 0 \\ \lim_{t\to\infty} u(t) - u_c(t, s(t)) &= 0 \end{aligned} \tag{3.39}$$

In the case of the surface vessel, the proposed guidance law was a law for the desired orientation of the body frame relative to the inertial frame ψ. However, in the 3D-case with rotation about several axes, it is no longer straightforward to define a desired absolute orientation ϕ, θ and ψ. As such, Børhaug introduces a coordinate frame c. This is obtained by rotating the b-frame an angle of α_c about the y-axis and an angle $-\beta_c$ about the rotated z-axis ($\boldsymbol{\Theta}_{cb} = [0, \alpha_c, -\beta_c]^T$).

$$\begin{aligned} \alpha_c &\triangleq \arctan\left(\frac{w}{u_c}\right), \\ \beta_c &\triangleq \arctan\left(\frac{v}{\sqrt{u_c^2 + w^2}}\right) \end{aligned} \tag{3.40}$$

The orientation of the c-frame relative to the f-frame is then described by $\boldsymbol{\Theta}_{fc} = [\phi_{fc}, \theta_{fc}, \psi_{fc}]^t$, which can be calculated based on the rotation matrix

$$\boldsymbol{R}_c^f(\boldsymbol{\Theta}_{fc}) \triangleq [\boldsymbol{R}_f^i(\boldsymbol{\Theta}_{if})]^T \boldsymbol{R}_b^i(\boldsymbol{\Theta}_{ib})[\boldsymbol{R}_b^c(\boldsymbol{\Theta}_{cb})]^T \tag{3.41}$$

Instead of defining guidance laws for θ and ψ, Børhaug suggests guidance laws for the relative orientation of the c-frame, θ_{fc} and ψ_{fc} (ϕ_{fc} does not affect the path following and as such a guidance law for this angle is not necessary). The update law is similar to that of the surface vessel.

$$\begin{aligned} \theta_{fc,d} &= \arctan\left(\frac{z_{b/f}}{\sqrt{\Delta^2 + y_{b/f}^2}}\right) \\ \psi_{fc,d} &= -\arctan\left(\frac{y_{b/f}}{\sqrt{\Delta^2 + x_{b/f}^2 + y_{b/f}^2}}\right) \end{aligned} \tag{3.42}$$

$$\begin{aligned} \dot{s} = \underbrace{U_c}_{\triangleq\sqrt{u_c^2+v^2+w^2}} & \frac{\sqrt{\Delta^2 + y_{b/f}^2}}{\sqrt{\Delta^2 + y_{b/f}^2 + z_{f/b}^2}} \frac{\sqrt{\Delta^2 + x_{b/f}^2 + z_{b/f}^2}}{\sqrt{\Delta^2 + x_{b/f}^2 + y_{b/f}^2 + z_{b/f}^2}} \\ & + U_c \frac{x_{b/f}}{\sqrt{\Delta^2 + x_{b/f}^2 + y_{b/f}^2 + z_{b/f}^2}} \end{aligned} \tag{3.43}$$

Børhaug also introduces an integrator backstepping controller to track $\theta_{fc,d}$ and $\psi_{fc,d}$. This controller is described in chapter 5.2.2. As with the surface vessel, a feedback linearization surge controller (such as the one described in chapter 5.2.1) can be applied to ensure that u tracks $u_c(t, s(t))$. This closed loop system achieves the control objectives exponentially under certain assumptions.

Chapter 4

Problem Formulation

The guidance and control of marine vessels is an area of focus within the research community. There are still challenges related to autonomous tracking tasks, especially for underwater vehicles. The basis for the proposed master thesis is advanced guidance and control of underactuated marine vehicles with the task of following a general path. The key challenge addressed is path following in the presence of unknown ocean currents.

The preliminary set of tasks for the master thesis are:

1. Perform and report literature study on state of the art guidance and control of marine vehicles and current compensation.
2. Develop guidance law for both surface and underwater vehicles based on existing methods for path following in the presence of unknown ocean currents.
3. Implement the proposed solution in Simulink and verify result by simulations.
4. Write an international conference article based on the main results.

Chapter 5

Simulation models

This chapter presents the EOMs and the controllers for the surface supply ship and the Hugin AUV that have been implemented in Simulink and form the basis for the simulations presented in chapter 7.

5.1 Supply ship

The supply ship is a surface vessel with 3 DOFs. The model is given in [13]:

$$\dot{\boldsymbol{\eta}} = \boldsymbol{R}_{z,\psi}(\psi)\boldsymbol{\nu_r} + \boldsymbol{V_c} \tag{5.1}$$

$$\boldsymbol{M}\dot{\boldsymbol{\nu_r}} + \boldsymbol{C}(\boldsymbol{\nu_r})\boldsymbol{\nu_r} + \boldsymbol{D}\boldsymbol{\nu_r} = \boldsymbol{B}\boldsymbol{f} \tag{5.2}$$

$$\boldsymbol{\eta} = \begin{bmatrix} x \\ y \\ \psi \end{bmatrix} \tag{5.3}$$

$$\boldsymbol{\nu_r} = \begin{bmatrix} u_r \\ v_r \\ r \end{bmatrix} \tag{5.4}$$

This model is given relative to the ship's CG. u_r and v_r are the vessel velocities relative to the ocean current $\boldsymbol{V_c}$, which is given in equation (5.5). The current is assumed constant and irrotational in the inertial frame as discussed in chapter 2.

$$\boldsymbol{V_c} = \begin{bmatrix} V_x \\ V_y \\ 0 \end{bmatrix} \tag{5.5}$$

The controlled input $\boldsymbol{f}$ contains the propeller force T and the rudder angle δ.

$$\boldsymbol{f} = \begin{bmatrix} T \\ \delta \end{bmatrix} \tag{5.6}$$

The model matrices are shown below (numeric values specified in [13]):

$$\boldsymbol{M} = \begin{bmatrix} m_{11} & 0 & 0 \\ 0 & m_{22} & m_{23} \\ 0 & m_{23} & m_{33} \end{bmatrix} \tag{5.7}$$

$$\boldsymbol{C}(\boldsymbol{\nu_r}) = \begin{bmatrix} 0 & 0 & -m_{22}v_r - m_{23}r \\ 0 & 0 & m_{11}u_r \\ m_{22}v_r + m_{23}r & -m_{11}u_r & 0 \end{bmatrix} \tag{5.8}$$

$$\boldsymbol{D} = \begin{bmatrix} d_{11} & 0 & 0 \\ 0 & d_{22} & md23 \\ 0 & d_{32} & d_{33} \end{bmatrix} \tag{5.9}$$

$$\boldsymbol{B} = \begin{bmatrix} b_{11} & 0 \\ 0 & b_{22} \\ 0 & b_{32} \end{bmatrix} \tag{5.10}$$

By rewriting equation (5.2), it is obvious that

$$\boldsymbol{\dot{\nu}_r} = \begin{bmatrix} \dot{u}_r \\ \dot{v}_r \\ \dot{r} \end{bmatrix} = \boldsymbol{M}^{-1}\boldsymbol{B}\boldsymbol{f} - \boldsymbol{M}^{-1}(\boldsymbol{C}(\boldsymbol{\nu_r})\boldsymbol{\nu_r} + \boldsymbol{D}\boldsymbol{\nu_r}). \tag{5.11}$$

It can easily be seen that the rudder angle δ affects both sway v_r and yaw r dynamics.

$$\boldsymbol{M}^{-1}\boldsymbol{B} = \begin{bmatrix} \frac{b_{11}}{m_{11}} & 0 \\ 0 & \frac{b_{22}m_{33} - b_{32}m_{23}}{m_{22}m_{33} - m_{23}^2} \\ 0 & \frac{b_{32}m_{22} - b_{22}m_{23}}{m_{22}m_{33} - m_{23}^2} \end{bmatrix} \tag{5.12}$$

By transforming the model as described in chapter 3.2 the model can be rewritten and the control problems will be simplified. Defining ϵ as

$$\epsilon \triangleq -\frac{m_{33}b_{22} - m_{23}b_{32}}{m_{22}b_{32} - m_{23}b_{22}} \tag{5.13}$$

and the transformation matrix $\boldsymbol{T}$ as in equation (5.14), the model can be transformed to a new point p. In this point the effect of the rudder has been removed from the sway dynamic. The transformed model is given in equation (5.15). Note that the states $\boldsymbol{\nu_r}$ and $\boldsymbol{\eta}$ now describe the motion in point p and not CG.

$$\boldsymbol{T} = \begin{bmatrix} 1 & 0 & 0 \\ 0 & 1 & \epsilon \\ 0 & 0 & 1 \end{bmatrix} \tag{5.14}$$

$$\begin{aligned} \boldsymbol{\dot{\eta}} &= \boldsymbol{R}_{z,\psi}(\psi)\boldsymbol{\nu_r} + \boldsymbol{V_c} \\ \boldsymbol{M}^p\boldsymbol{\dot{\nu}_r} + \boldsymbol{C}^p(\boldsymbol{\nu_r})\boldsymbol{\nu_r} + \boldsymbol{D}^p\boldsymbol{\nu_r} &= \boldsymbol{B}^p\boldsymbol{f} \end{aligned} \tag{5.15}$$

Defining $\boldsymbol{H} \triangleq \boldsymbol{T}^{-1}$, the transformed model matrices are given below:

$$\begin{aligned}
\boldsymbol{M}^p &= \boldsymbol{H}^T \boldsymbol{M} \boldsymbol{H} \\
\boldsymbol{D}^p &= \boldsymbol{H}^T \boldsymbol{D} \boldsymbol{H} \\
\boldsymbol{B}^p &= \boldsymbol{H}^T \boldsymbol{B} \\
\boldsymbol{C}^p(\boldsymbol{\nu}_r) &= \begin{bmatrix} 0 & 0 & -m_{22}^p v_r - m_{23}^p r \\ 0 & 0 & m_{11}^p u_r \\ m_{22}^p v_r + m_{23}^p r & -m_{11}^p u_r & 0 \end{bmatrix}
\end{aligned} \tag{5.16}$$

Through this transformation it can be shown that

$$\boldsymbol{\tau} = \begin{bmatrix} \tau_u \\ 0 \\ \tau_r \end{bmatrix} = (\boldsymbol{M}^p)^{-1} \boldsymbol{B}^p \boldsymbol{f} = \begin{bmatrix} \frac{b_{11}^p}{m_{11}^p} & 0 \\ 0 & 0 \\ 0 & \frac{b_{32}^p m_{22}^p - b_{22}^p m_{23}^p}{m_{22}^p m_{33}^p - {m_{23}^p}^2} \end{bmatrix} \begin{bmatrix} T \\ \delta \end{bmatrix}, \tag{5.17}$$

and the model can be written in component form as below.

$$\begin{aligned}
\dot{x} &= \cos(\psi) u_r - \sin(\psi) v_r + V_x \\
\dot{y} &= \sin(\psi) u_r + \cos(\psi) v_y + V_y \\
\dot{\psi} &= r \\
\dot{u_r} &= F_{u_r}(u_r, v_r, r) - \frac{d_{11}^p}{m_{11}^p} u_r + \tau_u \\
\dot{v_r} &= X(u_r) r + Y(u_r) v_r \\
\dot{r} &= F_r(u_r, v_r, r) + \tau_r
\end{aligned} \tag{5.18}$$

$$F_{u_r}(u_r, v_r, r) = \frac{m_{22}^p v_r + m_{23}^p r}{m_{11}^p} r \tag{5.19}$$

$$X(u_r) = \frac{{m_{23}^p}^2 - m_{11}^p m_{33}^p}{m_{22}^p m_{33}^p - {m_{23}^p}^2} u_r + \frac{d_{33}^p m_{23}^p - d_{23}^p m_{33}^p}{m_{22}^p m_{33}^p - {m_{23}^p}^2} \tag{5.20}$$

$$Y(u_r) = \frac{m_{22}^p m_{23}^p - m_{11}^p m_{23}^p}{m_{22}^p m_{33}^p - {m_{23}^p}^2} u_r - \frac{d_{22}^p m_{33}^p - d_{32}^p m_{23}^p}{m_{22}^p m_{33}^p - {m_{23}^p}^2} \tag{5.21}$$

$$\begin{aligned}
F_r(u_r, v_r, r) =& \frac{m_{23}^p d_{22}^p - m_{22}^p (d_{32}^p + (m_{22}^p - m_{11}^p) u_r)}{m_{22}^p m_{33}^p - {m_{23}^p}^2} v_r \\
&+ \frac{m_{23}^p (d_{23}^p + m_{11}^p u_r) - m_{22}^p (d_{33}^p + m_{23}^p u_r)}{m_{22}^p m_{33}^p - {m_{23}^p}^2} r
\end{aligned} \tag{5.22}$$

5.1.1 Feedback Linearization Controllers

This section presents feedback linearization controllers from [6] that ensure tracking of the references for u_r and ψ. Equation (5.18) shows that the supply ship has two inputs τ_u and τ_r that affect the surge and yaw dynamics respectively. The

surge controller is responsible for making the relative surge velocity u_r track the desired speed profile $u_{rd}(t)$ and the yaw controller ensure tracking of the desired yaw and yaw rate ψ_d and $\dot{\psi}_d$. By defining the errors in relative surge velocity as $\tilde{u}_r \triangleq u_r - u_{rd}$, yaw $\tilde{\psi} \triangleq \psi - \psi_d$ and yaw rate as $\dot{\tilde{\psi}} \triangleq r - \dot{\psi}_d$ and imposing the following controllers (k_{u_r}, k_ψ and $k_r > 0$),

$$\tau_u = -F_u(u_r, v_r, r) + \frac{d_{11}^p}{m_{11}^p} u_{rd} + \dot{u}_{rd} - k_{u_r}\tilde{u}_r \tag{5.23}$$

$$\tau_r = -F_r(u_r, v_r, r) + \ddot{\psi}_d - k_\psi \tilde{\psi} - k_r \dot{\tilde{\psi}} \tag{5.24}$$

it can easily be shown that the errors converges to zero exponentially.

$$\begin{aligned} \dot{\boldsymbol{\xi}} &= \begin{bmatrix} \dot{\tilde{u}}_r \\ \dot{\tilde{\psi}} \\ \ddot{\tilde{\psi}} \end{bmatrix} \\ &= \begin{bmatrix} -(k_{u_r} + \frac{d_{11}^p}{m_{11}^p}) & 0 & 0 \\ 0 & 0 & 1 \\ 0 & -k_\psi & -k_r \end{bmatrix} \begin{bmatrix} \tilde{u}_r \\ \tilde{\psi} \\ \dot{\tilde{\psi}} \end{bmatrix} \\ &= \boldsymbol{\Lambda}\boldsymbol{\xi} \end{aligned} \tag{5.25}$$

The closed loop system above is linear and time-invariant. All controller gains and $\frac{d_{11}^p}{m_{11}^p}$ are strictly positive, meaning that $\boldsymbol{\Lambda}$ is Hurwitz and the origin $\boldsymbol{\xi} = 0$ is UGES (theorem 4.5 in appendix A.3.2).

5.2 HUGIN

HUGIN is a torpedo-shaped AUV and the model is given by Kongsberg Maritime AS. As such, the model parameters are not specified in this thesis. A few assumptions have been made to simplify the model slightly.

1. The roll is assumed passively stabilized through fins or by gravity, and the model is subsequently reduced to 5 DOF: $\phi = 0$. This is a common assumption in maneuvering control of slender body AUVs [12].
2. Even though the HUGIN AUV have 4 rudders (top, bottom, port, starboard), it is assumed that the rudder angles are connected: $\delta_{top} = \delta_{bottom}$ and $\delta_{port} = \delta_{starboard}$.
3. The propeller force T is assumed independent of the vessel surge speed u.

The model is given below relative to Hugin's CG:

$$\dot{\boldsymbol{\eta}} = \boldsymbol{J}(\boldsymbol{\eta})\boldsymbol{\nu_r} + \boldsymbol{V_c} \tag{5.26}$$

$$\boldsymbol{M}\dot{\boldsymbol{\nu}}_{\boldsymbol{r}} + \boldsymbol{C}(\boldsymbol{\nu_r})\boldsymbol{\nu_r} + \boldsymbol{D}(\boldsymbol{\nu_r})\boldsymbol{\nu_r} + \boldsymbol{g}(\boldsymbol{\eta}) = \boldsymbol{B}\boldsymbol{f} \tag{5.27}$$

$$\boldsymbol{\eta} = \begin{bmatrix} x \\ y \\ z \\ \theta \\ \psi \end{bmatrix} \tag{5.28}$$

$$\boldsymbol{\nu_r} = \begin{bmatrix} u_r \\ v_r \\ w_r \\ q \\ r \end{bmatrix} \tag{5.29}$$

u_r, v_r and w_r are the vessel speeds relative to the current $\boldsymbol{V_c}$ given in equation (5.30). The current is assumed constant and irrotational in the inertial frame as discussed in chapter 2.

$$\boldsymbol{V_c} = \begin{bmatrix} V_x \\ V_y \\ V_z \\ 0 \\ 0 \end{bmatrix} \tag{5.30}$$

The controlled input $\boldsymbol{f}$ contains the propeller force T and the two rudder angles δ_q and δ_r (the angles of the side and top/bottom rudders respectively).

$$\boldsymbol{f} = \begin{bmatrix} T \\ \delta_q \\ \delta_r \end{bmatrix} \tag{5.31}$$

The matrices are shown below:

$$\boldsymbol{M} = \begin{bmatrix} m_{11} & 0 & 0 & 0 & 0 \\ 0 & m_{22} & 0 & 0 & m_{25} \\ 0 & 0 & m_{33} & m_{34} & 0 \\ 0 & 0 & m_{43} & m_{44} & 0 \\ 0 & m_{52} & 0 & 0 & m_{55} \end{bmatrix} \tag{5.32}$$

$$\boldsymbol{C}(\boldsymbol{\nu}_r) = \begin{bmatrix} 0 & 0 & 0 & m_{33}w_r + m_{34}q & -m_{22}v_r - m_{25}r \\ 0 & 0 & 0 & 0 & m_{11}u_r \\ 0 & 0 & 0 & -m_{11}u_r & 0 \\ -m_{33}w_r - m_{34}q & 0 & m_{11}u_r & 0 & 0 \\ m_{22}v_r + m_{25}r & -m_{11}u_r & 0 & 0 & 0 \end{bmatrix} \tag{5.33}$$

$$\boldsymbol{D}(\boldsymbol{\nu_r}) = \underbrace{-\begin{bmatrix} d_{11} & 0 & 0 & 0 & 0 \\ 0 & d_{22} & 0 & 0 & d_{25} \\ 0 & 0 & d_{33} & d_{34} & 0 \\ 0 & 0 & d_{43} & d_{44} & 0 \\ 0 & d_{52} & 0 & 0 & d_{55} \end{bmatrix}}_{\boldsymbol{D}_l} \underbrace{-\begin{bmatrix} d^n_{11}|u_r| & 0 & 0 & 0 & 0 \\ 0 & 0 & 0 & 0 & 0 \\ 0 & 0 & 0 & 0 & 0 \\ 0 & 0 & 0 & 0 & 0 \\ 0 & 0 & 0 & 0 & 0 \end{bmatrix}}_{\boldsymbol{D}_n(\boldsymbol{\nu_r})} \tag{5.34}$$

$$\boldsymbol{g}(\boldsymbol{\eta}) = \begin{bmatrix} 0 \\ 0 \\ 0 \\ BG_z W \sin(\theta) \\ 0 \end{bmatrix} \tag{5.35}$$

BG_z is the vertical distance between CG and CB, and $W = mg$ is the weight of the vehicle.

$$\boldsymbol{B} = \begin{bmatrix} b_{11} & 0 & 0 \\ 0 & 0 & b_{23} \\ 0 & b_{32} & 0 \\ 0 & b_{42} & 0 \\ 0 & 0 & b_{52} \end{bmatrix} \tag{5.36}$$

By rewriting equation (5.27), it is obvious that

$$\dot{\boldsymbol{\nu_r}} = \boldsymbol{M}^{-1}\boldsymbol{B}\boldsymbol{f} - \boldsymbol{M}^{-1}(\boldsymbol{C}(\boldsymbol{\nu_r})\boldsymbol{\nu_r} + \boldsymbol{D}(\boldsymbol{\nu_r})\boldsymbol{\nu_r} + \boldsymbol{g}(\boldsymbol{\eta})) \tag{5.37}$$

In this model, the pitch control δ_q affects both pitch and heave dynamics and the yaw control δ_r affects both yaw and sway dynamics.

$$\boldsymbol{M}^{-1}\boldsymbol{B} = \begin{bmatrix} \frac{b_{11}}{m_{11}} & 0 & 0 \\ 0 & 0 & \frac{b_{23}m_{55} - b_{53}m_{25}}{m_{22}m_{55} - m_{25}m_{52}} \\ 0 & \frac{b_{32}m_{44} - b_{42}m_{34}}{m_{33}m_{44} - m_{34}m_{43}} & 0 \\ 0 & \frac{b_{42}m_{33} - b_{32}m_{43}}{m_{33}m_{44} - m_{34}m_{43}} & 0 \\ 0 & 0 & \frac{b_{53}m_{22} - b_{23}m_{52}}{m_{22}m_{55} - m_{25}m_{52}} \end{bmatrix} \tag{5.38}$$

The model can be transformed similar to the supply ship model to simplify control problems. Defining ϵ_1 and ϵ_2 as

$$\begin{aligned} \epsilon_1 &\triangleq -\frac{m_{55}b_{23} - m_{25}b_{53}}{m_{22}b_{53} - m_{25}b_{23}} \\ \epsilon_2 &\triangleq -\frac{m_{44}b_{32} - m_{34}b_{42}}{m_{33}b_{42} - m_{34}b_{32}}. \end{aligned} \tag{5.39}$$

HUGIN has a cylindrical shape resulting in $\epsilon_1 = -\epsilon_2 = 0.4303$ m. Defining the transformation matrix $\boldsymbol{T}$ as in equation (5.40), the model can be transformed to a new point p 0.4303 meters from the CG, and in this point the effect of the rudders have been removed from the heave and sway dynamics. The transformed model is given in equation (5.41). Note that the states $\boldsymbol{\nu_r}$ and $\boldsymbol{\eta}$ now describe the motion in point p and not CG.

$$\boldsymbol{T} = \begin{bmatrix} 1 & 0 & 0 & 0 & 0 \\ 0 & 1 & 0 & 0 & \epsilon_1 \\ 0 & 0 & 1 & \epsilon_2 & 0 \\ 0 & 0 & 0 & 1 & 0 \\ 0 & 0 & 0 & 0 & 1 \end{bmatrix} \tag{5.40}$$

$$\begin{aligned}\dot{\boldsymbol{\eta}} &= \boldsymbol{J}(\boldsymbol{\eta})\boldsymbol{\nu_r} + \boldsymbol{V_c} \\ \boldsymbol{M}^p\dot{\boldsymbol{\nu}}_{\boldsymbol{r}} + \boldsymbol{C}^p(\boldsymbol{\nu_r})\boldsymbol{\nu_r} + \boldsymbol{D}^p(\boldsymbol{\nu_r})\boldsymbol{\nu_r} + \boldsymbol{g}^p(\boldsymbol{\eta}) &= \boldsymbol{B}^p\boldsymbol{f}\end{aligned} \tag{5.41}$$

Defining $\boldsymbol{H} \triangleq \boldsymbol{T}^{-1}$, the transformed model matrices are given below:

$$\begin{aligned}\boldsymbol{M}^p &= \boldsymbol{H}^T\boldsymbol{M}\boldsymbol{H} \\ \boldsymbol{D}^p(\boldsymbol{\nu_r}) &= \boldsymbol{H}^T\boldsymbol{D}_l\boldsymbol{H} + \boldsymbol{D}_n(\boldsymbol{\nu_r}) \\ \boldsymbol{g}^p(\boldsymbol{\eta}) &= \boldsymbol{H}^T\boldsymbol{g}(\boldsymbol{\eta}) = \boldsymbol{g}(\boldsymbol{\eta}) \\ \boldsymbol{B}^p &= \boldsymbol{H}^T\boldsymbol{B}\end{aligned}$$

$$\boldsymbol{C}(\boldsymbol{\nu}_r) = \begin{bmatrix} 0 & 0 & 0 & m^p_{33}w_r + m^p_{34}q & -m^p_{22}v_r - m^p_{25}r \\ 0 & 0 & 0 & 0 & m^p_{11}u_r \\ 0 & 0 & 0 & -m^p_{11}u_r & 0 \\ -m^p_{33}w_r - m^p_{34}q & 0 & m^p_{11}u_r & 0 & 0 \\ m^p_{22}v_r + m^p_{25}r & -m^p_{11}u_r & 0 & 0 & 0 \end{bmatrix} \tag{5.42}$$

Through this transformation it can be shown that

$$\boldsymbol{\tau} = \begin{bmatrix}\tau_u \\ 0 \\ 0 \\ \tau_q \\ \tau_r\end{bmatrix} = (\boldsymbol{M}^p)^{-1}\boldsymbol{B}^p\boldsymbol{f} = \begin{bmatrix} \frac{b_{11}}{m_{11}} & 0 & 0 \\ 0 & 0 & 0 \\ 0 & 0 & 0 \\ 0 & \frac{m_{33}b_{42} - m_{34}b_{32}}{m_{33}m_{44} - m_{34}m_{43}} & 0 \\ 0 & 0 & \frac{m_{22}b_{53} - m_{25}b_{23}}{m_{22}m_{55} - m_{25}m_{52}} \end{bmatrix} \begin{bmatrix} T \\ \delta_q \\ \delta_r \end{bmatrix}, \tag{5.43}$$

and the model can be written in component form as below.

$$\begin{aligned}\dot{x} &= \cos(\theta)\cos(\psi)u_r - \sin(\psi)v_r + \sin(\theta)\cos(\psi)w_r + V_x \\ \dot{y} &= \cos(\theta)\sin(\psi)u_r + \cos(\psi)v_r + \sin(\theta)\sin(\psi)w_r + V_y \\ \dot{z} &= -\sin(\theta)u_r + \cos(\theta)w_r + V_z \\ \dot{\theta} &= q \\ \dot{\psi} &= \frac{r}{\cos(\theta)} \\ \dot{u_r} &= F_{u_r}(u_r, v_r, w_r, r, q) + \tau_u \\ \dot{v_r} &= X_{v_r}(u_r)r + Y_{v_r}(u_r)v_r \\ \dot{w_r} &= X_{w_r}(u_r)q + Y_{w_r}(u_r)w_r + Z_{w_r}\sin(\theta) \\ \dot{q} &= F_q(\theta, u_r, w_r, q) + \tau_q \\ \dot{r} &= F_r(u_r, v_r, r) + \tau_r\end{aligned} \tag{5.44}$$

$$F_{u_r}(u_r, v_r, w_r, r, q) = \frac{(m^p_{22}v_r + m^p_{25}r)r - (m^p_{33}w_r + m^p_{34}q)q - d^p_{11}u_r - d^n_{11}|u_r|u_r}{m^p_{11}} \tag{5.45}$$

$$X_{v_r}(u_r) = \frac{{m^p_{25}}^2 - m^p_{11}m^p_{55}}{m^p_{22}m^p_{55} - {m^p_{25}}^2}u_r + \frac{d^p_{55}m^p_{25} - d^p_{25}m^p_{55}}{m^p_{22}m^p_{55} - {m^p_{25}}^2} \tag{5.46}$$

$$Y_{v_r}(u_r) = \frac{(m^p_{22} - m^p_{11})m^p_{25}}{m^p_{22}m^p_{55} - {m^p_{25}}^2}u_r - \frac{d^p_{22}m^p_{55} - d^p_{52}m^p_{25}}{m^p_{22}m^p_{55} - {m^p_{25}}^2} \tag{5.47}$$

$$X_{w_r}(u_r) = \frac{-{m^p_{34}}^2 + m^p_{11}m^p_{44}}{m^p_{33}m^p_{44} - {m^p_{34}}^2}u_r + \frac{d^p_{44}m^p_{34} - d^p_{34}m^p_{44}}{m^p_{33}m^p_{44} - {m^p_{34}}^2} \tag{5.48}$$

$$Y_{w_r}(u_r) = \frac{(m^p_{11} - m^p_{33})m^p_{34}}{m^p_{33}m^p_{44} - {m^p_{34}}^2}u_r - \frac{d^p_{33}m^p_{44} - d^p_{43}m^p_{34}}{m^p_{33}m^p_{44} - {m^p_{34}}^2} \tag{5.49}$$

$$Z_{w_r} = \frac{BG_zWm^p_{34}}{m^p_{33}m^p_{44} - {m^p_{34}}^2} \tag{5.50}$$

$$\begin{aligned} F_q(\theta, u_r, w_r, q) =& \frac{m^p_{34}d^p_{33} - m^p_{33}(d^p_{43} - (m^p_{33} - m^p_{11})u_r)}{m^p_{33}m^p_{44} - {m^p_{34}}^2}w_r \\ &+ \frac{m^p_{34}(d^p_{34} - m^p_{11}u_r) - m^p_{33}(d^p_{44} - m^p_{34}u_r)}{m^p_{33}m^p_{44} - {m^p_{34}}^2}q \\ &- \frac{BG_zWm^p_{33}\sin(\theta)}{m^p_{33}m^p_{44} - {m^p_{34}}^2} \end{aligned} \tag{5.51}$$

$$\begin{aligned} F_r(u_r, w_r, r) =& \frac{m^p_{25}d^p_{22} - m^p_{22}(d^p_{52} + (m^p_{22} - m^p_{11})u_r)}{m^p_{22}m^p_{55} - {m^p_{25}}^2}v_r \\ &+ \frac{m^p_{25}(d^p_{25} + m^p_{11}u_r) - m^p_{22}(d^p_{55} + m^p_{25}u_r)}{m^p_{22}m^p_{55} - {m^p_{25}}^2}r \end{aligned} \tag{5.52}$$

5.2.1 Feedback Linearization Controllers

This section presents feedback linearization controllers from [6] that ensure tracking of the references for u_r, θ and ψ. Equation (5.44) shows that Hugin has three inputs τ_u, τ_q and τ_r that affect the surge, pitch and yaw dynamics respectively. The surge controller is responsible for making the relative surge velocity u_r track the desired speed profile $u_{rd}(t)$, the pitch controller ensure tracking of the desired pitch and pitch rate θ_d and $\dot{\theta}_d$ and the yaw controller ensure tracking of the desired yaw and yaw rate ψ_d and $\dot{\psi}_d$. By defining the error in relative surge velocity as $\tilde{u}_r \triangleq u_r - u_{rd}$, pitch $\tilde{\theta} \triangleq \theta - \theta_d$, pitch rate $\dot{\tilde{\theta}} \triangleq q - \dot{\theta}_d$, yaw $\tilde{\psi} \triangleq \psi - \psi_d$ and yaw rate as $\dot{\tilde{\psi}} \triangleq \frac{r}{\cos(\theta)} - \dot{\psi}_d$ and imposing the following controllers (k_{u_r}, k_θ, k_q, k_ψ and $k_r > 0$),

$$\tau_u = -F_{u_r}(u_r, v_r, w_r, r, q) + \dot{u}_{rd} - k_{u_r}\tilde{u}_r \tag{5.53}$$

$$\tau_q = -F_q(\theta, u_r, w_r, q) + \ddot{\theta}_d - k_\theta\tilde{\theta} - k_q\dot{\tilde{\theta}} \tag{5.54}$$

$$\tau_r = -F_r(u_r, w_r, r) - q\sin(\theta)\dot{\psi} + \cos(\theta)(\ddot{\psi}_d - k_\psi\tilde{\psi} - k_r\dot{\tilde{\psi}}) \tag{5.55}$$

it can easily be shown that the errors converge to zero exponentially.

$$\begin{aligned}\dot{\boldsymbol{\xi}} &= \begin{bmatrix}\dot{\tilde{u}}_r \\ \dot{\tilde{\theta}} \\ \ddot{\tilde{\theta}} \\ \dot{\tilde{\psi}} \\ \ddot{\tilde{\psi}}\end{bmatrix} \\ &= \begin{bmatrix}-k_{u_r} & 0 & 0 & 0 & 0 \\ 0 & 0 & 1 & 0 & 0 \\ 0 & -k_\theta & -k_q & 0 & 0 \\ 0 & 0 & 0 & 0 & 1 \\ 0 & 0 & 0 & -k_\psi & -k_r\end{bmatrix}\begin{bmatrix}\tilde{u}_r \\ \tilde{\theta} \\ \dot{\tilde{\theta}} \\ \tilde{\psi} \\ \dot{\tilde{\psi}}\end{bmatrix} \\ &= \boldsymbol{\Lambda}\boldsymbol{\xi}\end{aligned} \tag{5.56}$$

The closed loop system above is linear and time-invariant. All controller gains are strictly positive, meaning that $\boldsymbol{\Lambda}$ is Hurwitz and the origin $\boldsymbol{\xi} = 0$ is UGES (theoren 4.5 in appendix A.3.2).

5.2.2 Integrator Backstepping Controller

This section presents an integrator backstepping controller developed in [6]. The goal is to track the desired relative orientation provided by the guidance laws for path following of underwater vehicles presented in chapter 3.7. As explained in said chapter, the guidance laws provides a reference for θ_{fc} and ψ_{fc} denoted $\theta_{fc,d}$ and $\psi_{fc,d}$. $\boldsymbol{\Theta}_{fc} = [\phi_{fc}, \theta_{fc}, \psi_{fc}]^T$ is calculated based on the known rotation matrix $\boldsymbol{R}_c^f(\boldsymbol{\Theta}_{fc})$. To track the desired orientation, Børhaug defines the error

$$\boldsymbol{z}_1 \triangleq \begin{bmatrix}\tilde{\theta}_{fc} \\ \tilde{\psi}_{fc}\end{bmatrix} \triangleq \begin{bmatrix}\theta_{fc} \\ \psi_{fc}\end{bmatrix} - \begin{bmatrix}\theta_{fc,d} \\ \psi_{fc,d}\end{bmatrix}. \tag{5.57}$$

It is known that $\dot{\boldsymbol{\Theta}}_{fc} = \boldsymbol{T}_\Theta(\boldsymbol{\Theta}_{fc})\boldsymbol{\omega}_{c/f}^c$ (see chapter 2), where

$$\boldsymbol{T}_\Theta(\boldsymbol{\Theta}_{fc}) = \begin{bmatrix}1 & \sin(\phi_{fc})\tan(\theta_{fc}) & \cos(\phi_{fc})\tan(\theta_{fc}) \\ 0 & \cos(\phi_{fc}) & -\sin(\phi_{fc}) \\ 0 & \frac{\sin(\phi_{fc})}{\cos(\theta_{fc})} & \frac{\cos(\phi_{fc})}{\cos(\theta_{fc})}\end{bmatrix}. \tag{5.58}$$

The error dynamics is then given as

$$\begin{aligned}\dot{\boldsymbol{z}}_1 &= \begin{bmatrix}\dot{\theta}_{fc} \\ \dot{\psi}_{fc}\end{bmatrix} - \begin{bmatrix}\dot{\theta}_{fc,d} \\ \dot{\psi}_{fc,d}\end{bmatrix} \\ &= \begin{bmatrix}\cos(\phi_{fc}) & -\sin(\phi_{fc}) \\ \frac{\sin(\phi_{fc})}{\cos(\theta_{fc})} & \frac{\cos(\phi_{fc})}{\cos(\theta_{fc})}\end{bmatrix}\underbrace{\begin{bmatrix}0 & 1 & 0 \\ 0 & 0 & 1\end{bmatrix}}_{\boldsymbol{H}}\boldsymbol{\omega}_{c/f}^c - \begin{bmatrix}\dot{\theta}_{fc,d} \\ \dot{\psi}_{fc,d}\end{bmatrix}\end{aligned} \tag{5.59}$$

$\boldsymbol{\omega}^c_{c/f}$ can be decomposed as below.

$$\boldsymbol{\omega}^c_{c/f} = \boldsymbol{\omega}^c_{c/i} - \boldsymbol{\omega}^c_{f/i} = \boldsymbol{\omega}^c_{b/i} + \boldsymbol{\omega}^c_{c/b} - \boldsymbol{\omega}^c_{f/i} = \boldsymbol{R}^c_b(\boldsymbol{\Theta}_{cb})\boldsymbol{\omega}^b_{b/i} + \boldsymbol{\omega}^c_{c/b} - \boldsymbol{R}^c_f(\boldsymbol{\Theta}_{fc})\boldsymbol{\omega}^f_{f/i} \tag{5.60}$$

$\boldsymbol{\Theta}_{cb} = [0, \alpha_c, -\beta_c]^T$ (α_c and β_c defined in equation (3.40)), $\boldsymbol{\omega}^b_{b/i} = [0, q, r]^T$, $\boldsymbol{\omega}^c_{c/b} = -\boldsymbol{\omega}^c_{b/c} = \boldsymbol{T}^{-1}_{\Theta}(\boldsymbol{\Theta}_{cb})\dot{\boldsymbol{\Theta}}_{cb} = [-\dot{\beta}_c \sin(\alpha_c), -\dot{\alpha}_c, \dot{\beta}_c \cos(\alpha_c)]^T$ and $\boldsymbol{\omega}^f_{f/i}$ is defined in equation (3.30). This can be substituted into the error dynamics.

$$\dot{\boldsymbol{z}}_1 = \boldsymbol{A}(\phi_{fc}, \theta_{fc}, \alpha_c, \beta_c) \begin{bmatrix} q \\ r \end{bmatrix} + \boldsymbol{\Phi}(t, \boldsymbol{\omega^c_{c/b}}, \boldsymbol{\Theta}_{fc}, \boldsymbol{\omega}^f_{f/i}) \tag{5.61}$$

$$\boldsymbol{A} \triangleq \begin{bmatrix} \cos(\phi_{fc}) & -\sin(\phi_{fc}) \\ \frac{\sin(\phi_{fc})}{\cos(\theta_{fc})} & \frac{\cos(\phi_{fc})}{\cos(\theta_{fc})} \end{bmatrix} \begin{bmatrix} \cos(\beta_c) & -\sin(\beta_c)\sin(\alpha_c) \\ 0 & \cos(\alpha_c), \end{bmatrix} \tag{5.62}$$

$$\boldsymbol{\Phi} = -\begin{bmatrix} \dot{\theta}_{fc,d} \\ \dot{\psi}_{fc,d} \end{bmatrix} + \begin{bmatrix} \cos(\phi_{fc}) & -\sin(\phi_{fc}) \\ \frac{\sin(\phi_{fc})}{\cos(\theta_{fc})} & \frac{\cos(\phi_{fc})}{\cos(\theta_{fc})} \end{bmatrix} \boldsymbol{H}(\boldsymbol{\omega}^c_{c/b} - \boldsymbol{R}^c_f(\boldsymbol{\Theta}_{fc})\boldsymbol{\omega}^f_{f/i}) \tag{5.63}$$

By introducing a new error variable,

$$\boldsymbol{z}_2 \triangleq \begin{bmatrix} \tilde{q} \\ \tilde{r} \end{bmatrix} \triangleq \begin{bmatrix} q \\ r \end{bmatrix} - \begin{bmatrix} q_d \\ r_d \end{bmatrix}, \tag{5.64}$$

and defining

$$\begin{bmatrix} q_d \\ r_d \end{bmatrix} \triangleq -\boldsymbol{A}^{-1}(\boldsymbol{\Phi} + \boldsymbol{K}_1\boldsymbol{z}_1), \tag{5.65}$$

it is easy to see that $\boldsymbol{\Phi} = -\boldsymbol{A}\begin{bmatrix} q_d \\ r_d \end{bmatrix} - \boldsymbol{K}_1\boldsymbol{z}_1$, and

$$\dot{\boldsymbol{z}}_1 = \boldsymbol{A}\boldsymbol{z}_2 - \boldsymbol{K}_1\boldsymbol{z}_1. \tag{5.66}$$

$\boldsymbol{K}_1$ is a symmetric positive definite controller gain matrix. Furthermore, by looking at the error dynamics of $\boldsymbol{z}_2$ and inserting from equation (5.44),

$$\begin{aligned} \dot{\boldsymbol{z}}_2 &= \begin{bmatrix} \dot{q} \\ \dot{r} \end{bmatrix} - \begin{bmatrix} \dot{q_d} \\ \dot{r_d} \end{bmatrix} \\ &= \begin{bmatrix} F_q(\theta, u_r, w_r, q) + \tau_q \\ F_r(u_r, v_r, r) + \tau_r \end{bmatrix} - \begin{bmatrix} \dot{q_d} \\ \dot{r_d} \end{bmatrix}, \end{aligned} \tag{5.67}$$

the control laws can be chosen as below.

$$\begin{bmatrix} \tau_q \\ \tau_r \end{bmatrix} = \begin{bmatrix} \dot{q_d} \\ \dot{r_d} \end{bmatrix} - \begin{bmatrix} F_q(\theta, u_r, w_r, q) \\ F_r(u_r, v_r, r) \end{bmatrix} - \boldsymbol{A}^T\boldsymbol{z}_1 - \boldsymbol{K}_2\boldsymbol{z}_2 \tag{5.68}$$

$\boldsymbol{K}_2$ is also a symmetric positive definite controller gain matrix. The closed loop dynamics of the defined errors are then

$$\begin{bmatrix} \dot{z}_1 \\ \dot{z}_2 \end{bmatrix} = \begin{bmatrix} -\boldsymbol{K}_1 & \boldsymbol{A} \\ -\boldsymbol{A}^T & -\boldsymbol{K}_2 \end{bmatrix} \begin{bmatrix} \boldsymbol{z}_1 \\ \boldsymbol{z}_2 \end{bmatrix}. \tag{5.69}$$

The origin $(\boldsymbol{z}_1, \boldsymbol{z}_2) = (\mathbf{0}, \mathbf{0})$ is an exponentially stable equilibrium of the closed loop system. This is shown using the positive definite, decrescent and radially unbounded Lyapunov function $V = 0.5||\boldsymbol{z}_1^2|| + 0.5||\boldsymbol{z}_2^2||$.

$$\dot{V} = -\boldsymbol{z}_1^T \boldsymbol{K}_1 \boldsymbol{z}_1 - \boldsymbol{z}_2^T \boldsymbol{K}_2 \boldsymbol{z}_2 \leq -\lambda ||\boldsymbol{z}||^2 \tag{5.70}$$

$\dot{V}$ is bounded upper bounded by a negative definite quadratic function ($\lambda > 0$ is less than the minimum eigenvalue of $\boldsymbol{K}_1$ and $\boldsymbol{K}_2$), and as such the closed loop system is UES according to the theorem 4.10 in appendix A.3.3. Due to the fact that the matrix $\boldsymbol{A}$ is not defined for $\cos(\theta_{fc}) = 0$, the system is *not* globally stable.

Chapter 6

Path Following in the Presence of Unknown Ocean Currents

This chapter presents two theorems that guarantee path following in the presence of unknown ocean currents. The desired path is assumed continuously differentiable and parametrized as a function of the traveled distance along the path s, and the ocean current is assumed constant and irrotational.

The theorems are based on a combination of the ocean current observer presented in 3.4 and the path following theorems of Børhaug described in chapter 3.7.

6.1 Path Following of Space Curves in the Presence of Unknown Ocean Currents, Underactuated Surface Ship

6.1.1 Theorem 1

As discussed in chapter 3.7, the control objective is to follow the desired path with a commanded relative surge velocity. The Serret-Frenet reference frame $\{f\}$ propagates along the desired path. In the presented theorem, estimates of the ocean current in the inertial frame as described in chapter 3.4 are used, and the

following notation is introduced.

$$\begin{aligned}
\boldsymbol{V}_c^f &= [\boldsymbol{R}_f^i(\psi_f)]^T \boldsymbol{V}_c \\
\hat{\boldsymbol{V}_c^f} &= [\boldsymbol{R}_f^i(\psi_f)]^T \hat{\boldsymbol{V}}_c \\
&\Downarrow \\
V_x^f &\triangleq \cos(\psi_f) V_x + \sin(\psi_f) V_y \\
V_y^f &\triangleq -\sin(\psi_f) V_x + \cos(\psi_f) V_y \\
\hat{V_x^f} &\triangleq \cos(\psi_f) \hat{V}_x + \sin(\psi_f) \hat{V}_y \\
\hat{V_y^f} &\triangleq -\sin(\psi_f) \hat{V}_x + \cos(\psi_f) \hat{V}_y
\end{aligned} \tag{6.1}$$

Theorem 1: Consider a 3-DOF underactuated surface vessel described by equation (6.2)
$\Big(F_u(u_r, v_r, r)$, $X(u_r)$, $Y(u_r)$ and $F_r(u_r, v_r, r)$ defined in chapter 5.1$\Big)$ in closed loop with the feedback linearization controllers in equation (6.3 with the goal of following a general path with a constant relative surge velocity U_{rd} when affected by unknown constant, irrotational ocean current V_x and V_y.

$$\begin{aligned}
\dot{x} &= \cos(\psi) u_r - \sin(\psi) v_r + V_x \\
\dot{y} &= \sin(\psi) u_r + \cos(\psi) v_y + V_y \\
\dot{\psi} &= r \\
\dot{u_r} &= F_u(u_r, v_r, r) - \frac{d_{11}^p}{m_{11}^p} u_r + \tau_u \\
\dot{v_r} &= X(u_r) r + Y(u_r) v_r \\
\dot{r} &= F_r(u_r, v_r, r) + \tau_r
\end{aligned} \tag{6.2}$$

$$\begin{aligned}
\tau_u &= -F_u(u_r, v_r, r) + \frac{d_{11}^p}{m_{11}^p} U_{rd} - k_{u_r}(u_r - U_{rd}), && k_{u_r} > 0 \\
\tau_r &= -F_r(u_r, v_r, r) + \ddot{\psi}_d - k_\psi(\psi - \psi_d) - k_r(r - \dot{\psi}_d), && k_\psi, k_r > 0
\end{aligned} \tag{6.3}$$

The controllers are discussed in detail in chapter 5.1.1. By introducing a Serret-Frenet coordinate frame anchored in and propagating along the desired path with velocity $\dot{s}$, the control objectives are described by equation (6.4).

$$\begin{aligned}
\lim_{t\to\infty} x_{b/f}(t) &= 0 \\
\lim_{t\to\infty} y_{b/f}(t) &= 0 \\
\lim_{t\to\infty} u_r(t) &= U_{rd}
\end{aligned} \tag{6.4}$$

Through the use of the following current estimates, update law and guidance law, the control objectives are achieved with uniform, global, asymptotic stabil-

ity (UGAS) if assumptions **A1**-**A4** are satisfied.

$$\begin{aligned}
\dot{\tilde{x}} &= \cos(\psi)u_r - \sin(\psi)v_r + \hat{V}_x + k_{x1}\tilde{x}, \quad k_{x1} > 0 \\
\dot{\tilde{y}} &= \sin(\psi)u_r + \cos(\psi)v_r + \hat{V}_y + k_{y1}\tilde{y}, \quad k_{y1} > 0 \\
\dot{\hat{V}}_x &= k_{x2}\tilde{x}, \quad k_{x2} > 0 \\
\dot{\hat{V}}_y &= k_{y2}\tilde{y}, \quad k_{y2} > 0
\end{aligned} \tag{6.5}$$

$$\dot{s} = \underbrace{\sqrt{U_{rd}^2 + v_r^2}}_{\triangleq U_c} \frac{\sqrt{\Delta^2 + x_{b/f}^2} + x_{b/f}}{\sqrt{\Delta^2 + x_{b/f}^2 + (y_{f/b} + f)^2}} + \hat{V_x^f} \tag{6.6}$$

$$\psi_d = \psi_f - \arctan\left(\frac{v_r}{U_{rd}}\right) - \arctan\left(\frac{y_{b/f} + f}{\sqrt{\Delta^2 + \left(x_{b/f}\right)^2}}\right), \tag{6.7}$$

where f is the solution to the second order equation

$$\left(\hat{V_y^f}^2 - U_c^2\right) f^2 + 2\hat{V_y^f}^2 y_{b/f} f + \hat{V_y^f}^2 \left(\Delta^2 + x_{b/f}^2 + y_{b/f}^2\right) = 0. \tag{6.8}$$

Assumptions:

$X^{max} \triangleq |X(U_{rd})|$, $Y^{min} \triangleq |Y(U_{rd})|$

A1 - The functions $X(u_r)$ and $Y(u_r)$ satisfy
$Y(U_{rd}) \leq -Y^{min} < 0$,
$-U_{rd} + a \leq X(U_{rd}) \leq X^{max}$, where a is a positive constant.

A2 - The curvature of the desired path is bounded such that
$\kappa_{max} \triangleq \underset{s \in \Re}{max} |\kappa(s)| < \frac{1}{3}\left(\frac{Y^{min}}{X^{max}}\right)$.

A3 - The parameter Δ of the guidance law (6.7) satisfies $\Delta > \frac{\frac{3}{2}X^{max}}{Y^{min} - 3X^{max}\kappa_{max}}$.

A4 - The ocean current is assumed bounded and less than the desired relative surge velocity, $0 \leq |\boldsymbol{V_c}| \leq V_{max} < U_{rd}$. This saturation is also used on the estimated of the current, $|\hat{\boldsymbol{V}}_c| \leq V_{max} < U_{rd}$.

Remark 1 - $Y(U_{rd}) < 0$ is a natural assumption since $Y(U_{rd}) = 0$ would imply that the supply ship is undamped in sway and $Y(U_{rd}) > 0$ would imply that some small perturbation in sway would result in an accelerating sway velocity for $u_r = U_{rd}$ [6]. In reality it would indicate that a push in the sway-direction would result in a constantly increasing sway velocity, a response that is physically impossible. $-U_{rd} + a \leq X(U_{rd}) \leq X^{max}$ is not a very strict demand since U_{rd} is a design parameter that can be chosen to fulfill this inequality.

Remark 2 - Assumptions **A1-A3** is used to prove boundedness for v_r, see chapter 6.1.3.

Remark 3 - Assumption **A4** ensures that the solution of f is real and finite, see chapter 6.1.4.

6.1.2 Body Serret-Frenet Kinematics including Current

The differential kinematic relationship between the body and Serret-Frenet frame is derived in [6] and is shown in equation (6.9). Here, $\psi_{fb} = \psi - \psi_f$, where ψ is the orientation of the body frame and ψ_f is the orientation of the Serret-Frenet frame relative to the NED coordinate system.

$$\begin{bmatrix} \dot{x}_{b/f} \\ \dot{y}_{b/f} \end{bmatrix} = \begin{bmatrix} \cos(\psi_{fb}) & -\sin(\psi_{fb}) \\ \sin(\psi_{fb}) & \cos(\psi_{fb}) \end{bmatrix} \begin{bmatrix} u \\ v \end{bmatrix} - \begin{bmatrix} \dot{s} \\ 0 \end{bmatrix} - \dot{s} \begin{bmatrix} 0 & -\kappa \\ \kappa & 0 \end{bmatrix} \begin{bmatrix} x_{b/f} \\ y_{b/f} \end{bmatrix} \tag{6.9}$$

The ocean current is given in inertial reference frame as

$$\boldsymbol{V}_c = \begin{bmatrix} V_x \\ V_y \end{bmatrix} \tag{6.10}$$

and in the body reference frame as

$$\begin{aligned} \boldsymbol{V}_c^b &= \boldsymbol{R}_b^i(\psi)^T \boldsymbol{V}_c \\ &= \begin{bmatrix} \cos(\psi) & \sin(\psi) \\ -\sin(\psi) & \cos(\psi) \end{bmatrix} \begin{bmatrix} V_x \\ V_y \end{bmatrix} \\ &= \begin{bmatrix} u_c \\ v_c \end{bmatrix}. \end{aligned} \tag{6.11}$$

The relative linear velocity is defined as

$$\begin{bmatrix} u_r \\ v_r \end{bmatrix} = \begin{bmatrix} u \\ v \end{bmatrix} - \begin{bmatrix} u_c \\ v_c \end{bmatrix}. \tag{6.12}$$

This can be used to rewrite equation (6.9).

$$\begin{aligned} \begin{bmatrix} \dot{x}_{b/f} \\ \dot{y}_{b/f} \end{bmatrix} &= \boldsymbol{R}_b^f(\psi_{fb}) \begin{bmatrix} u \\ v \end{bmatrix} - \begin{bmatrix} \dot{s} \\ 0 \end{bmatrix} - \dot{s} \begin{bmatrix} 0 & -\kappa \\ \kappa & 0 \end{bmatrix} \begin{bmatrix} x_{b/f} \\ y_{b/f} \end{bmatrix} \\ &= \boldsymbol{R}_b^f(\psi_{fb}) \left(\begin{bmatrix} u_r \\ v_r \end{bmatrix} + \boldsymbol{V}_c^b \right) - \begin{bmatrix} \dot{s} \\ 0 \end{bmatrix} - \dot{s} \begin{bmatrix} 0 & -\kappa \\ \kappa & 0 \end{bmatrix} \begin{bmatrix} x_{b/f} \\ y_{b/f} \end{bmatrix} \\ &= \boldsymbol{R}_b^f(\psi_{fb}) \left(\begin{bmatrix} u_r \\ v_r \end{bmatrix} + \boldsymbol{R}_b^i(\psi)^T \boldsymbol{V}_c \right) - \begin{bmatrix} \dot{s} \\ 0 \end{bmatrix} - \dot{s} \begin{bmatrix} 0 & -\kappa \\ \kappa & 0 \end{bmatrix} \begin{bmatrix} x_{b/f} \\ y_{b/f} \end{bmatrix} \\ &= \boldsymbol{R}_b^f(\psi_{fb}) \begin{bmatrix} u_r \\ v_r \end{bmatrix} - \begin{bmatrix} \dot{s} \\ 0 \end{bmatrix} - \dot{s} \begin{bmatrix} 0 & -\kappa \\ \kappa & 0 \end{bmatrix} \begin{bmatrix} x_{b/f} \\ y_{b/f} \end{bmatrix} + \boldsymbol{R}_f^i(\psi_f)^T \boldsymbol{V}_c \end{aligned} \tag{6.13}$$

6.1.3 Stability Proof

This proof concludes that the control objectives are achieved with uniform global asymptotic stability under the conditions of Theorem 1. Equation (6.13) is rewritten and shown to be a cascaded system that includes the error dynamics of the controlled states and current estimates. Stability is then proven using Lyapunov analysis of cascaded systems. Through the current observer, controllers, update and guidance law in Theorem 1, equation (6.13) can be rewritten to equation (6.14). The proof is described in detail in Appendix B.1.

$$\begin{bmatrix}\dot{x}_{b/f}\\ \dot{y}_{b/f}\end{bmatrix} = \begin{bmatrix}-U_c\frac{x_{b/f}}{\sqrt{\Delta^2+x_{b/f}^2+(y_{b/f}+f)^2}}\\ -U_c\frac{y_{b/f}}{\sqrt{\Delta^2+x_{b/f}^2+(y_{b/f}+f)^2}}\end{bmatrix} - \dot{s}\begin{bmatrix}0 & -\kappa\\ \kappa & 0\end{bmatrix}\begin{bmatrix}x_{b/f}\\ y_{b/f}\end{bmatrix} + \boldsymbol{H}(t,U_c,\boldsymbol{\xi})\boldsymbol{\xi} \quad (6.14)$$

$$\boldsymbol{H}(t,U_c,\boldsymbol{\xi})\boldsymbol{\xi} = \begin{bmatrix}\cos(\psi_{fb}) & h_1(t,U_c,\boldsymbol{\xi}) & 0 & \cos(\psi_f) & \sin(\psi_f) & 0 & 0\\ \sin(\psi_{fb}) & h_2(t,U_c,\boldsymbol{\xi}) & 0 & -\sin(\psi_f) & \cos(\psi_f) & 0 & 0\end{bmatrix}\begin{bmatrix}\tilde{u_r}\\ \tilde{\psi}\\ \tilde{r}\\ \tilde{V}_x\\ \tilde{V}_y\\ \tilde{x}\\ \tilde{y}\end{bmatrix} \quad (6.15)$$

$$h_1(t,U_c,\boldsymbol{\xi}) = \frac{\cos(\tilde{\psi})-1}{\tilde{\psi}}U_c\frac{\sqrt{\Delta^2+x_{b/f}^2}}{\sqrt{\Delta^2+x_{b/f}^2+(y_{b/f}+f)^2}} + \frac{\sin(\tilde{\psi})}{\tilde{\psi}}U_c\frac{y_{b/f}+f}{\sqrt{\Delta^2+x_{b/f}^2+(y_{b/f}+f)^2}}$$
$$h_2(t,U_c,\boldsymbol{\xi}) = \frac{\sin(\tilde{\psi})}{\tilde{\psi}}U_c\frac{\sqrt{\Delta^2+x_{b/f}^2}}{\sqrt{\Delta^2+x_{b/f}^2+(y_{b/f}+f)^2}} - \frac{\cos(\tilde{\psi})-1}{\tilde{\psi}}U_c\frac{y_{b/f}+f}{\sqrt{\Delta^2+x_{b/f}^2+(y_{b/f}+f)^2}} \quad (6.16)$$

The system in equation (6.14) and the dynamics of $\boldsymbol{\xi}$ (6.19) can be seen as a cascaded system where the error dynamics perturbs the nominal system in equation (6.17) through the term $\boldsymbol{H}(t,U_c,\boldsymbol{\xi})\boldsymbol{\xi}$ (appendix A.3.4).

$$\begin{bmatrix}\dot{x}_{b/f}\\ \dot{y}_{b/f}\end{bmatrix} = \begin{bmatrix}-U_c\frac{x_{b/f}}{\sqrt{\Delta^2+x_{b/f}^2+(y_{b/f}+f)^2}}\\ -U_c\frac{y_{b/f}}{\sqrt{\Delta^2+x_{b/f}^2+(y_{b/f}+f)^2}}\end{bmatrix} - \dot{s}\begin{bmatrix}0 & -\kappa\\ \kappa & 0\end{bmatrix}\begin{bmatrix}x_{b/f}\\ y_{b/f}\end{bmatrix} \quad (6.17)$$

Stability of the nominal system can be shown using the quadratic positive definite, decrescent and radially unbounded Lyapunov function $V = \frac{1}{2}(x_{b/f}^2 + y_{b/f}^2)$.

$$\begin{aligned}
\dot{V} &= \dot{x}_{b/f} x_{b/f} + \dot{y}_{b/f} y_{b/f} \\
&= -U_c \frac{x_{b/f}^2 + y_{b/f}^2}{\sqrt{\Delta^2 + x_{b/f}^2 + (y_{b/f} + f)^2}} + \dot{s}\kappa x_{b/f} y_{b/f} - \dot{s}\kappa x_{b/f} y_{b/f} \\
&\leq -U_{rd} \frac{x_{b/f}^2 + y_{b/f}^2}{\sqrt{\Delta^2 + x_{b/f}^2 + (y_{b/f} + f)^2}} \\
&\triangleq W(x_{b/f}, y_{b/f}) < 0
\end{aligned} \tag{6.18}$$

$\dot{V}$ is negative definite and as such the nominal system is UGAS (theorem 4.8 and 4.9 in appendix A.3.3). However, it is not possible to prove ULES stability cf. Børhaug [6] due to the time-varying term f. In particular, in any ball $\mathcal{B}_r = \left\{(x_{b/f}, y_{b/f}) \in \mathbb{R}^2 : \; x_{b/f}^2 + (y_{b/f} + f)^2 \leq r^2 \right\}$, $W \leq -\lambda x_{b/f}^2 - \lambda y_{b/f}^2$ for all $0 < \lambda \leq U_{rd}/\sqrt{\Delta^2 + r^2}$. However, due to the time-varying term f, $\mathcal{B}_r$ does not contain the origin $x_{b/f} = 0$, $y_{b/f} = 0$ for all $r > 0$, only for $r > |f|$. As such, exponential stability can not be guaranteed according to theorem 4.10 in appendix A.3.3.

The error dynamics is shown in equation (6.19) and is based on the feedback linearization controllers in chapter 5.1.1 and the current and position observers in chapter 3.4.

$$\begin{aligned}
\dot{\boldsymbol{\xi}} = \begin{bmatrix} \dot{\tilde{u}_r} \\ \dot{\tilde{\psi}} \\ \dot{\tilde{r}} \\ \dot{\tilde{V}}_x \\ \dot{\tilde{V}}_y \\ \dot{\tilde{x}} \\ \dot{\tilde{y}} \end{bmatrix} &= \begin{bmatrix} -(k_{u_r} + \frac{d_{11}^p}{m_{11}}) & 0 & 0 & 0 & 0 & 0 & 0 \\ 0 & 0 & 1 & 0 & 0 & 0 & 0 \\ 0 & -k_\psi & -k_r & 0 & 0 & 0 & 0 \\ 0 & 0 & 0 & 0 & 0 & -k_{x2} & 0 \\ 0 & 0 & 0 & 0 & 0 & 0 & -k_{y2} \\ 0 & 0 & 0 & 1 & 0 & -k_{x1} & 0 \\ 0 & 0 & 0 & 0 & 1 & 0 & -k_{y1} \end{bmatrix} \begin{bmatrix} \tilde{u_r} \\ \tilde{\psi} \\ \tilde{r} \\ \tilde{V}_x \\ \tilde{V}_y \\ \tilde{x} \\ \tilde{y} \end{bmatrix} \\
&= \boldsymbol{\Lambda} \boldsymbol{\xi}
\end{aligned} \tag{6.19}$$

System (6.19) is a linear system, and $\boldsymbol{\Lambda}$ is Hurwitz. Hence, the error dynamics is UGES according to the theorem 4.5 in appendix A.3.2.

Based on this, the entire system cascaded system (6.14) and (6.19) can be proven UGAS according to theorem 2 in appendix A.3.4 if $\boldsymbol{H}(t, U_c, \boldsymbol{\xi})$ is globally bounded. Equation (6.15) shows that $\boldsymbol{H}(t, U_c, \boldsymbol{\xi})$ is bounded for bounded values of $h_1(t, U_c, \boldsymbol{\xi})$ and $h_2(t, U_c, \boldsymbol{\xi})$. These are again bounded if U_c is bounded: It is trivial to see that

$\left|\frac{\sqrt{\Delta^2+x_{b/f}^2}}{\sqrt{\Delta^2+x_{b/f}^2+(y_{b/f}+f)^2}}\right| \leq 1$ and $\left|\frac{y_{b/f}+f}{\sqrt{\Delta^2+x_{b/f}^2+(y_{b/f}+f)^2}}\right| < 1$. Furthermore, $\frac{\sin(\tilde{\psi})}{\tilde{\psi}}$ and $\frac{\cos(\tilde{\psi})-1}{\tilde{\psi}}$ have defined limits as $\tilde{\psi}$ approaches zero and are otherwise defined and bounded for all values of ψ (see figure 6.1).

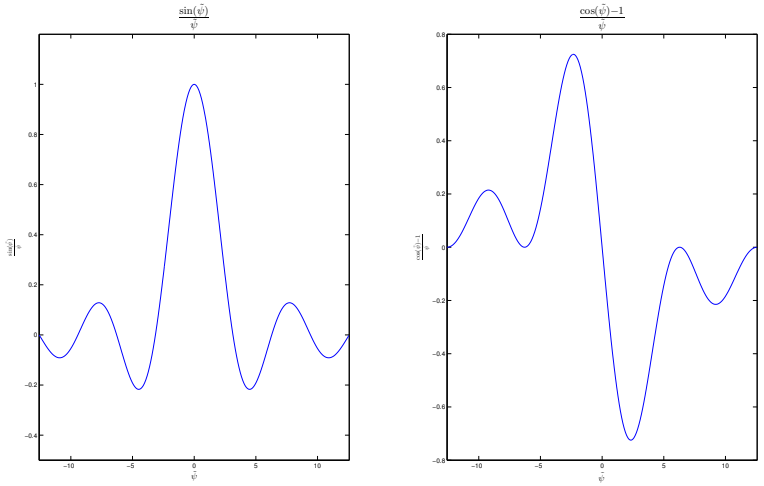

Figure 6.1: Illustration of $\frac{\sin(\tilde{\psi})}{\tilde{\psi}}$ and $\frac{\cos(\tilde{\psi})-1}{\tilde{\psi}}$ as $\tilde{\psi}$ approaches zero.

The total relative speed $U_c = \sqrt{U_{rd}^2 + v_r^2}$ is clearly bounded for bounded v_r. The proof in chapter 9.A in [6] can be applied to show that v_r is in fact bounded. Originally, this proof affirm the boundedness of the sway velocity v given that certain conditions are satisfied, but it can also be applied to relative sway velocity v_r. The proof assumes $u_r(t) \in [U_{min}, U_{max}]$, $\forall t \geq t_0$. In Theorem 1, $u_{rd}(t,s) = U_{rd} = constant$. The feedback linearization controller drives $\tilde{u}_r \to 0$ exponentially, so $u_r(t) = U_{rd}$, $\forall\ t \geq t_0 \geq 0$ for some t_0. Hence, $U_{min} = U_{max} = U_{rd}$, and if assumptions **A1-A3** are satisfied, it can be concluded that v_r is uniformly bounded $\forall t \geq t_0$.

Consequently, all conditions of theorem 2 in appendix A.3.4 are satisfied. In particular, the nominal system is UGAS with a quadratic Lyapunov-function. The error dynamics is UGES, and the interconnection matrix $\boldsymbol{H}$ is globally bounded. Consequently, the cascaded system in equation (6.14) and (6.19) is UGAS, and $x_{b/f}$, $y_{b/f}$ and $\tilde{u}_r$ converge to zero with uniform global asymptotic stability. Thus the control objectives are satisfied.

Proving exponential stability for the cascaded system remains a topic for future work.

6.1.4 Solving for f

As stated in Theorem 1, f is the solution to the second order equation

$$\underbrace{\left(\hat{V_y^f}^2 - U_c^2\right)}_{a} f^2 + 2\underbrace{\hat{V_y^f}^2 y_{b/f}}_{b} f + \underbrace{\hat{V_y^f}^2\left(\Delta^2 + x_{b/f}^2 + y_{b/f}^2\right)}_{c} = 0. \tag{6.20}$$

This equation is chosen as a direct result of the stability proof. As can be seen from equation (B.8) in appendix B.1, the dynamics of $y_{b/f}$ includes a term

$$U_c \frac{f}{\sqrt{\Delta^2 + x_{b/f}^2 + (y_{b/f} + f)^2}}. \tag{6.21}$$

To prove stability, it is desirable that this term is equal to $\hat{V}_y^f = -\sin(\psi_f)\hat{V}_x + \cos(\psi_f)\hat{V}_y$, which rewritten results in equation (6.20). This equation has two solutions:

$$\begin{aligned} f_1 &= \frac{-b - \sqrt{b^2 - ac}}{a} \\ f_2 &= \frac{-b + \sqrt{b^2 - ac}}{a} \end{aligned} \tag{6.22}$$

Based on assumption **A4**, the current and the estimates of the current are limited and less than U_{rd}. As such, it can easily be seen that $a < 0$:

$$\hat{V_y^f}^2 - U_c^2 \leq |\hat{\boldsymbol{V}}_c^f|^2 - U_c^2 = |\hat{\boldsymbol{V}}_c|^2 - U_c^2 < U_{rd}^2 - U_c^2 = U_{rd}^2 - (U_{rd}^2 + v_r^2) = -v_r^2 \leq 0 \tag{6.23}$$

Furthermore, $c \geq 0$. As such, the expression $b^2 - ac \geq 0$ and f_1 and f_2 are always real. Furthermore, division by a is safe since a will never be equal to zero.

As time progresses, $y_{b/f}$ and consequently b approach zero and the expressions for f_1 and f_2 can be simplified to

$$\begin{aligned} f_1 &= \frac{-\sqrt{-ac}}{a} \\ f_2 &= \frac{\sqrt{-ac}}{a} \end{aligned} \tag{6.24}$$

Hence, f_1 will always be positive (≥ 0), f_2 will always be negative (≤ 0), and the two solutions will be equal with opposite signs. This is illustrated in figure 6.2. As such, it is not arbitrary which solution for f one should chose, and it may be necessary to alternate between the two. This depends on the path and ocean current estimates. As mentioned, f is chosen to satisfy the following equation:

$$U_c \frac{f}{\sqrt{\Delta^2 + x_{b/f}^2 + (y_{b/f} + f)^2}} = \hat{V_y^f} \tag{6.25}$$

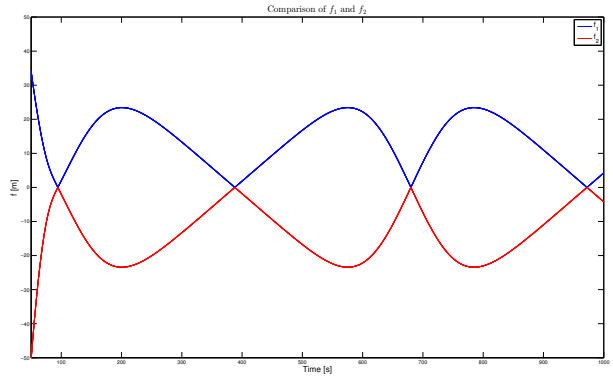

Figure 6.2: Comparison of f_1 and f_2 over time when the supply ship converges to and follows a circular path.

As such, f should have the same sign as $\hat{V}_y^f$, since U_c and $\sqrt{\Delta^2 + x_{b/f}^2 + (y_{b/f} + f)^2}$ are strictly positive:

$$
\begin{aligned}
f_1 &= \frac{-b - \sqrt{b^2 - ac}}{a} \\
f_2 &= \frac{-b + \sqrt{b^2 - ac}}{a} \\
f &= \begin{cases} f_1 & \hat{V}_y^f \geq 0 \\ f_2 & \hat{V}_y^f < 0 \end{cases}
\end{aligned}
\tag{6.26}
$$

By applying this method for a circular path, f is chosen by alternating between the two solutions as shown in figure 6.3.

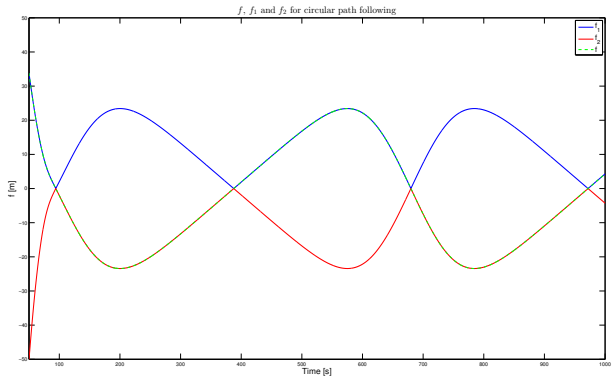

Figure 6.3: f is chosen as equation (6.26) when the supply ship converges to and follows a circular path.

6.2 Path Following of Space Curves in the Presence of Unknown Ocean Currents, Underactuated Underwater Vehicle

6.2.1 Theorem 2

In Theorem 2, the following notation is introduced.

$$\begin{aligned} \boldsymbol{V}_c^f &= [\boldsymbol{R}_f^i(\boldsymbol{\Theta}_{if})]^T \boldsymbol{V}_c \\ \hat{\boldsymbol{V}_c^f} &= [\boldsymbol{R}_f^i(\boldsymbol{\Theta}_{if})]^T \hat{\boldsymbol{V}}_c \end{aligned} \tag{6.27}$$

Theorem 2: Consider a 5-DOF underwater vehicle described by equation (6.28) $\Big(F_{u_r}(u_r, v_r, w_r, r, q),\ X_{v_r}(u_r),\ Y_{v_r},\ X_{w_r}(u_r),\ Y_{w_r}(u_r),\ Z_{w_r},\ F_q(\theta, u_r, w_r, q)$ and $F_r(u_r, v_r, r)$ specified in chapter 5.2$\Big)$ in closed loop with the controllers in equation (6.29) with the goal of following a general path with a constant surge velocity U_{rd} when affected by unknown constant, irrotational ocean current V_x, V_y and V_z.

$$\begin{aligned} \dot{x} &= \cos(\theta)\cos(\psi)u_r - \sin(\psi)v_r + \sin(\theta)\cos(\psi)w_r + V_x \\ \dot{y} &= \cos(\theta)\sin(\psi)u_r + \cos(\psi)v_r + \sin(\theta)\sin(\psi)w_r + V_y \\ \dot{z} &= -\sin(\theta)u_r + \cos(\theta)w_r + V_z \\ \dot{\theta} &= q \\ \dot{\psi} &= \frac{r}{\cos(\theta)} \\ \dot{u_r} &= F_{u_r}(u_r, v_r, w_r, r, q) + \tau_u \\ \dot{v_r} &= X_{v_r}(u_r)r + Y_{v_r}(u_r)v_r \\ \dot{w_r} &= X_{w_r}(u_r)q + Y_{w_r}(u_r)w_r + Z_{w_r}\sin(\theta) \\ \dot{q} &= F_q(\theta, u_r, w_r, q) + \tau_q \\ \dot{r} &= F_r(u_r, v_r, r) + \tau_r \end{aligned} \tag{6.28}$$

$$\begin{aligned} \tau_u &= -F_{u_r}(u_r, v_r, w_r, r, q) - k_{u_r}(u_r - U_{rd}), \qquad k_{u_r} > 0 \\ \begin{bmatrix} \tau_q \\ \tau_r \end{bmatrix} &= \begin{bmatrix} \dot{q_d} \\ \dot{r_d} \end{bmatrix} - \begin{bmatrix} F_q(\theta, u_r, w_r, q) \\ F_r(u_r, v_r, r) \end{bmatrix} - \boldsymbol{A}^T \boldsymbol{z}_1 - \boldsymbol{K}_2 \boldsymbol{z}_2, \qquad \boldsymbol{K}_2 > 0 \end{aligned} \tag{6.29}$$

The controllers are discussed in detail in chapter 5.2.1 and 5.2.2. By introducing a Serret-Frenet coordinate frame anchored in and propagating along the desired path, the control objectives are described by equation (6.30).

$$\begin{aligned} \lim_{t\to\infty} x_{b/f}(t) &= 0 \\ \lim_{t\to\infty} y_{b/f}(t) &= 0 \\ \lim_{t\to\infty} z_{b/f}(t) &= 0 \\ \lim_{t\to\infty} u_r(t) &= U_{rd} \end{aligned} \tag{6.30}$$

Through the use of following current estimates, update law and guidance law, the control objectives are achieved with asymptotic stability if assumptions **B1**-**B3** are satisfied.

$$\begin{aligned}
\dot{\hat{x}} &= \cos(\theta)\cos(\psi)u_r - \sin(\psi)v_r + \sin(\theta)\cos(\psi)w_r + \hat{V}_x + k_{x1}\tilde{x}, \quad k_{x1} > 0 \\
\dot{\hat{y}} &= \cos(\theta)\sin(\psi)u_r + \cos(\psi)v_r + \sin(\theta)\sin(\psi)w_r + \hat{V}_y + k_{y1}\tilde{y}, \quad k_{y1} > 0 \\
\dot{\hat{z}} &= -\sin(\theta)u_r + \cos(\theta)w_r + \hat{V}_z + k_{z1}\tilde{z}, \qquad\qquad\qquad\quad k_{z1} > 0 \\
\dot{\hat{V}}_x &= k_{x2}\tilde{x}, \quad k_{x2} > 0 \\
\dot{\hat{V}}_y &= k_{y2}\tilde{y}, \quad k_{y2} > 0 \\
\dot{\hat{V}}_z &= k_{z2}\tilde{z}, \quad k_{z2} > 0
\end{aligned} \tag{6.31}$$

$$\begin{aligned}
\dot{s} = & \underbrace{U_c}_{\triangleq\sqrt{U_{rd}^2+v_r^2+w_r^2}} \frac{\sqrt{\Delta^2+y_{b/f}^2}}{\sqrt{\Delta^2+y_{b/f}^2+(z_{b/f}+f)^2}} \frac{\sqrt{\Delta^2+x_{b/f}^2+z_{b/f}^2}}{\sqrt{\Delta^2+x_{b/f}^2+(y_{b/f}+g)^2+z_{b/f}^2}} \\
& + U_c \frac{x_{b/f}}{\sqrt{\Delta^2+x_{b/f}^2+y_{b/f}^2+z_{b/f}^2}} + \hat{V}_x^f
\end{aligned} \tag{6.32}$$

$$\begin{aligned}
\theta_{fc,d} &= \arctan\left(\frac{z_{b/f}+f}{\sqrt{\Delta^2+y_{b/f}^2}}\right) \\
\psi_{fc,d} &= -\arctan\left(\frac{y_{b/f}+g}{\sqrt{\Delta^2+x_{b/f}^2+z_{b/f}^2}}\right),
\end{aligned} \tag{6.33}$$

where f is the solution to the second order equation

$$\left(\hat{V_z^f}^2 - U_c^2\right) f^2 + 2\hat{V_z^f}^2 z_{b/f} f + \hat{V_z^f}^2 \left(\Delta^2 + y_{b/f}^2 + z_{b/f}^2\right) = 0 \tag{6.34}$$

and g is the solution to the second order equation

$$\left(\hat{V_y^f}^2 - \cos^2(\theta_{fc,d})U_c^2\right) g^2 + 2\hat{V_y^f}^2 y_{b/f} g + \hat{V_y^f}^2 \left(\Delta^2 + x_{b/f}^2 + y_{b/f}^2 + z_{b/f}^2\right) = 0 \tag{6.35}$$

Assumptions:

B1 - θ_{fc} and $\theta_{fc,d}$ are bounded. $|\theta_{fc}| < \pi/2$ and $\cos(\theta_{fc,d}) > k$, $0 < k < 1$. This implies that $|\theta_{fc,d}| < \arccos(k)$.

B2 - The ocean current is assumed bounded and less than the desired relative surge velocity scaled by a constant k, $0 \leq |\boldsymbol{V_c}| \leq V_{max} < kU_{rd}$, $0 < k < 1$. This saturation is also used on the estimated of the current, $|\hat{\boldsymbol{V}}_c| \leq V_{max} < kU_{rd}$.

B3 - The controllers and ocean current observer are assumed to be fast compared to the guidance law. As such, $\tilde{u}_r$, $\boldsymbol{z}_1$, $\boldsymbol{z}_2$, $\hat{\boldsymbol{V}}_c$, $\hat{x}$, $\hat{y}$ and $\hat{z}$ can be assumed zero.

Remark 1 - $|\theta_{fc}| = \pi/2$ is a singularity in the backstepping controller, see chapter 5.2.1. $|\theta_{fc}| < \pi/2$ ensure that this singularity is not reached.

Remark 2 - $|\theta_{fc,d}| < \arccos(k)$ and assumption **B2** ensures that the solutions of f and g are real and finite, see chapter 6.2.4.

Assumption **B1** define a domain $\mathbb{D}$ in which theorem 2 is valid:

$$\mathbb{D} = \left\{(\theta_{fc,d}, \theta_{fc}) \in \mathbb{R}^2 : |\theta_{fc,d}| < \arccos(k), |\theta_{fc}| < \pi/2\right\} \tag{6.36}$$

6.2.2 Body Serret-Frenet Kinematics including Current

The differential kinematic relationship between the body and Serret-Frenet for an underwater vehicle in the presence of ocean currents is very similar to that of a surface vessel. The vehicle now operates in 3D space rather than a plane. As such, the rotation matrices are functions of $\boldsymbol{\Theta}_{fb}$ and $\boldsymbol{\Theta}_{if}$ rather than ψ_{fb} and ψ_f, and $z_{b/f}$ is included in the dynamics.

$$\begin{bmatrix} \dot{x}_{b/f} \\ \dot{y}_{b/f} \\ \dot{z}_{b/f} \end{bmatrix} = \boldsymbol{R}_b^f(\boldsymbol{\Theta}_{fb}) \begin{bmatrix} u_r \\ v_r \\ w_r \end{bmatrix} - \begin{bmatrix} \dot{s} \\ 0 \\ 0 \end{bmatrix} - \dot{s} \begin{bmatrix} 0 & -\kappa & 0 \\ \kappa & 0 & -\tau \\ 0 & \tau & 0 \end{bmatrix} \begin{bmatrix} x_{b/f} \\ y_{b/f} \\ z_{b/f} \end{bmatrix} + \boldsymbol{R}_f^i(\boldsymbol{\Theta}_{if})^T \boldsymbol{V}_c \tag{6.37}$$

6.2.3 Stability Proof

This proof concludes that the control objectives $x_{b/f} = 0$, $y_{b/f} = 0$, $z_{b/f} = 0$ and $\tilde{u}_r = 0$ are achieved with asymptotic stability under the conditions of Theorem 2. To do this, equation (6.37) is rewritten and shown to be a cascaded system that includes the error dynamics of the controlled states and current estimates. Stability is proven using Lyapunov analysis. Through the current observer, controllers, update and guidance law in Theorem 2, equation (6.37) can be rewritten to equation (6.38). The proof is described in detail in Appendix B.2.

$$\begin{aligned} \begin{bmatrix} \dot{x}_{b/f} \\ \dot{y}_{b/f} \\ \dot{z}_{b/f} \end{bmatrix} = & \begin{bmatrix} -U_c \frac{x_{b/f}}{\sqrt{\Delta^2 + x_{b/f}^2 + y_{b/f}^2 + z_{b/f}^2}} \\ -U_c \frac{\sqrt{\Delta^2 + y_{b/f}^2}}{\sqrt{\Delta^2 + y_{b/f}^2 + (z_{b/f}+f)^2}} \frac{y_{b/f}}{\sqrt{\Delta^2 + x_{b/f}^2 + (y_{b/f}+g)^2 + z_{b/f}^2}} \\ -U_c \frac{z_{b/f}}{\sqrt{\Delta^2 + y_{b/f}^2 + (z_{b/f}+f)^2}} \end{bmatrix} \\ & - \dot{s} \begin{bmatrix} 0 & -\kappa & 0 \\ \kappa & 0 & -\tau \\ 0 & \tau & 0 \end{bmatrix} \begin{bmatrix} x_{b/f} \\ y_{b/f} \\ z_{b/f} \end{bmatrix} + \boldsymbol{H}(t, U_c, \boldsymbol{\xi})\boldsymbol{\xi} \end{aligned} \tag{6.38}$$

$$
\boldsymbol{H}(t, U_c, \boldsymbol{\xi})^T =
$$

$$
\begin{bmatrix}
\cos(\theta_{fb})\cos(\psi_{fb}) & \cos(\theta_{fb})\sin(\psi_{fb}) & -\sin(\theta_{fb}) \\
h_{11} & h_{21} & h_{31} \\
h_{12} & h_{22} & h_{32} \\
0 & 0 & 0 \\
0 & 0 & 0 \\
\cos(\psi_f)\cos(\theta_f) & \cos(\psi_f)\sin(\phi_f)\sin(\theta_f) - \cos(\phi_f)\sin(\psi_f) & \cos(\phi_f)\cos(\psi_f)\sin(\theta_f) + \sin(\phi_f)\sin(\psi_f) \\
\cos(\theta_f)\sin(\psi_f) & \sin(\phi_f)\sin(\psi_f)\sin(\theta_f) + \cos(\phi_f)\cos(\psi_f) & \cos(\phi_f)\sin(\psi_f)\sin(\theta_f) - \cos(\psi_f)\sin(\phi_f) \\
-\sin(\theta_f) & \cos(\theta_f)\sin(\phi_f) & \cos(\phi_f)\cos(\theta_f) \\
0 & 0 & 0 \\
0 & 0 & 0 \\
0 & 0 & 0
\end{bmatrix}
$$

$$
\boldsymbol{\xi}^T = \begin{bmatrix} \tilde{u_r} & \tilde{\theta}_{fc} & \tilde{\psi}_{fc} & \tilde{q} & \tilde{r} & \tilde{V}_x & \tilde{V}_y & \tilde{V}_z & \tilde{x} & \tilde{y} & \tilde{z} \end{bmatrix} \tag{6.39}
$$

$$
\begin{aligned}
h_{11} &= -U_c \frac{\sin(\tilde{\theta}_{fc})}{\tilde{\theta}_{fc}} \sin(\theta_{fc,d}) \cos(\psi_{fc,d}) \cos(\tilde{\psi}_{fc}) + U_c \frac{\sin(\tilde{\theta}_{fc})}{\tilde{\theta}_{fc}} \sin(\theta_{fc,d}) \sin(\psi_{fc,d}) \sin(\tilde{\psi}_{fc}) \\
&\quad + U_c \frac{\cos(\tilde{\theta}_{fc}) - 1}{\tilde{\theta}_{fc}} \cos(\theta_{fc,d}) \cos(\psi_{fc,d}) \\
h_{12} &= -U_c \frac{\sin(\tilde{\psi}_{fc})}{\tilde{\psi}_{fc}} \cos(\theta_{fc,d}) \cos(\tilde{\theta}_{fc}) \sin(\psi_{fc,d}) + U_c \frac{\cos(\tilde{\psi}_{fc}) - 1}{\tilde{\psi}_{fc}} \cos(\theta_{fc,d}) \cos(\tilde{\theta}_{fc}) \cos(\psi_{fc,d}) \\
h_{21} &= -U_c \frac{\sin(\tilde{\theta}_{fc})}{\tilde{\theta}_{fc}} \sin(\theta_{fc,d}) \sin(\psi_{fc,d}) \cos(\tilde{\psi}_{fc}) - U_c \frac{\sin(\tilde{\theta}_{fc})}{\tilde{\theta}_{fc}} \sin(\theta_{fc,d}) \cos(\psi_{fc,d}) \sin(\tilde{\psi}_{fc}) \\
&\quad + U_c \frac{\cos(\tilde{\theta}_{fc}) - 1}{\tilde{\theta}_{fc}} \cos(\theta_{fc,d}) \sin(\psi_{fc,d}) \\
h_{22} &= U_c \frac{\sin(\tilde{\psi}_{fc})}{\tilde{\psi}_{fc}} \cos(\theta_{fc,d}) \cos(\tilde{\theta}_{fc}) \cos(\psi_{fc,d}) + U_c \frac{\cos(\tilde{\psi}_{fc}) - 1}{\tilde{\psi}_{fc}} \cos(\theta_{fc,d}) \cos(\tilde{\theta}_{fc}) \sin(\psi_{fc,d}) \\
h_{31} &= -U_c \frac{\sin(\tilde{\theta}_{fc})}{\tilde{\theta}_{fc}} \cos(\theta_{fc,d}) - U_c \frac{\cos(\tilde{\theta}_{fc}) - 1}{\tilde{\theta}_{fc}} \sin(\theta_{fc,d}) \\
h_{32} &= 0
\end{aligned} \tag{6.40}
$$

The system in equation (6.38) and the dynamics of $\boldsymbol{\xi}$ (6.43) can be seen as a cascaded system where the error dynamics perturbs the nominal system in equation (6.41) through the term $\boldsymbol{H}(t, U_c, \boldsymbol{\xi})\boldsymbol{\xi}$ (appendix A.3.4).

$$\begin{bmatrix} \dot{x}_{b/f} \\ \dot{y}_{b/f} \\ \dot{z}_{b/f} \end{bmatrix} = \begin{bmatrix} -U_c \frac{x_{b/f}}{\sqrt{\Delta^2 + x_{b/f}^2 + y_{b/f}^2 + z_{b/f}^2}} \\ -U_c \frac{\sqrt{\Delta^2 + y_{b/f}^2}}{\sqrt{\Delta^2 + y_{b/f}^2 + (z_{b/f}+f)^2}} \frac{y_{b/f}}{\sqrt{\Delta^2 + x_{b/f}^2 + (y_{b/f}+g)^2 + z_{b/f}^2}} \\ -U_c \frac{z_{b/f}}{\sqrt{\Delta^2 + y_{b/f}^2 + (z_{b/f}+f)^2}} \end{bmatrix} - \dot{s} \begin{bmatrix} 0 & -\kappa & 0 \\ \kappa & 0 & -\tau \\ 0 & \tau & 0 \end{bmatrix} \begin{bmatrix} x_{b/f} \\ y_{b/f} \\ z_{b/f} \end{bmatrix} \tag{6.41}$$

Stability of the nominal system can be shown using the quadratic, positive definite, decrescent and radially unbounded Lyapunov function $V = \frac{1}{2}(x_{b/f}^2 + y_{b/f}^2 + z_{b/f}^2)$.

$$\begin{aligned} \dot{V} &= \dot{x}_{b/f} x_{b/f} + \dot{y}_{b/f} y_{b/f} + \dot{z}_{b/f} z_{b/f} \\ &= -U_c \frac{x_{b/f}^2}{\sqrt{\Delta^2 + x_{b/f}^2 + y_{b/f}^2 + z_{b/f}^2}} - U_c \frac{z_{b/f}^2}{\sqrt{\Delta^2 + y_{b/f}^2 + (z_{b/f}+f)^2}} \\ &\quad - U_c \frac{\sqrt{\Delta^2 + y_{b/f}^2}}{\sqrt{\Delta^2 + y_{b/f}^2 + (z_{b/f}+f)^2}} \frac{y_{b/f}^2}{\sqrt{\Delta^2 + x_{b/f}^2 + (y_{b/f}+g)^2 + z_{b/f}^2}} \\ &\leq -U_{rd} \left(\frac{x_{b/f}^2}{\sqrt{\Delta^2 + x_{b/f}^2 + y_{b/f}^2 + z_{b/f}^2}} + \frac{z_{b/f}^2}{\sqrt{\Delta^2 + y_{b/f}^2 + (z_{b/f}+f)^2}} \right. \\ &\quad \left. + \frac{\sqrt{\Delta^2 + y_{b/f}^2}}{\sqrt{\Delta^2 + y_{b/f}^2 + (z_{b/f}+f)^2}} \frac{y_{b/f}^2}{\sqrt{\Delta^2 + x_{b/f}^2 + (y_{b/f}+g)^2 + z_{b/f}^2}} \right) \\ &\triangleq W(x_{b/f}, y_{b/f}, z_{b/f}) < 0 \end{aligned} \tag{6.42}$$

$\dot{V}$ is negative definite and the nominal system is UGAS according to theorem 4.8/4.9 in appendix A.3.3.

The error dynamics is shown in equation (6.43) and is based on the feedback linearization controller and integrator backstepping controller in chapter 5.2.1 and 5.2.2 and the current and position observers in chapter 3.4.

$$\dot{\boldsymbol{\xi}} = \begin{bmatrix} \dot{\tilde{u}}_r \\ \dot{\tilde{\theta}}_{fc} \\ \dot{\tilde{\psi}}_{fc} \\ \dot{\tilde{q}} \\ \dot{\tilde{r}} \\ \dot{\tilde{V}}_x \\ \dot{\tilde{V}}_y \\ \dot{\tilde{V}}_z \\ \dot{\tilde{x}} \\ \dot{\tilde{y}} \\ \dot{\tilde{z}} \end{bmatrix} = \begin{bmatrix} \dot{\tilde{u}}_r \\ \dot{\boldsymbol{z}}_1 \\ \dot{\boldsymbol{z}}_2 \\ \dot{\tilde{V}}_x \\ \dot{\tilde{V}}_y \\ \dot{\tilde{V}}_z \\ \dot{\tilde{x}} \\ \dot{\tilde{y}} \\ \dot{\tilde{z}} \end{bmatrix} = \begin{bmatrix} -k_{u_r} & \mathbf{0} & \mathbf{0} & 0 & 0 & 0 & 0 & 0 & 0 \\ 0 & -\boldsymbol{K}_1 & \boldsymbol{A} & 0 & 0 & 0 & 0 & 0 & 0 \\ 0 & -\boldsymbol{A}^T & -\boldsymbol{K}_2 & 0 & 0 & 0 & 0 & 0 & 0 \\ 0 & \mathbf{0} & \mathbf{0} & 0 & 0 & 0 & -k_{x2} & 0 & 0 \\ 0 & \mathbf{0} & \mathbf{0} & 0 & 0 & 0 & 0 & -k_{y2} & 0 \\ 0 & \mathbf{0} & \mathbf{0} & 0 & 0 & 0 & 0 & 0 & -k_{z2} \\ 0 & \mathbf{0} & \mathbf{0} & 1 & 0 & 0 & -k_{x1} & 0 & 0 \\ 0 & \mathbf{0} & \mathbf{0} & 0 & 1 & 0 & 0 & -k_{y1} & 0 \\ 0 & \mathbf{0} & \mathbf{0} & 0 & 0 & 1 & 0 & 0 & -k_{z1} \end{bmatrix} \begin{bmatrix} \tilde{u}_r \\ \boldsymbol{z}_1 \\ \boldsymbol{z}_2 \\ \tilde{V}_x \\ \tilde{V}_y \\ \tilde{V}_z \\ \tilde{x} \\ \tilde{y} \\ \tilde{z} \end{bmatrix}$$
$$= \boldsymbol{\Lambda}\boldsymbol{\xi} \tag{6.43}$$

Equation (6.43) has an UES equilbrium point in $\boldsymbol{\xi} = 0$. This is shown using Lyapunov analysis. It is known that

$$\begin{aligned} \begin{bmatrix} \dot{\tilde{x}} \\ \dot{\tilde{V}}_x \end{bmatrix} &= \underbrace{\begin{bmatrix} -k_{x1} & 1 \\ -k_{x2} & 0 \end{bmatrix}}_{\boldsymbol{A}_x} \begin{bmatrix} \tilde{x} \\ \tilde{V}_x \end{bmatrix} \\ \begin{bmatrix} \dot{\tilde{y}} \\ \dot{\tilde{V}}_y \end{bmatrix} &= \underbrace{\begin{bmatrix} -k_{y1} & 1 \\ -k_{y2} & 0 \end{bmatrix}}_{\boldsymbol{A}_y} \begin{bmatrix} \tilde{y} \\ \tilde{V}_y \end{bmatrix} \\ \begin{bmatrix} \dot{\tilde{z}} \\ \dot{\tilde{V}}_z \end{bmatrix} &= \underbrace{\begin{bmatrix} -k_{z1} & 1 \\ -k_{z2} & 0 \end{bmatrix}}_{\boldsymbol{A}_z} \begin{bmatrix} \tilde{z} \\ \tilde{V}_z \end{bmatrix}. \end{aligned} \tag{6.44}$$

Under the constraints of Theorem 2, $k_{x1}, k_{x2}, k_{y1}, k_{y2}, k_{z1}, k_{z2} > 0$ and $\boldsymbol{A}_x$, $\boldsymbol{A}_y$ and $\boldsymbol{A}_z$ are Hurwitz. Thus, there exists three symmetric positive definite matrices $\boldsymbol{P}_x$, $\boldsymbol{P}_y$ and $\boldsymbol{P}_z$ (theorem 4.6 in appendix A.3.2) such that

$$\begin{aligned} \boldsymbol{P}_x\boldsymbol{A}_x + \boldsymbol{A}_x^T\boldsymbol{P}_x &= -\begin{bmatrix} 1 & 0 \\ 0 & 1 \end{bmatrix} \\ \boldsymbol{P}_y\boldsymbol{A}_y + \boldsymbol{A}_y^T\boldsymbol{P}_y &= -\begin{bmatrix} 1 & 0 \\ 0 & 1 \end{bmatrix} \\ \boldsymbol{P}_z\boldsymbol{A}_z + \boldsymbol{A}_z^T\boldsymbol{P}_z &= -\begin{bmatrix} 1 & 0 \\ 0 & 1 \end{bmatrix}. \end{aligned} \tag{6.45}$$

Taking the positive definite, decresent, radially unbounded Lyapunov candidate

$$V = \frac{1}{2}\tilde{u}_r^2 + \frac{1}{2}\boldsymbol{z}_1^T\boldsymbol{z}_1 + \frac{1}{2}\boldsymbol{z}_2^T\boldsymbol{z}_2 + \begin{bmatrix}\tilde{x} & \tilde{V}_x\end{bmatrix}\boldsymbol{P}_x\begin{bmatrix}\tilde{x}\\ \tilde{V}_x\end{bmatrix} + \begin{bmatrix}\tilde{y} & \tilde{V}_y\end{bmatrix}\boldsymbol{P}_y\begin{bmatrix}\tilde{y}\\ \tilde{V}_y\end{bmatrix} + \begin{bmatrix}\tilde{z} & \tilde{V}_z\end{bmatrix}\boldsymbol{P}_z\begin{bmatrix}\tilde{z}\\ \tilde{V}_z\end{bmatrix}. \tag{6.46}$$

It can easily be seen that the time-derivative of V is given as

$$\begin{aligned}\dot{V} &= \tilde{u}_r\dot{\tilde{u}}_r + \frac{1}{2}\dot{\boldsymbol{z}}_1^T\boldsymbol{z}_1 + \frac{1}{2}\boldsymbol{z}_1^T\dot{\boldsymbol{z}}_1 + \frac{1}{2}\dot{\boldsymbol{z}}_2^T\boldsymbol{z}_2 + \frac{1}{2}\boldsymbol{z}_2^T\dot{\boldsymbol{z}}_2 + \begin{bmatrix}\dot{\tilde{x}} & \dot{\tilde{V}}_x\end{bmatrix}\boldsymbol{P}_x\begin{bmatrix}\tilde{x}\\ \tilde{V}_x\end{bmatrix} + \begin{bmatrix}\tilde{x} & \tilde{V}_x\end{bmatrix}\boldsymbol{P}_x\begin{bmatrix}\dot{\tilde{x}}\\ \dot{\tilde{V}}_x\end{bmatrix}\\ &\quad + \begin{bmatrix}\dot{\tilde{y}} & \dot{\tilde{V}}_y\end{bmatrix}\boldsymbol{P}_y\begin{bmatrix}\tilde{y}\\ \tilde{V}_y\end{bmatrix} + \begin{bmatrix}\tilde{y} & \tilde{V}_y\end{bmatrix}\boldsymbol{P}_y\begin{bmatrix}\dot{\tilde{y}}\\ \dot{\tilde{V}}_y\end{bmatrix} + \begin{bmatrix}\dot{\tilde{z}} & \dot{\tilde{V}}_z\end{bmatrix}\boldsymbol{P}_z\begin{bmatrix}\tilde{z}\\ \tilde{V}_z\end{bmatrix} + \begin{bmatrix}\tilde{z} & \tilde{V}_z\end{bmatrix}\boldsymbol{P}_z\begin{bmatrix}\dot{\tilde{z}}\\ \dot{\tilde{V}}_z\end{bmatrix}\\ &= -k_{u_r}\tilde{u}_r^2 - \boldsymbol{z}_1^T\boldsymbol{K}_1\boldsymbol{z}_1 - \boldsymbol{z}_2^T\boldsymbol{K}_2\boldsymbol{z}_2 - \tilde{x}^2 - \tilde{V}_x^2 - \tilde{y}^2 - \tilde{V}_y^2 - \tilde{z}^2 - \tilde{V}_z^2.\end{aligned} \tag{6.47}$$

$\dot{V}$ is negative definite (the controller gain $k_{u_r} > 0$ and the controller gain matrices $\boldsymbol{K}_1 = \boldsymbol{K}_1^T$ and $\boldsymbol{K}_2 = \boldsymbol{K}_2^T$ are symmetric positive definite). Hence, the equilibrium point $\boldsymbol{\xi} = \boldsymbol{0}$ is UAS (theorem 4.8/4.9 in appendix A.3.3). Furthermore, the Lyapunov function satisfies the conditions of theorem 4.10 in appendix A.3.3, so $\boldsymbol{\xi} = \boldsymbol{0}$ is UES. However, the error dynamics is *not* globally stable due to the singularity $\theta_{fc} = \pi/2$ in the matrix $\boldsymbol{A}$ (discussed in chapter 5.2.2). This singularity is not contained in the domain $\mathbb{D}$ (6.36) in which Theorem 2 is valid, so the error dynamics is UES in $\mathbb{D}$.

Theorem 2 in appendix A.3.4 regarding the stability of cascaded systems is not applicable due to the fact that the error dynamics is not UGAS. However, since $\boldsymbol{\xi} \to \boldsymbol{0}$, one can apply assumption **B3** and assume $\boldsymbol{\xi} = \boldsymbol{0}$. As such, equation (6.38) reduces to the nominal system in equation (6.41), which is known UGAS. Hence, it is possible to conclude that the control objectives are achieved asymptotically.

Proving stability of the cascaded system (6.38) and (6.43) remains a topic for future work.

6.2.4 Solving for f and g

This chapter is very similar to chapter 6.1.4 describing how to solve for f in the case of surface vessles. The same principles apply for underwater vehicles.

As stated in Theorem 2, f is the solution to the second order equation

$$\underbrace{\left(\hat{V_z^f}^2 - U_c^2\right)}_{a_f} f^2 + 2\underbrace{\hat{V_z^f}^2 z_{b/f}}_{b_f} f + \underbrace{\hat{V_z^f}^2\left(\Delta^2 + y_{b/f}^2 + z_{b/f}^2\right)}_{c_f} = 0 \tag{6.48}$$

and g is the solution to the second order equation

$$\underbrace{\left(\hat{V_y^f}^2 - \cos^2(\theta_{fc,d})U_c^2\right)}_{a_g} g^2 + 2\underbrace{\hat{V_y^f}^2 y_{b/f}}_{b_g} g + \underbrace{\hat{V_y^f}^2\left(\Delta^2 + x_{b/f}^2 + y_{b/f}^2 + z_{b/f}^2\right)}_{c_g} = 0 \tag{6.49}$$

These equations are chosen as a direct result of the stability proof. As can be seen from equation (B.30) and (B.33) in Appendix B.2, the dynamics of $y_{b/f}$ has a term

$$U_c \cos(\theta_{fc,d}) \frac{g}{\sqrt{\Delta^2 + x_{b/f}^2 + (y_{b/f} + g)^2 + z_{b/f}^2}} \tag{6.50}$$

and the dynamics of $z_{b/f}$ has a term

$$U_c \frac{f}{\sqrt{\Delta^2 + y_{b/f}^2 + (z_{b/f} + f)^2}}. \tag{6.51}$$

To prove stability, it is desirable that these terms are equal to $\hat{V}_y^f$ and $\hat{V}_z^f$ respectively. Rewritten, this results in equation (6.48) and (6.49). These equations both have two solutions:

$$\begin{aligned} f_1 &= \frac{-b_f - \sqrt{b_f^2 - a_f c_f}}{a_f} \\ f_2 &= \frac{-b_f + \sqrt{b_f^2 - a_f c_f}}{a_f} \end{aligned} \tag{6.52}$$

$$\begin{aligned} g_1 &= \frac{-b_g - \sqrt{b_g^2 - a_g c_g}}{a_g} \\ g_2 &= \frac{-b_g + \sqrt{b_g^2 - a_g c_g}}{a_g} \end{aligned} \tag{6.53}$$

Based on assumption **B2**, the current is limited and less than kU_{rd} for some constant $0 < k < 1$. As such, by using this saturation also on the estimated current, it can easily be seen that $a_f < 0$:

$$\begin{aligned} \hat{V_z^f}^2 - U_c^2 \leq |\hat{\boldsymbol{V}}_c^f|^2 - U_c^2 &= |\hat{\boldsymbol{V}}_c|^2 - U_c^2 < k^2 U_{rd}^2 - U_c^2 \\ &= k^2 U_{rd}^2 - (U_{rd}^2 + v_r^2 + w_r^2) = \underbrace{(k^2 - 1)}_{<0} U_{rd}^2 - v_r^2 - w_r^2 < 0 \end{aligned} \tag{6.54}$$

Furthermore, $c_f \geq 0$. As such, the expression $b_f^2 - a_f c_f \geq 0$ and f_1 and f_2 are always real. Furthermore, division by a_f is safe since a_f will never be equal to zero.

As time progresses, $z_{b/f}$ and consequently b_f approach zero. The expressions for f_1 and f_2 can be simplified to

$$\begin{aligned} f_1 &= \frac{-\sqrt{-a_f c_f}}{a_f} \\ f_2 &= \frac{\sqrt{-a_f c_f}}{a_f} \end{aligned} \tag{6.55}$$

Thus, f_1 will always be positive (≥ 0), f_2 will always be negative (≤ 0), and the two solutions will be equal with opposite signs. As such, it is not arbitrary which solution for f one should chose, and it may be necessary to alternate between the two. This depends on the path and ocean current estimates. As mentioned, f is chosen to satisfy the following equation:

$$U_c \frac{f}{\sqrt{\Delta^2 + y_{b/f}^2 + (z_{b/f} + f)^2}} = \hat{V}_z^f \tag{6.56}$$

As such, f should have the same sign as $\hat{V_z^f}$, since U_c and $\sqrt{\Delta^2 + y_{b/f}^2 + (z_{b/f} + f)^2}$ are strictly positive:

$$\begin{aligned} f_1 &= \frac{-b_f - \sqrt{b_f^2 - a_f c_f}}{a_f} \\ f_2 &= \frac{-b_f + \sqrt{b_f^2 - a_f c_f}}{a_f} \\ f &= \begin{cases} f_1 & \hat{V_z^f} \geq 0 \\ f_2 & \hat{V_z^f} < 0 \end{cases} \end{aligned} \tag{6.57}$$

The analysis of g is very similar. By assumption **B2** the current and the current estimates are limited and less than kU_{rd} for some constant $0 < k < 1$. Furthermore, $\theta_{fc,d}$ is bounded so $\cos(\theta_{fc,d}) > k$ based on assumption **B1**. As such, it is easy to see that $a_g < 0$:

$$\begin{aligned} \hat{V_y^f}^2 - \cos^2(\theta_{fc,d}) U_c^2 &\leq |\hat{\boldsymbol{V}}_c^f|^2 - \cos^2(\theta_{fc,d}) U_c^2 = |\hat{\boldsymbol{V}}_c|^2 - \cos^2(\theta_{fc,d}) U_c^2 \\ &< k^2 U_{rd}^2 - k^2 U_c^2 = -k^2 (v_r^2 + w_r^2) \leq 0 \end{aligned} \tag{6.58}$$

The solution of g is chosen in the same manner as f:

$$\begin{aligned} g_1 &= \frac{-b_g - \sqrt{b_g^2 - a_g c_g}}{a_g} \\ g_2 &= \frac{-b_g + \sqrt{b_g^2 - a_g c_g}}{a_g} \\ g &= \begin{cases} g_1 & \hat{V_y^f} \geq 0 \\ g_2 & \hat{V_y^f} < 0 \end{cases} \end{aligned} \tag{6.59}$$

Chapter 7

Simulation

The developed theorems are based on the path following methods of Børhaug discussed in chapter 3.7. The same controller systems are used, but the guidance and update laws have been extended to include the terms f, g and $\hat{\boldsymbol{V}}_c$ to compensate for the ocean current. The original guidance and update laws of Børhaug (f, g and $\hat{\boldsymbol{V}}_c$ equal to zero) have been simulated to test how unknown ocean currents affect the path following of the marine vessel. The results are shown in chapter 7.1.4 and 7.2.4.

The simulation results for Theorem 1 and 2 are shown in chapter 7.1.5 and 7.2.5. These simulations are first and foremost conducted to confirm the correctness of the developed theorems, and for this purpose the simulation conditions are ideal: All states are measured without measurement noise, and the vessel model is assumed known and perfectly accurate. However, these assumptions are not realistic for a real-life application. Furthermore, these simulation results are more extensive due to the fact that Theorem 1 and 2 are the main contributions of this thesis. Both the feedack linearization controllers and integrator backstepping controllers in Theorem 1 and 2 are known to be sensitive to modeling uncertainty. As such, some simulations were run with modeling errors in the controllers. These results are shown in chapter 7.3.

7.1 Simulations on supply ship

7.1.1 Implementation

The Simulink diagram is shown in figure 7.1. To simplify the block diagram, some of the connections are color coded. For instance, the signal for the traveled distance s is marked with red.

The block named "supply ship" contains the dynamic model presented in chapter 5.1. It takes as input the ocean current, motor thruster force T and rudder angle

δ_r, and calculates the ship states $\boldsymbol{\eta} = [x, y, \psi]^T$ and $\boldsymbol{\nu}_r = [u_r, v_r, r]^T$. T and δ_r are calculated by the controller system, which contains the feedback linearization controllers described in chapter 5.1.1. The inputs to this subsystem are the ship states, the desired heading $\psi_{desired}$ and the desired relative surge velocity $u_{r,desired}$. $\psi_{desired}$ is calculated based on the guidance law in equation (6.7) in the block called "Guidance law" and $u_{r,desired} = U_{rd} = constant$. The ocean current is estimated as described in chapter 3.4 in the block named "Ocean current observer".

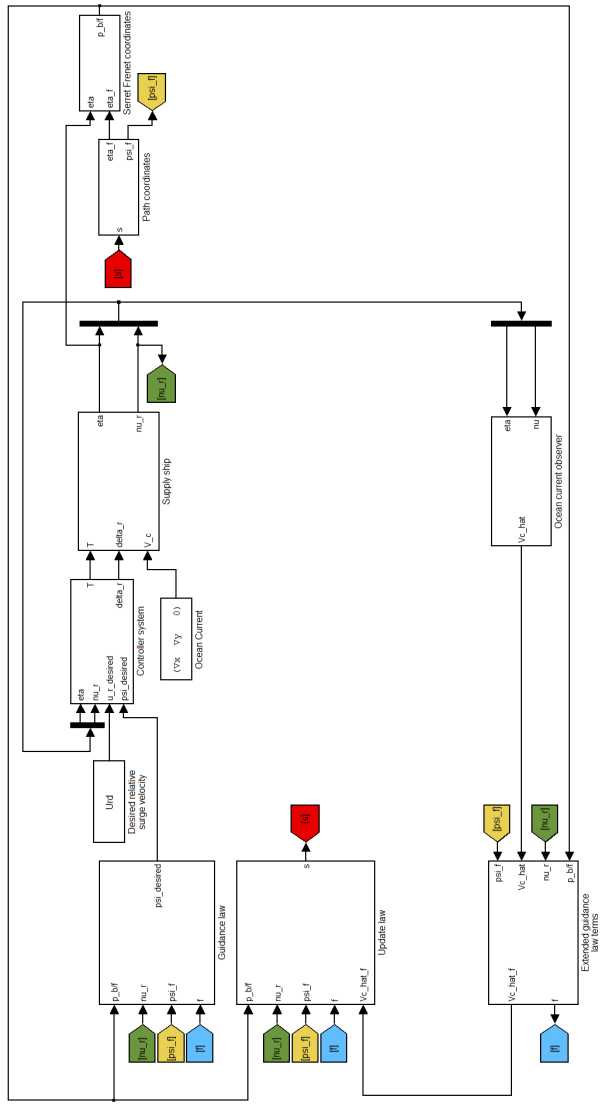

Figure 7.1: Simulink implementation of closed-loop system with supply ship, feedback linearization controllers and guidance and update law from Theorem 1.

The desired path is defined in the inertial coordinate system as $\boldsymbol{\eta}_f = [x_f, y_f, \psi_f]^T$ and is calculated in the block called "Path coordinates". As figure 7.1 shows, the desired path is parametrized as a function of the traveled distance s (this is described in greater detail in chapter 7.1.2). The update law for $\dot{s}$ is calculated and integrated in the block called "Update law".

As described in Theorem 1, one of the control objectives is to make $\boldsymbol{p}_{b/f}^f = [x_{b/f}, y_{b/f}]^T$ converge to zero. These terms are calculated in the block named "Serret Frenet coordinates" using equation (7.1).

$$\boldsymbol{p}_{b/f}^f = \begin{bmatrix} x_{b/f} \\ y_{b/f} \end{bmatrix} = [\boldsymbol{R}_f^i(\psi_f)]^T (\underbrace{\boldsymbol{p}_{b/i}^i - \boldsymbol{p}_{f/i}^i}_{\boldsymbol{p}_{b/f}^i}) = [\boldsymbol{R}_f^i(\psi_f)]^T (\begin{bmatrix} x \\ y \end{bmatrix} - \begin{bmatrix} x_f \\ y_f \end{bmatrix}) \tag{7.1}$$

$\boldsymbol{p}_{b/f}^f$ is used in a feedback along with $\boldsymbol{\nu}_r$, $\hat{\boldsymbol{V}}_c$ and ψ_f to solve for the extended guidance and update law terms f and $\hat{\boldsymbol{V}}_c^f$ as described in chapter 6.1.

7.1.2 Desired paths

In the simulations, 3 different paths have been implemented: A straight line, a circle and a piecewise curved and straight path. The parametrizations are presented below.

Path 1: Straight line The desired path is a straight line starting in the origin of the inertial system and has a heading of 30° as shown in figure 7.2.

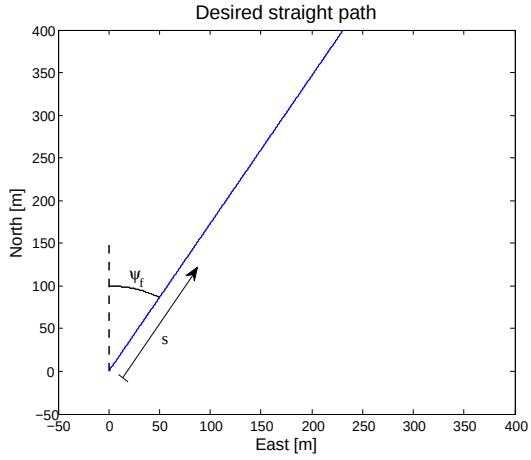

Figure 7.2: Illustration of the implemented desired straight path for the supply ship.

$$\begin{aligned} x_f(s) &= s\cos(\psi_f) \\ y_f(s) &= s\sin(\psi_f) \\ \psi_f(s) &= \frac{\pi}{6} \end{aligned} \tag{7.2}$$

Path 2: Circular The desired path is a clockwise circle with radius $R = 400$ m and center in $C = [0, 800]^T$ m as shown in figure 7.3.

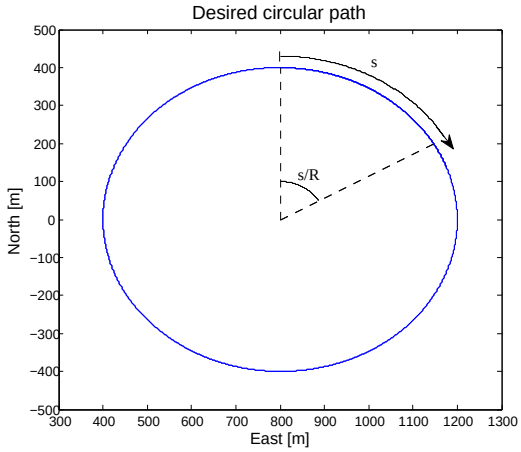

Figure 7.3: Illustration of the implemented desired circular path for the supply ship.

$$\begin{aligned} x_f(s) &= R\cos\left(\frac{s}{R}\right) \\ y_f(s) &= R\sin\left(\frac{s}{R}\right) + 800 \\ \psi_f(s) &= \frac{s}{R} + \frac{\pi}{2} \end{aligned} \tag{7.3}$$

Path 3: Piecewise straight and circular The desired path has the shape of an athletics track. The path is to be followed clockwise and starts at the top point of the easternmost half circle as shown in figure 7.4. The half circles both have radius $R = 400$ m and center in $C_1 = [0, 0]^T$ m and $C_2 = [0, 800]^T$ m respectively. The first round of the path is parametrized as below.

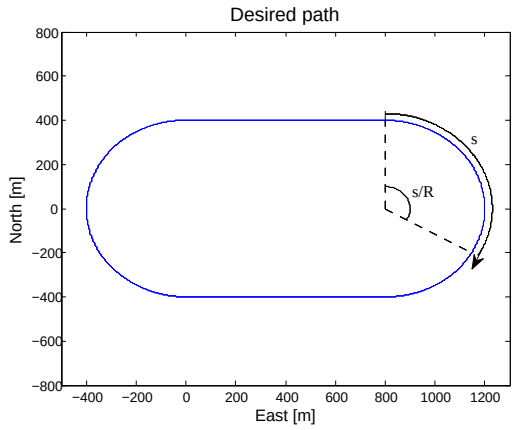

Figure 7.4: Illustration of the implemented desired piecewise circular and straight path for the supply ship.

$$
\begin{aligned}
&\left.\begin{aligned} x_f(s) &= R\cos\left(\frac{s}{R}\right) \\ y_f(s) &= R\sin\left(\frac{s}{R}\right) + 800 \\ \psi_f(s) &= \frac{s}{R} + \frac{\pi}{2} \end{aligned}\right\} s \leq \pi R \\
&\left.\begin{aligned} x_f(s) &= -R \\ y_f(s) &= 800 - (s - \pi R) \\ \psi_f(s) &= \frac{3\pi}{2} \end{aligned}\right\} \pi R < s \leq \pi R + 800 \\
&\left.\begin{aligned} x_f(s) &= R\cos\left(\frac{s-800}{R}\right) \\ y_f(s) &= R\sin\left(\frac{s-800}{R}\right) \\ \psi_f(s) &= \frac{s-800}{R} + \frac{\pi}{2} \end{aligned}\right\} \pi R + 800 < s \leq 2\pi R + 800 \\
&\left.\begin{aligned} x_f(s) &= R \\ y_f(s) &= s - 800 - 2\pi R \\ \psi_f(s) &= 2\pi R + \frac{\pi}{2} \end{aligned}\right\} s \leq 2\pi R + 800 < s \leq 2\pi R + 1600
\end{aligned}
\tag{7.4}
$$

7.1.3 Simulation parameters

In all simulations on the supply ship, the following parameters are used:

$$\begin{array}{llll} U_{rd} = 5\frac{m}{s} & \boldsymbol{V}_c = [-1.5, 1.5]^T \frac{m}{s} & V_{max} = 5\frac{m}{s} & \Delta = 50m \\ k_{u_r} = 0.1\frac{1}{s} & k_\psi = 0.04\frac{1}{s^2} & k_r = 0.9\frac{1}{s} & \\ k_{x1} = 1\frac{1}{s} & k_{x2} = 1\frac{1}{s^2} & k_{y1} = 1\frac{1}{s} & k_{y2} = 1\frac{1}{s^2} \end{array}$$

In addition, the motor thrust T is saturated at 5 MN and the rudder is saturated at $\pm\frac{\pi}{2}$ radians with a rate limitation of $\pm\frac{\pi}{18}$ radians per second (meaning that the rudder can change approximately 10 degrees per second). The given parameters and desired paths satisfy the assumptions of Theorem 1:

Assumptions:

A1 - $Y(U_{rd}) = -Y^{min} = -0.3774 < 0$, and
$-U_{rd} + a = -5 + a \leq X(U_{rd}) = -2.8480 \leq X^{max} = 2.8480$,
for any $0 < a < 2.152$.

A2 - The curvature of the desired path is bounded such that
$\kappa_{max} \triangleq \underset{s\in\Re}{max}|\kappa(s)| < \frac{1}{3}\left(\frac{Y^{min}}{X^{max}}\right) = 0.04417$. For a straight line, $\kappa(s) = 0$ for all s, so $\kappa_{max} = 0$, and for the circular and piecewise circular desired paths described above, $\kappa_{max} = \frac{1}{R} = 0.0025$.

A3 - The parameter Δ of the guidance law (6.7) safisfies $\Delta > \frac{\frac{3}{2}X^{max}}{Y^{min} - 3X^{max}\kappa_{max}}$. This means that $\Delta > 11.32$ for the straight line path and $\Delta > 12.0$ for the circular and piecewise circular paths. As such, the chosen value $\Delta = 50$ satisfies this demand.

A4 - The ocean current is assumed bounded and less than the desired relative surge velocity, $0 \leq \sqrt{(-1.5)^2 + 1.5^2} = 2.12 < V_{max} = 5 \leq U_{rd} = 5$. This saturation is also used on the estimated of the current.

7.1.4 Simulation results: Original Guidance and Update Law

The original guidance and update law of Børhaug discussed in chapter 3.7 was simulated by setting the output of the "Extended guidance law terms"-block in figure 7.1 identically equal to zero.

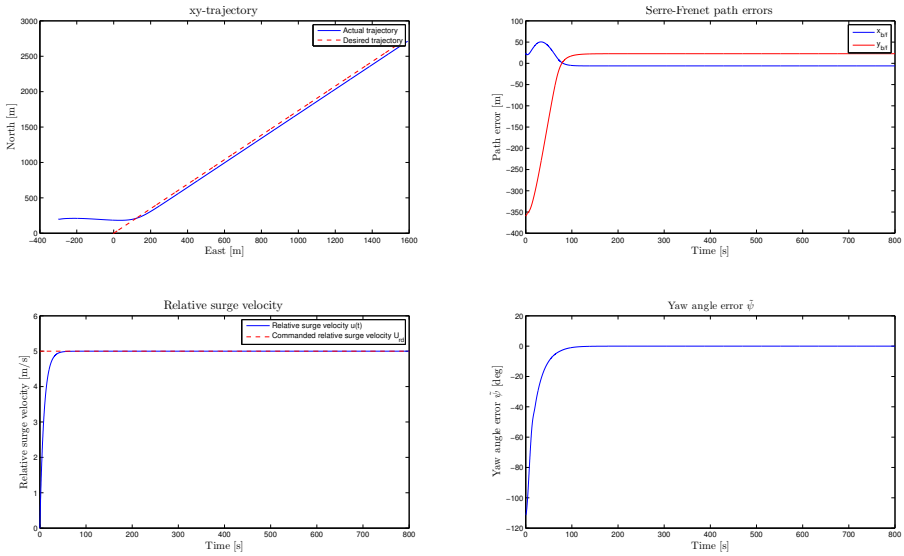

Figure 7.5: **Path 1** - Simulation results of original guidance and update law in the presence of unknown ocean currents.

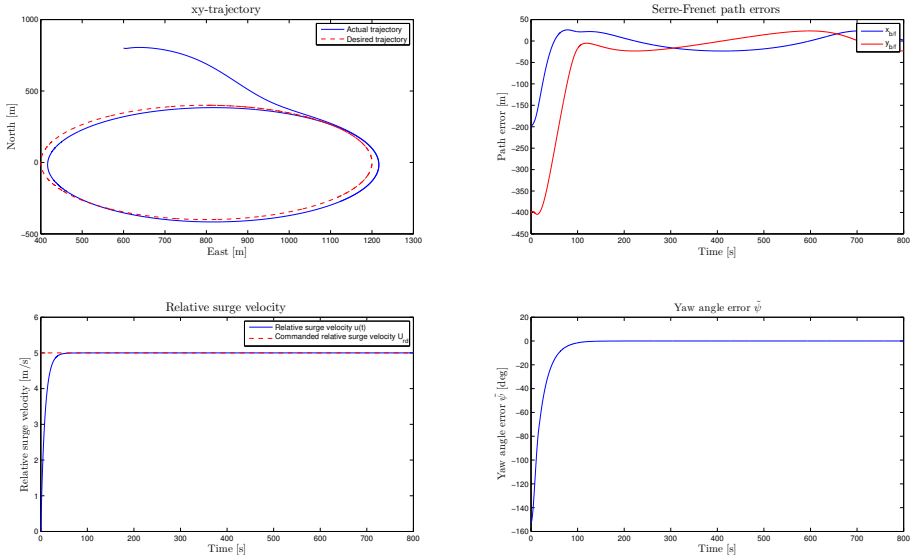

Figure 7.6: **Path 2** - Simulation results of original guidance and update law in the presence of unknown ocean currents.

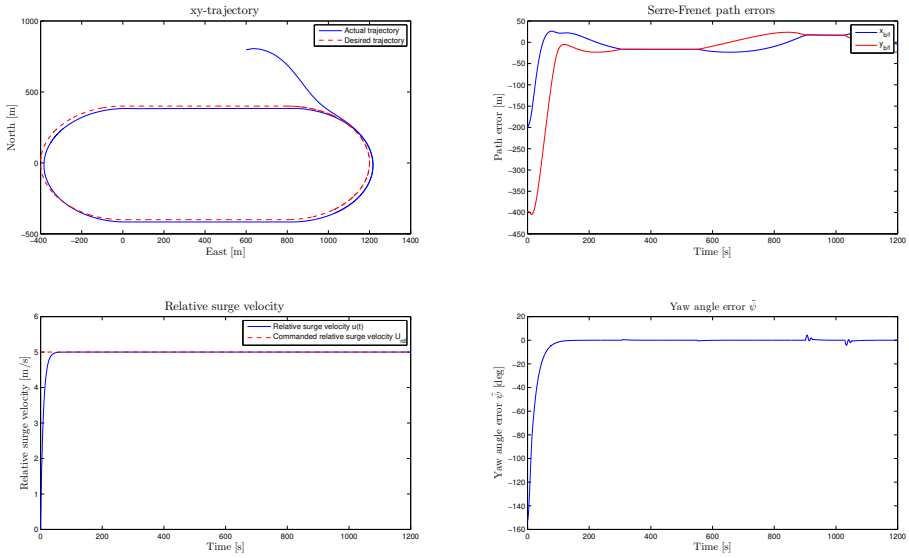

Figure 7.7: **Path 3** - Simulation results of original guidance and update law in the presence of unknown ocean currents.

7.1.5 Simulation results: Theorem 1

This chapter presents the simulation results of Theorem 1.

Path 1

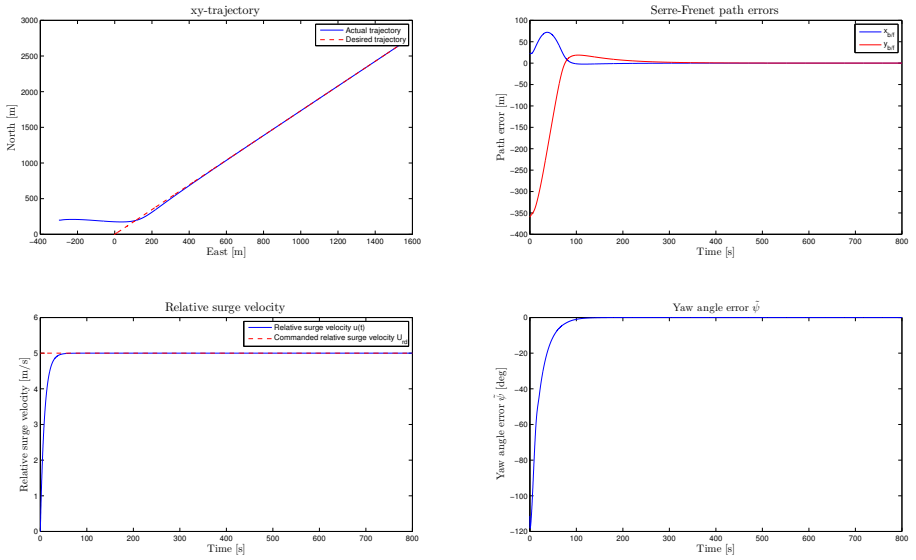

Figure 7.8: Actual versus desired trajectory, Serret-Frenet path errors, actual versus desired relative surge velocity and yaw angle error.

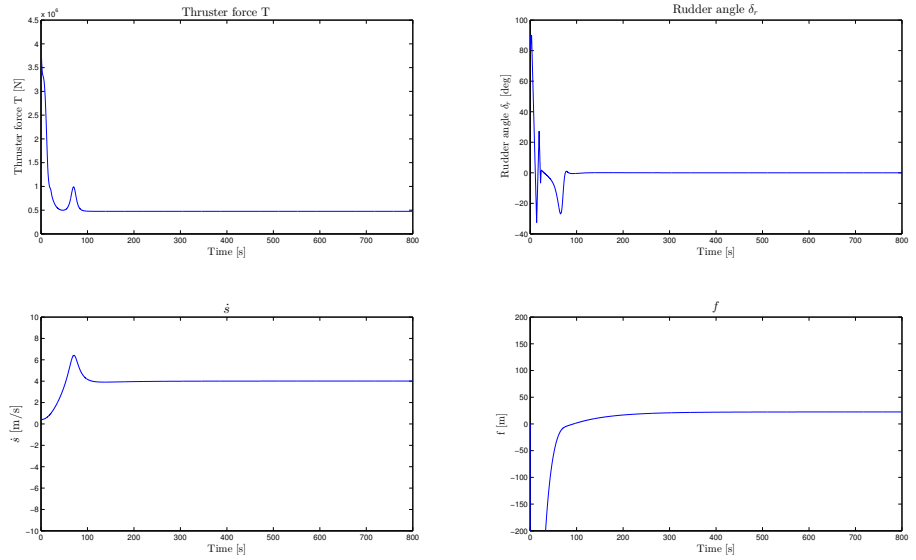

Figure 7.9: Thruster force, rudder angle, speed of Serret-Frenet frame along path and guidance law term f.

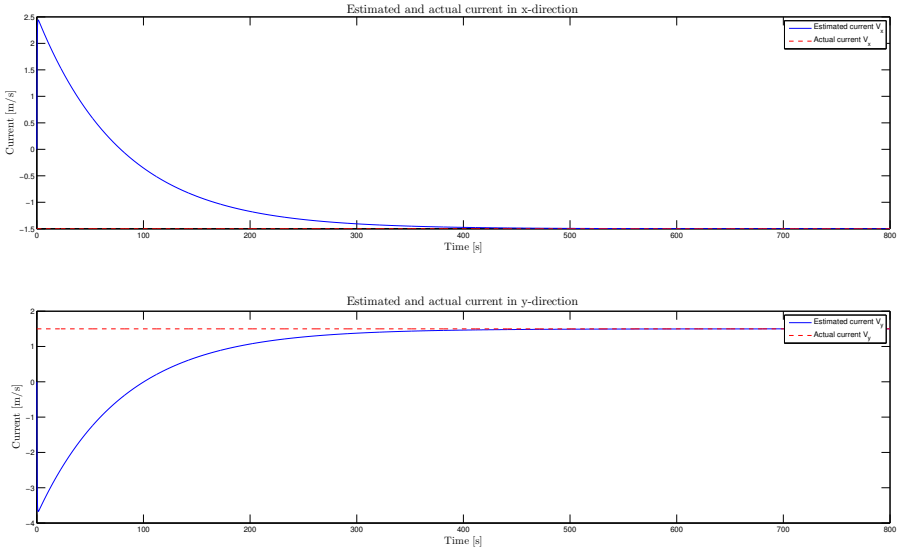

Figure 7.10: Actual versus estimated ocean current V_x and V_y.

Path 2

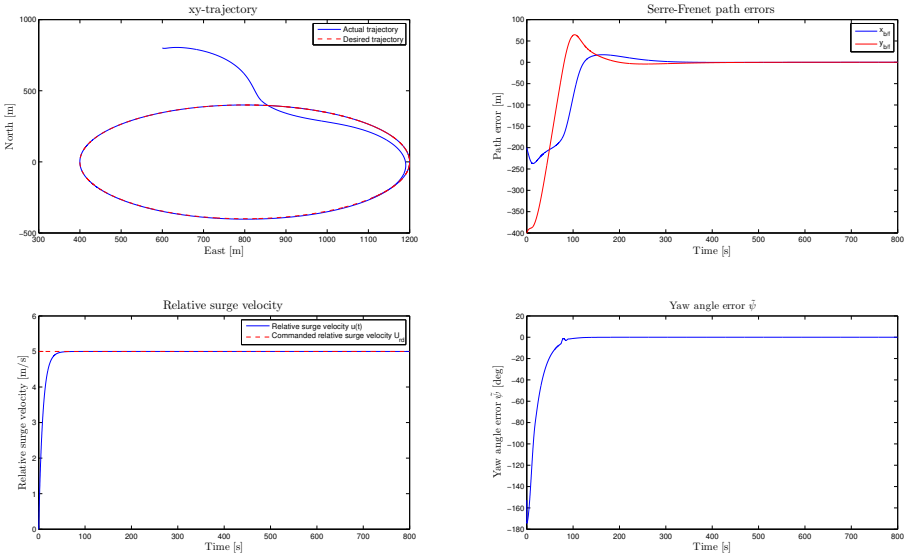

Figure 7.11: Actual versus desired trajectory, Serret-Frenet path errors, actual versus desired relative surge velocity and yaw angle error.

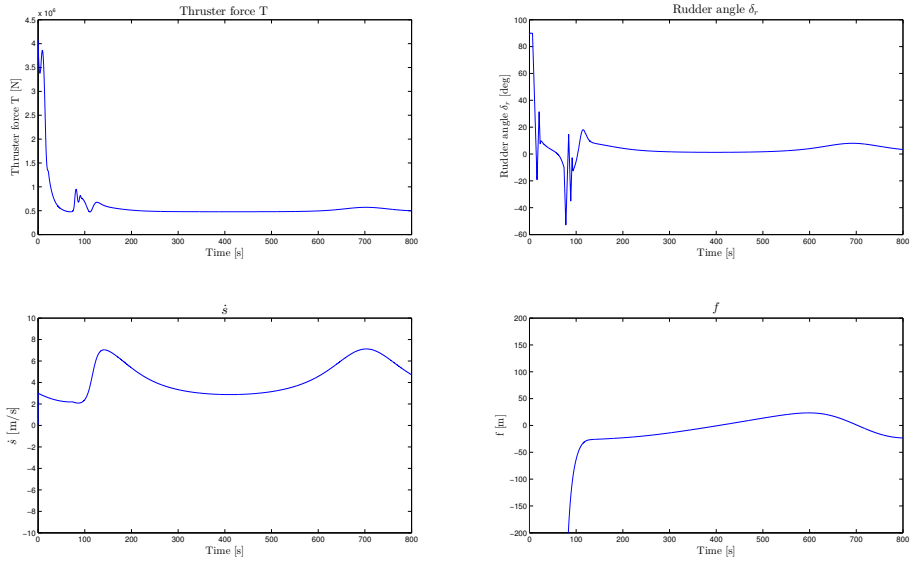

Figure 7.12: Thruster force, rudder angle, speed of Serret-Frenet frame along path and guidance law term f.

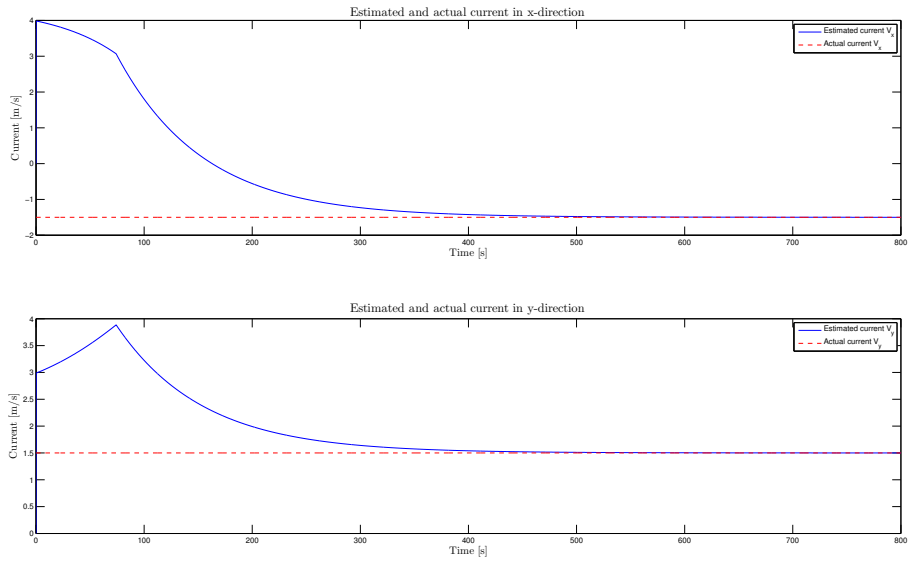

Figure 7.13: Actual versus estimated ocean current V_x and V_y.

Path 3

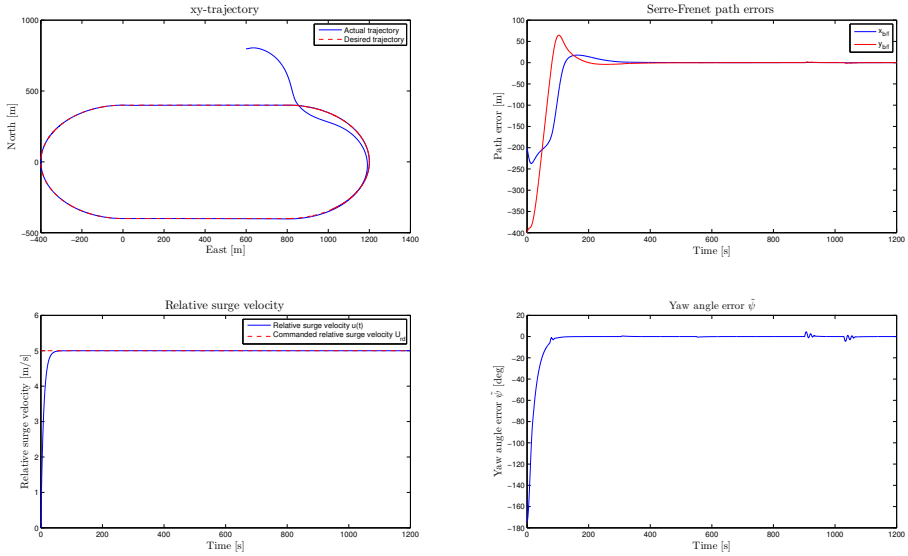

Figure 7.14: Actual versus desired trajectory, Serret-Frenet path errors, actual versus desired relative surge velocity and yaw angle error.

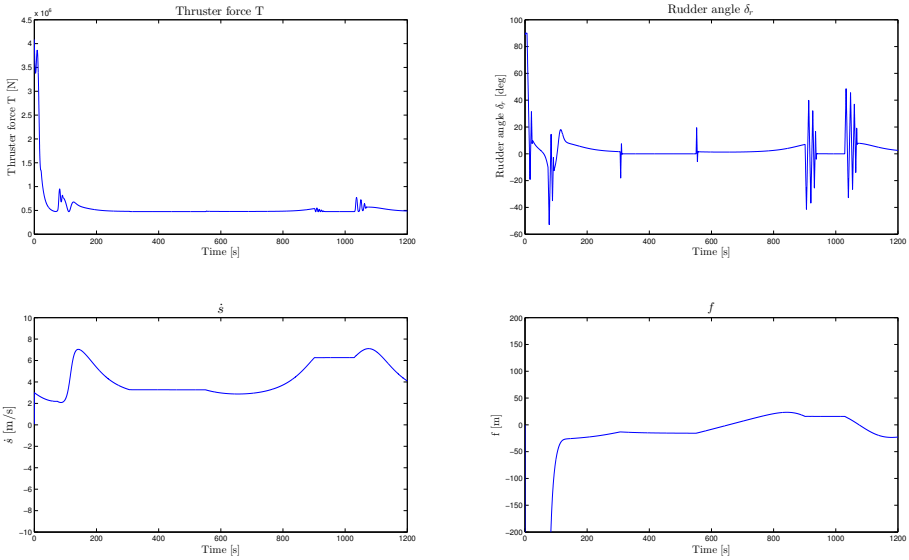

Figure 7.15: Thruster force, rudder angle, speed of Serret-Frenet frame along path and guidance law term f.

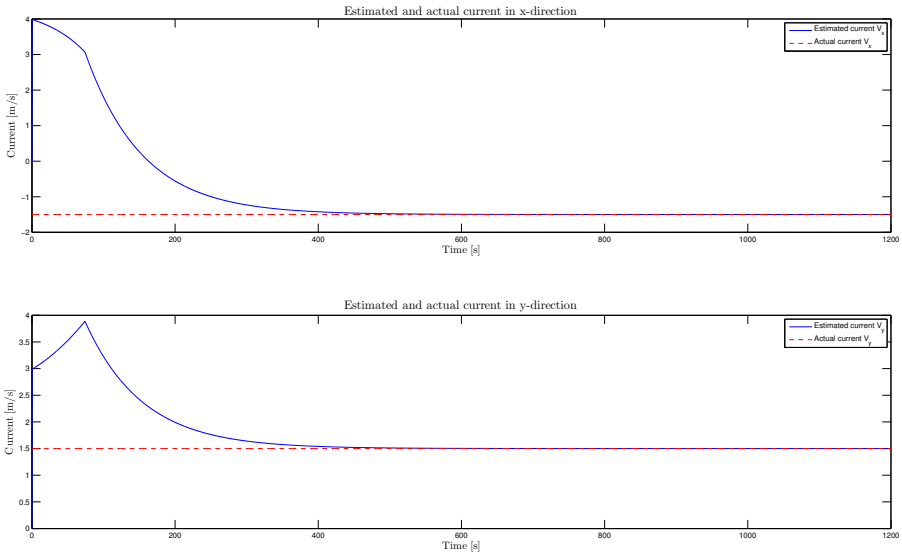

Figure 7.16: Actual versus estimated ocean current V_x and V_y.

7.2 Simulations on Hugin

7.2.1 Implementation

The implementation in Simulink is shown in figure 7.17 and is very similar to the implementation of the supply ship. The same color codes are used to simplify the block diagram.

The states $\boldsymbol{\eta} = [x, y, z, \theta, \psi]^T$ and $\boldsymbol{\nu}_r = [u_r, v_r, w_r, q, r]^T$ are computed in the block named "Hugin" based on the three controlled inputs T, δ_q and δ_r and ocean current. T, δ_q and δ_r are calculated by the controller system, which contains the feedback linearization surge controller described in chapter 5.2.1 and the integrator backstepping controller described in chapter 5.2.2. The desired relative surge velocity is still equal to a constant value U_{rd} and the guidance law calculates references for θ_{fc} and ψ_{fc}. The ocean current is estimated as described in chapter 3.4 in the block named "Ocean current observer".

The desired path is defined in the inertial coordinate system as $\boldsymbol{\eta}_f = [x_f, y_f, z_f, \phi_f, \theta_f, \psi_f]^T$ and is the output of the "Path coordinates" subsystem. This subsystem also calculates the path curvature and torsion $\mathcal{C}_f = [\kappa(s), \tau(s)]^T$, which is necessary in the integrator backstepping controller. The update law $\dot{s}$ is calculated and integrated to traveled distance s in the block called "Update law".

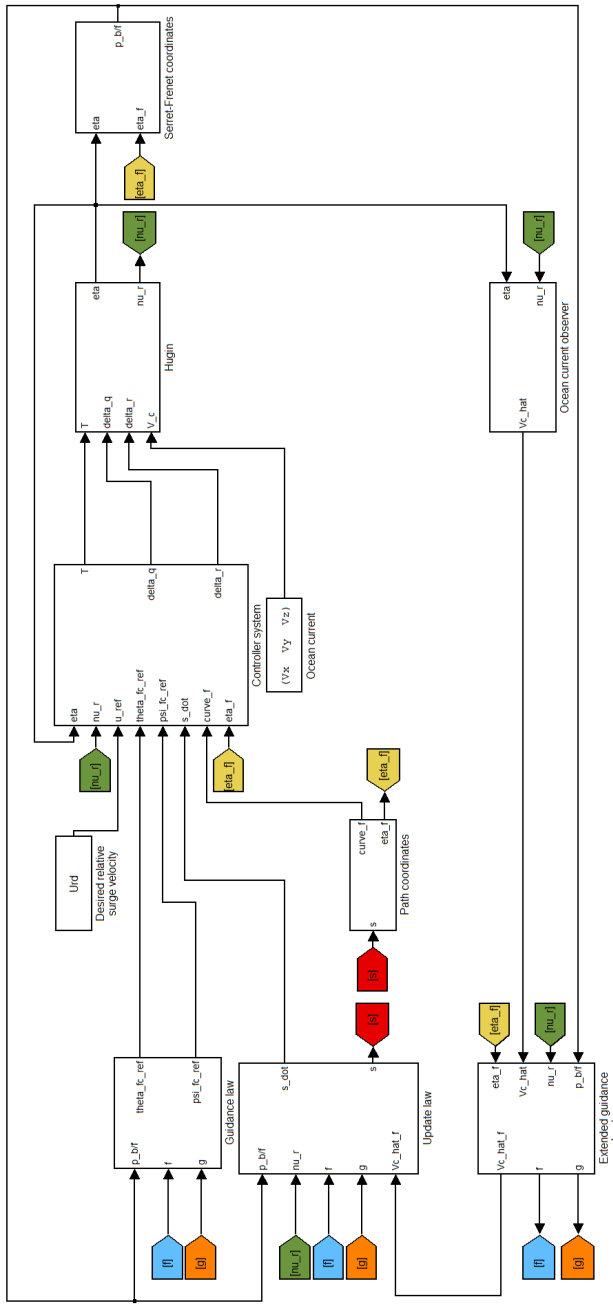

Figure 7.17: Simulink implementation of closed-loop system with Hugin, feedback linearization and integrator backstepping controllers and guidance and update law from Theorem 2.

As described in Theorem 2, one of the control objectives is to make $\boldsymbol{p}^f_{b/f} = [x_{b/f}, y_{b/f}, z_{b/f}]^T$ converge to zero. These terms are calculated in the block named "Serret Frenet coordinates" using equation 7.5.

$$\boldsymbol{p}^f_{b/f} = \begin{bmatrix} x_{b/f} \\ y_{b/f} \\ z_{b/f} \end{bmatrix} = [\boldsymbol{R}^i_f(\underbrace{\phi_f, \theta_f, \psi_f}_{\boldsymbol{\Theta}_{if}})]^T(\underbrace{\boldsymbol{p}^i_{b/i} - \boldsymbol{p}^i_{f/i}}_{\boldsymbol{p}^i_{b/f}}) = [\boldsymbol{R}^i_f(\boldsymbol{\Theta}_{if})]^T(\begin{bmatrix} x \\ y \\ z \end{bmatrix} - \begin{bmatrix} x_f \\ y_f \\ z_f \end{bmatrix}) \tag{7.5}$$

$\boldsymbol{p}^f_{b/f}$ is used in a feedback along with $\boldsymbol{\nu}_r$, $\hat{\boldsymbol{V}}_c$ and $\boldsymbol{\eta}_f$ to solve for the extended guidance and update law terms f, g and $\hat{\boldsymbol{V}}^f_c$ as described in chapter 6.2.

7.2.2 Desired path

In the simulations, 3 different paths have been implemented: A straight line, a circle in the plane and a helix. The parametrizations are presented below. In the case of underwater vehicles, the parametrizations also include the curvature $\kappa(s)$ and torsion $\tau(s)$. These are used in the integrator backstepping controller.

Path 4: Straight line The desired path is a straight line starting in the origin $(0, 0, 0)$ of the inertial system passes through the point $(a, 0, a)$. This corresponds to a constant attitude $\phi_f = 0°$, $\theta_f = -45°$ and $\psi_f = 0°$ as shown in figure 7.18.

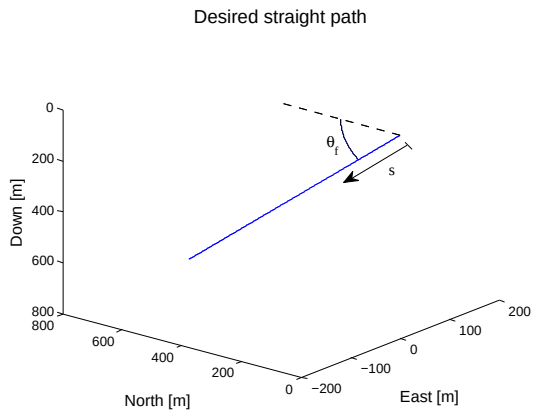

Figure 7.18: Illustration of the implemented desired straight path for Hugin.

$$
\begin{aligned}
x_f(s) &= s\cos(\theta_f) \\
y_f(s) &= 0 \\
z_f(s) &= -s\sin(\theta_f) \\
\phi_f(s) &= 0 \\
\theta_f(s) &= -\frac{\pi}{4} \\
\psi_f(s) &= 0 \\
\kappa(s) &= 0 \\
\tau(s) &= 0
\end{aligned}
\tag{7.6}
$$

Path 5: Circle in plane The desired path is a clockwise circle in the plane $z = 50$ m with radius $R = 400$ m and center in $(0, 0, 50)$ m.

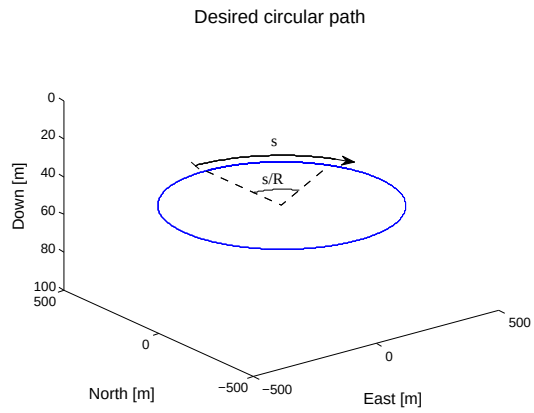

Figure 7.19: Illustration of the implemented desired circular path for Hugin.

$$
\begin{aligned}
x_f(s) &= R\cos\left(\frac{s}{R}\right) \\
y_f(s) &= R\sin\left(\frac{s}{R}\right) \\
z_f(s) &= 50 \\
\phi_f(s) &= 0 \\
\theta_f(s) &= 0 \\
\psi_f(s) &= \frac{s}{R} + \frac{\pi}{2} \\
\kappa(s) &= \frac{1}{R} \\
\tau(s) &= 0
\end{aligned}
\tag{7.7}
$$

Path 6: Helix The desired path is a clockwise helix moving downwards. The circle has radius $R = 400m$ and a vertical separation of $h = 40m$ between the helix loops.

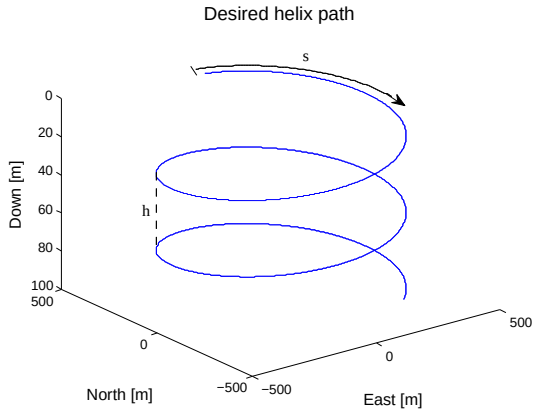

Figure 7.20: Illustration of the implemented desired helix path for Hugin.

$$
\begin{aligned}
x_f(s) &= R\cos\left(\frac{s}{\sqrt{R^2+\left(\frac{h}{2\pi}\right)^2}}\right) \\
y_f(s) &= R\sin\left(\frac{s}{\sqrt{R^2+\left(\frac{h}{2\pi}\right)^2}}\right) \\
z_f(s) &= \frac{h}{2\pi}\frac{s}{\sqrt{R^2+\left(\frac{h}{2\pi}\right)^2}} \\
\phi_f(s) &= 0 \\
\theta_f(s) &= -\arctan\left(\frac{\frac{h}{2\pi}}{R}\right) \\
\psi_f(s) &= \frac{s\cos(\theta_f(s)}{R}+\frac{\pi}{2} \\
\kappa(s) &= \frac{R}{\sqrt{R^2+\left(\frac{h}{2\pi}\right)^2}} \\
\tau(s) &= \frac{\frac{h}{2\pi}}{\sqrt{R^2+\left(\frac{h}{2\pi}\right)^2}}
\end{aligned}
\tag{7.8}
$$

7.2.3 Simulation parameters

In all simulations, the following parameters are used:

$$
\begin{array}{lll}
U_{rd} = 5\frac{m}{s} & \boldsymbol{V}_c = [0.5, -0.5, 0.5]^T \frac{m}{s} & V_{max} = 1\frac{m}{s} \quad \Delta = 50m \quad k = 0.2 \\
k_{u_r} = 0.1\frac{1}{s} & \boldsymbol{K}_1 = \boldsymbol{I} & \boldsymbol{K}_2 = \boldsymbol{I} \\
k_{x1} = 4\frac{1}{s} & k_{x2} = 0.05\frac{1}{s^2} & \\
k_{y1} = 4\frac{1}{s} & k_{y2} = 0.05\frac{1}{s^2} & \\
k_{z1} = 4\frac{1}{s} & k_{z2} = 0.05\frac{1}{s^2} &
\end{array}
$$

In addition, the motor thruster force is saturated at 80 kN and the rudders are saturated at $\pm\frac{\pi}{2}$ radians. The assumptions of Theorem 2 are not as straightforward to verify as those of Theorem 1. For one, Theorem 2 is valid only in the domain $\mathbb{D}$ defined by assumption **B1**. In retrospect the simulation results can determine whether or not this assumption is satisfied. Furthermore, assumption **B3** is applied in the stability proof and does not contain any explicit conditions that can be tested. The simulation parameters satisfy assumption **B2**: $0 \leq |\boldsymbol{V}_c| = \sqrt{0.5^2 + (-0.5)^2 + 0.5^2} = 0.866 < V_{max} = 1 \leq kU_{rd} = 1$. This saturation is used on the estimated of the current, so $0 \leq |\hat{\boldsymbol{V}}_c| < V_{max} \leq kU_{rd}$.

7.2.4 Simulation results: Original Guidance and Update Law

The original guidance and update law of Børhaug discussed in chapter 3.7 was simulated by setting the output of the "Extended guidance law terms"-block in figure 7.1 identically equal to zero.

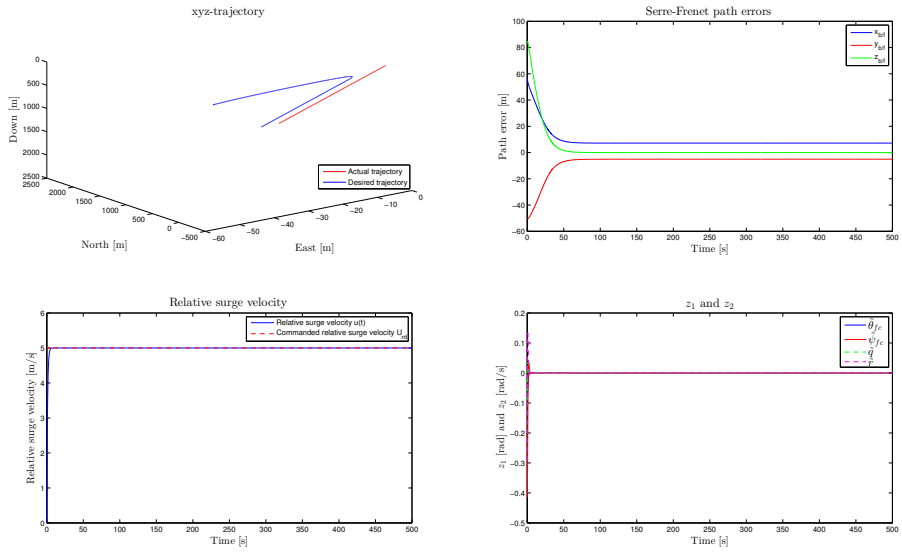

Figure 7.21: **Path 4** - Simulation results of original guidance and update law in the presence of unknown ocean currents.

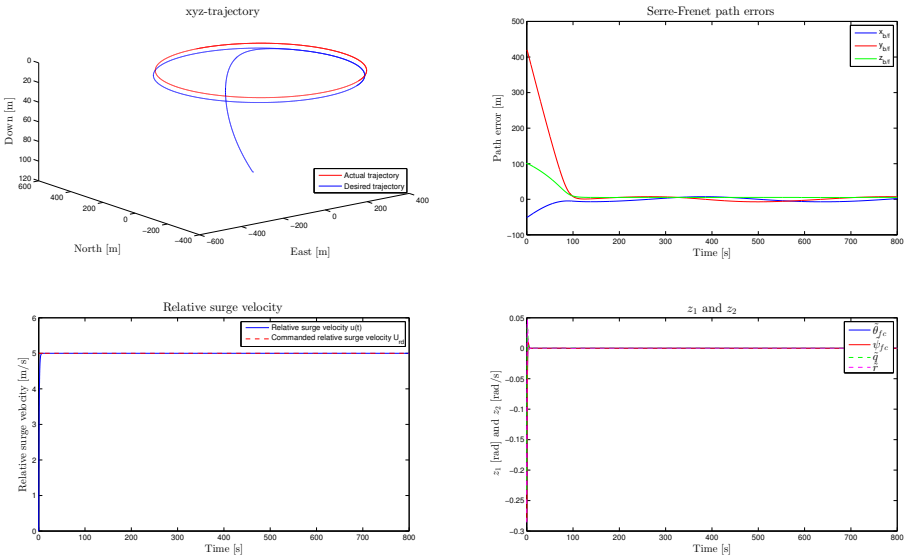

Figure 7.22: **Path 5** - Simulation results of original guidance and update law in the presence of unknown ocean currents.

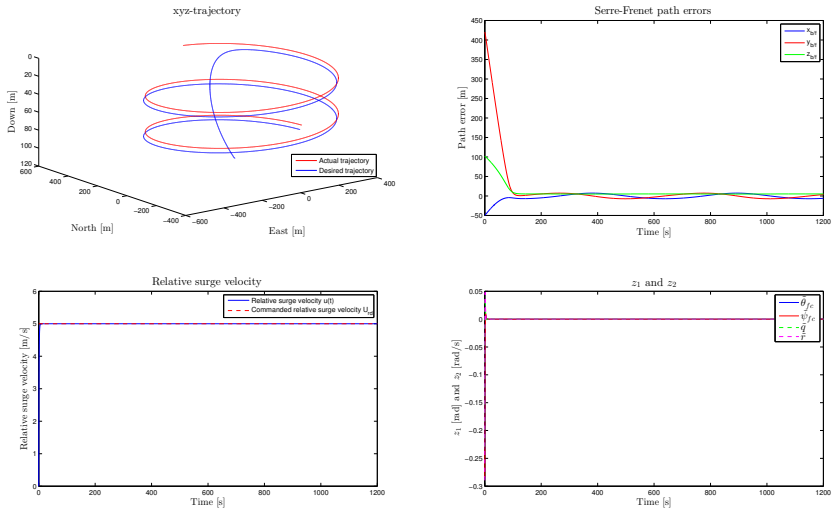

Figure 7.23: **Path 6** - Simulation results of original guidance and update law in the presence of unknown ocean currents.

7.2.5 Simulation results: Theorem 2

This chapter presents the simulation results of Theorem 1.

Path 4

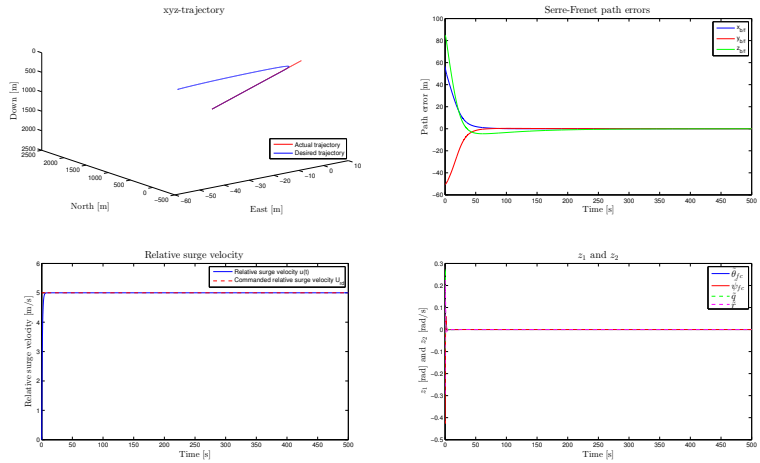

Figure 7.24: Actual versus desired trajectory, Serret-Frenet path errors, actual versus desired relative surge velocity and errors $\boldsymbol{z}_1$ and $\boldsymbol{z}_2$.

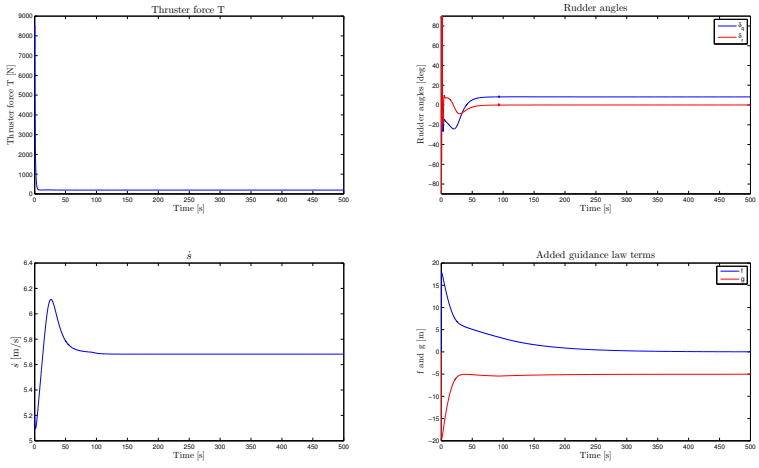

Figure 7.25: Thruster force, rudder angles, speed of Serret-Frenet frame along path and guidance law terms f and g.

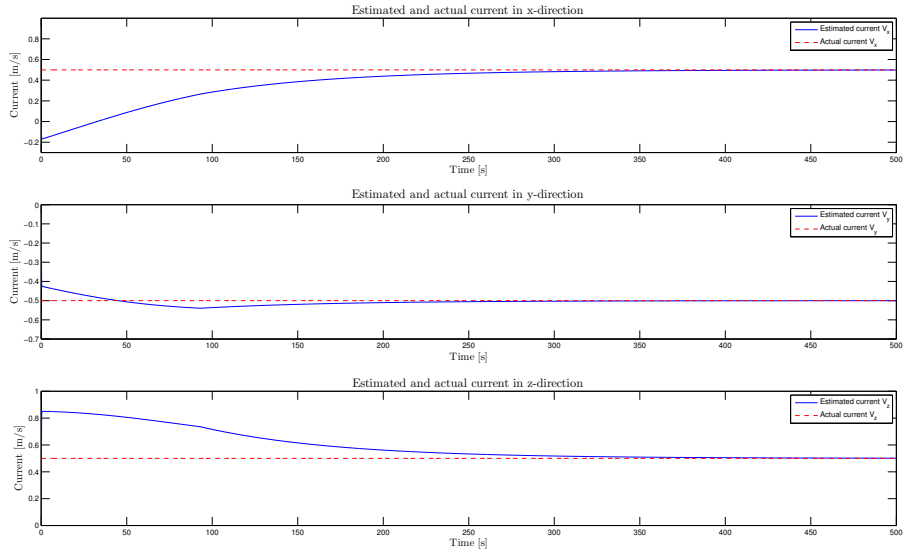

Figure 7.26: Actual versus estimated ocean current V_x, V_y and V_z.

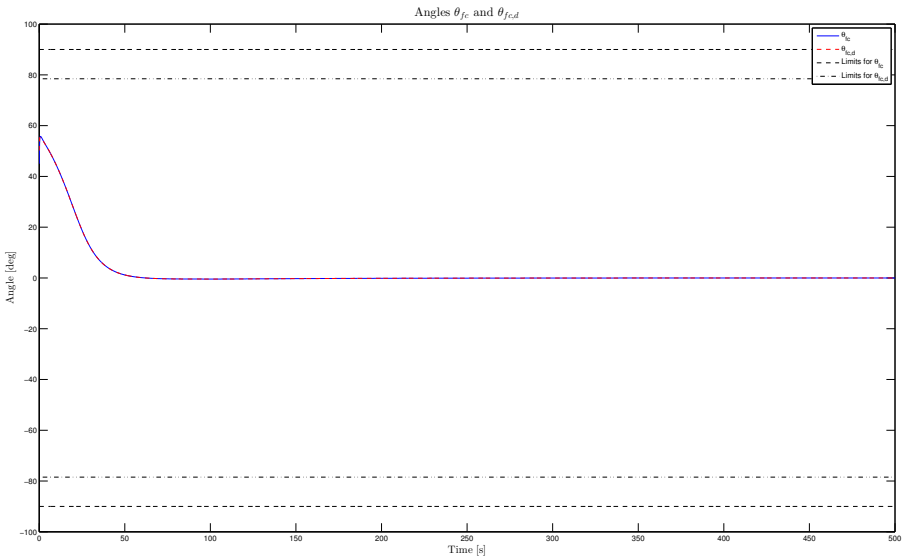

Figure 7.27: Relative orientation θ_{fc} and $\theta_{fc,d}$ and their respective limits that define $\mathbb{D}$.

Path 5

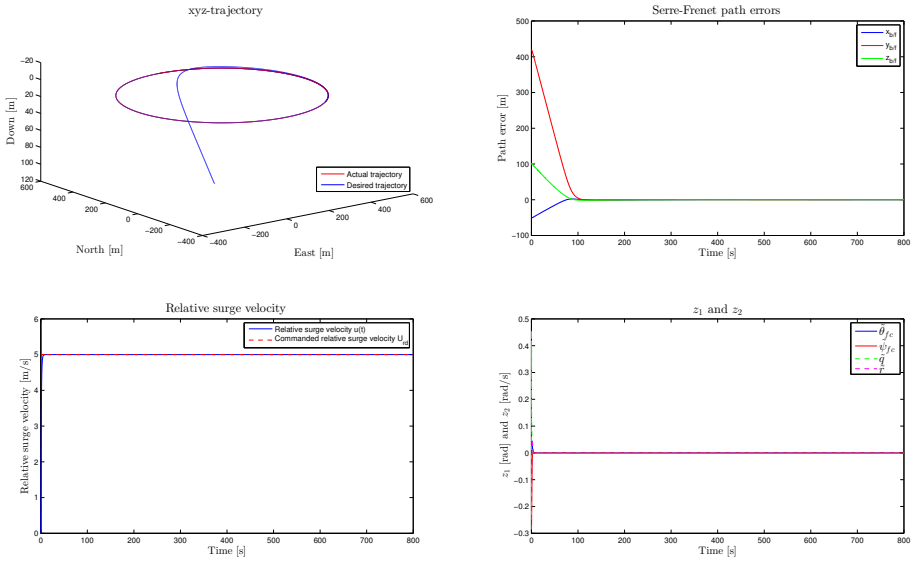

Figure 7.28: Actual versus desired trajectory, Serret-Frenet path errors, actual versus desired relative surge velocity and errors $\boldsymbol{z}_1$ and $\boldsymbol{z}_2$.

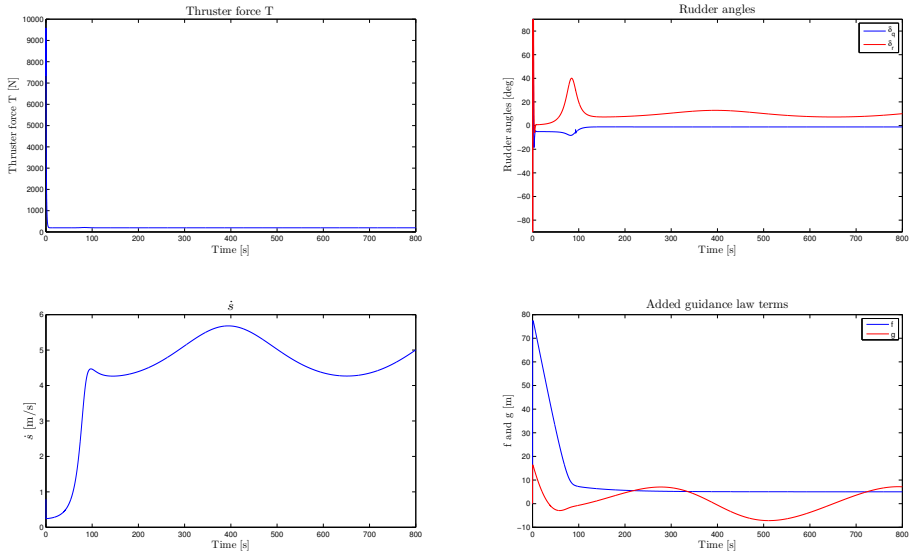

Figure 7.29: Thruster force, rudder angles, speed of Serret-Frenet frame along path and guidance law terms f and g.

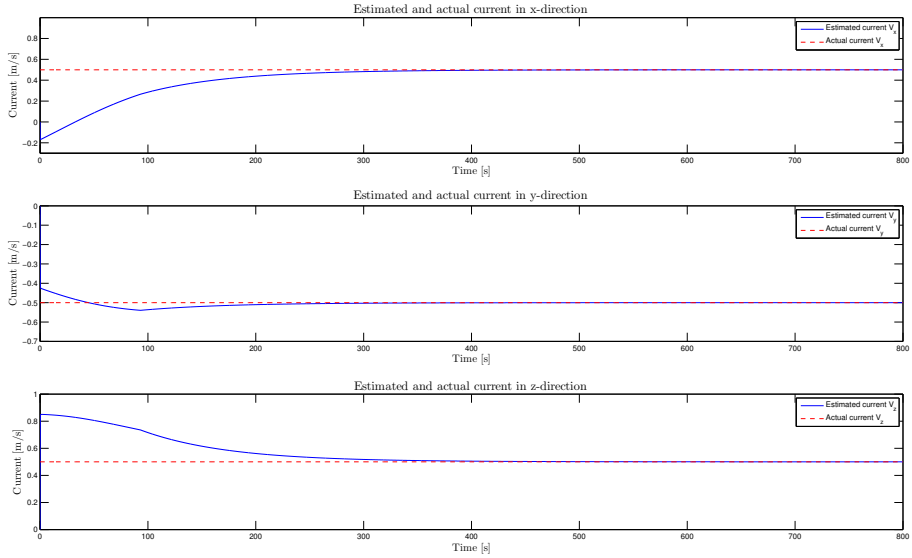

Figure 7.30: Actual versus estimated ocean current V_x, V_y and V_z.

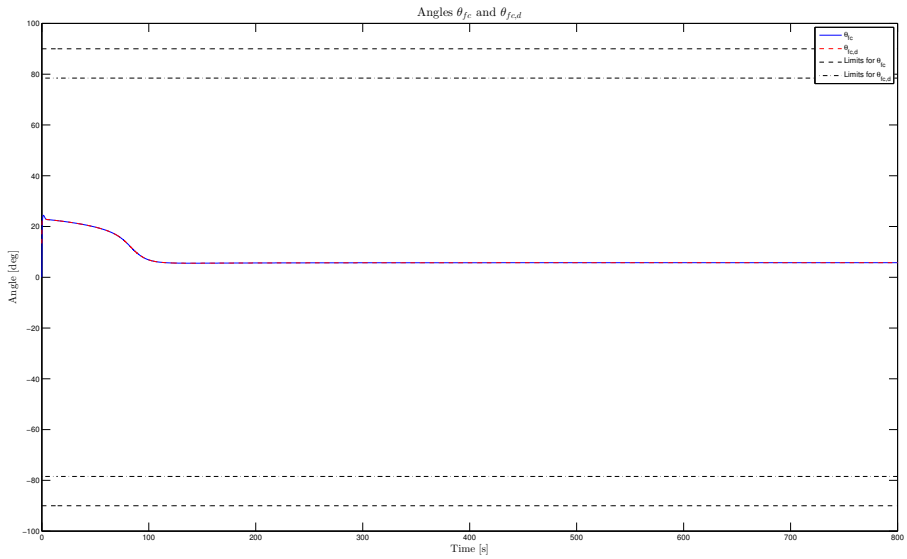

Figure 7.31: Relative orientation θ_{fc} and $\theta_{fc,d}$ and their respective limits that define $\mathbb{D}$.

Path 6

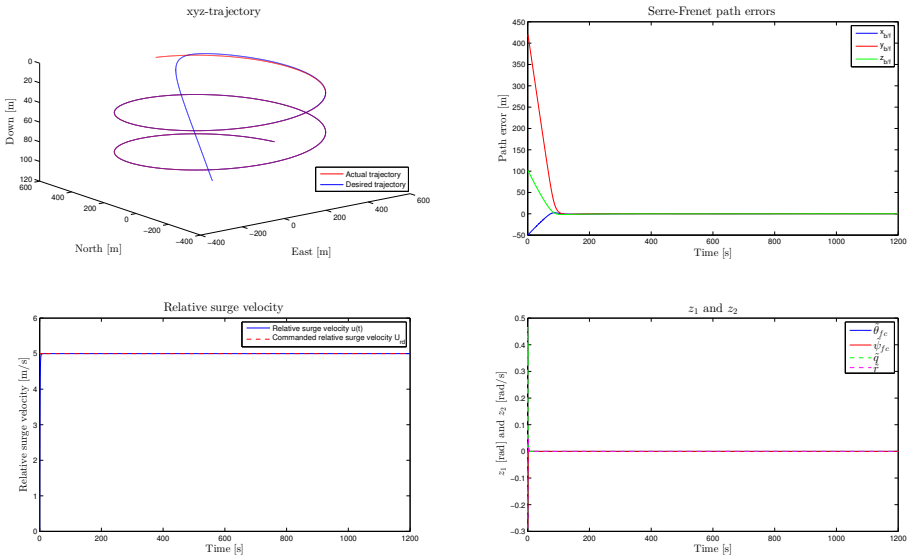

Figure 7.32: Actual versus desired trajectory, Serret-Frenet path errors, actual versus desired relative surge velocity and errors $\boldsymbol{z}_1$ and $\boldsymbol{z}_2$.

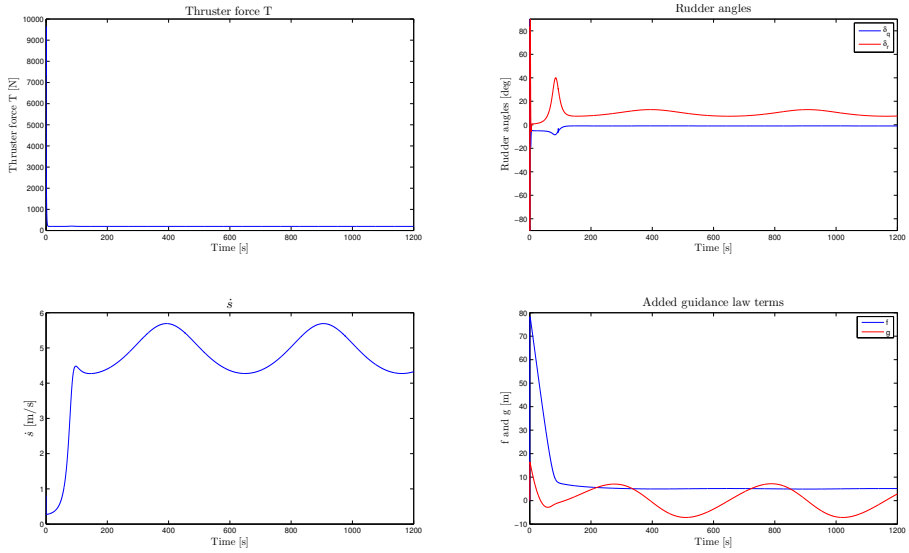

Figure 7.33: Thruster force, rudder angles, speed of Serret-Frenet frame along path and guidance law terms f and g.

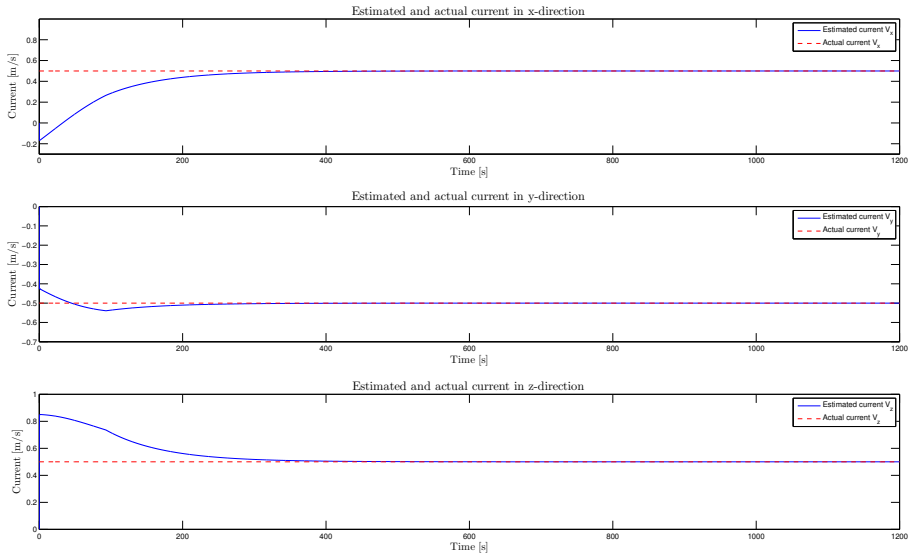

Figure 7.34: Actual versus estimated ocean current V_x, V_y and V_z.

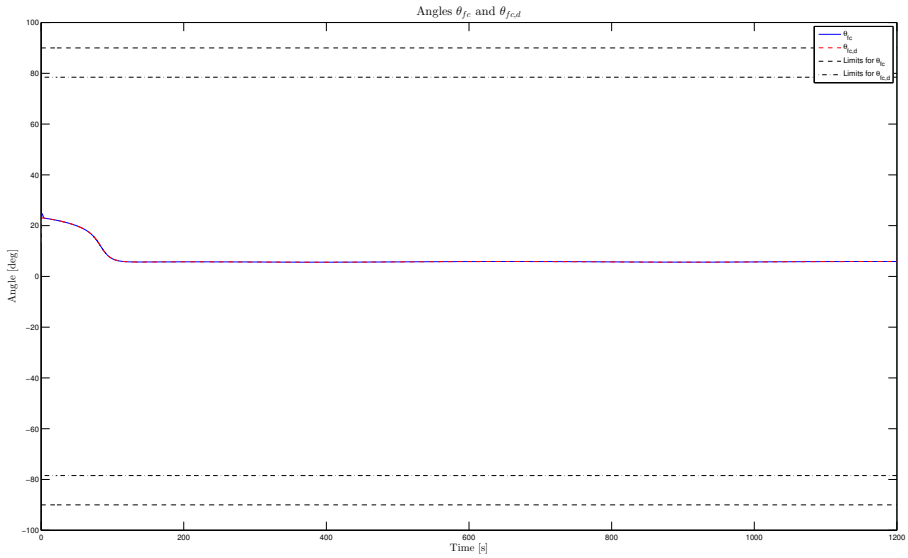

Figure 7.35: Relative orientation θ_{fc} and $\theta_{fc,d}$ and their respective limits that define $\mathbb{D}$.

7.3 Simulations with Modeling Errors

Theorem 1 and 2 were simulated with an incorrect vessel model in the feedback linearization controllers and integrator backstepping controllers. As such, the model used in the controllers to cancel non-linearities and ensure tracking of the references is slightly different than that of the actual vessel, and some of the non-linear effects will not be canceled from the dynamics. The model in the controller has the same structure as the supply ship, but the numeric values have been changed by as much as $\pm 40\%$ of their correct value.

Simulations were run with all of the desired paths for both Hugin and the supply ship. However, only a few results are included in this chapter due to the unanimity of the results and the fact that modeling errors are not the main focus of this thesis. Hence, the results shown below are representative responses for all the conducted simulations.

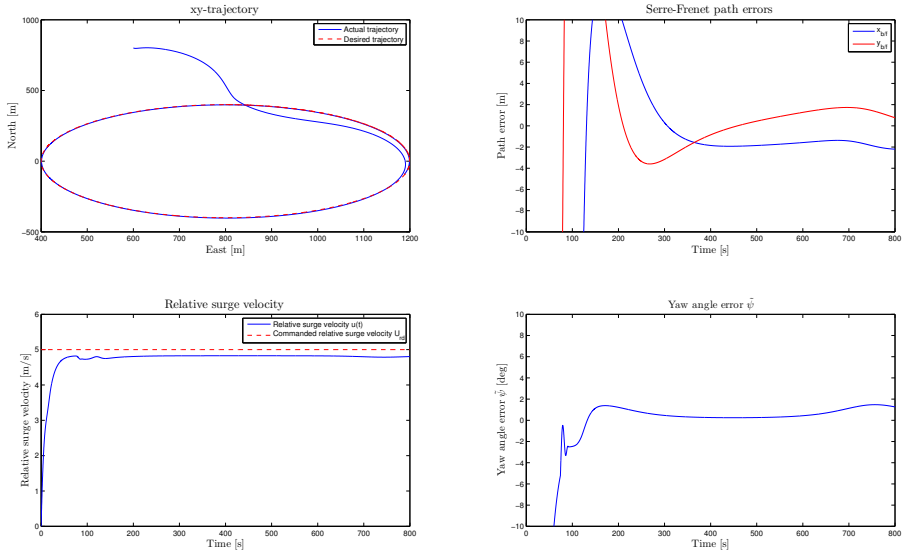

Figure 7.36: Actual versus desired trajectory, Serret-Frenet path errors, actual versus desired relative surge velocity and yaw angle error of supply ship with modeling error in controller.

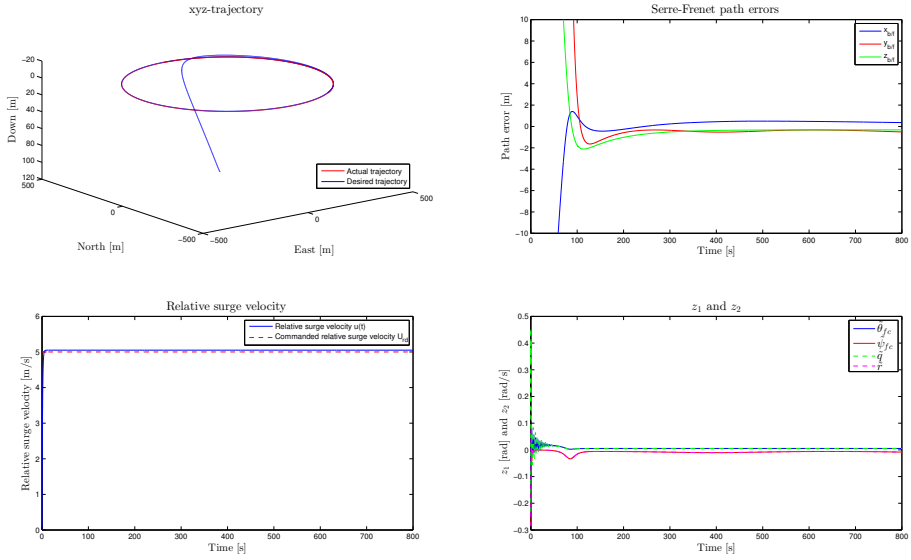

Figure 7.37: Actual versus desired trajectory, Serret-Frenet path errors, actual versus desired relative surge velocity and errors $\boldsymbol{z}_1$ and $\boldsymbol{z}_2$ of Hugin with modeling error in controller.

Chapter 8

Discussion

8.1 Basis for this thesis

The preliminary objective of this thesis was guidance and control of marine vehicles with the goal of following a general path in the presence of unknown ocean currents. A possible approach was to use Line of Sight guidance scheme described in chapter 3.6 as a starting point. This is a widely used method, and the literature review concluded that there are several established LOS guidance laws for path following of straight lines and circular paths. Furthermore, there exists a LOS strategy with integral effect that allows for straight line path following in the presence of unknown, constant, irrotational ocean currents. However, the LOS approach requires calculation of the cross-track error e and the path heading $\chi_p(t)$ based on the marine vessel position. This is straightforward when considering geometrically simple paths such as a line or circle, but can be difficult for a general curved path. Furthermore, the integral LOS technique is based on straight line path following in the presence of currents. In this case, the necessary side-slip angle to counteract the current and follow the desired path is constant since the current is constant and attacks the marine vehicle from the same direction when following the straight line. As such, the integral effect converges to this stationary side-slip angle. However, when the desired path is not straight, the current will affect the vessel from different directions along the path, and the necessary side-slip angle is no longer constant. As such, an integral effect will not be able to stabilize on a given value. Based on this, LOS was discarded as a basis for this thesis.

The path following methods of Even Børhaug [6] described in chapter 3.7 ensure path following of continuously differentiable curves for both surface and underwater vehicles when no ocean current is present. In this approach, the desired path coordinates are parametrized as a function of the traveled distance s along the path, which allows for relative easy modeling of a general curved path. As such, these methods were assessed to be an excellent basis for the challenge addressed in thesis, and the goal was to expand the guidance and update laws of Børhaug to

achieve path following also when ocean currents affect the vessel in question.

The literature review revealed that marine vessels, underwater vehicles in particular, have numerous potential applications within research and industry, and that such vessels are becoming increasingly more autonomous. General path following in the presence of unknown ocean currents forms the basis for numerous, more complex marine operations. Hence, it is highly applicable ability in a real-life scenario.

8.2 Simulation Results of Original Guidance and Update Law

The path following methods discussed in chapter 3.7 were implemented in Simulink for both the supply ship and Hugin. As expected, the control objectives were satisfied when there was no ocean current. However, as can be seen in figure 7.5-7.7 and 7.21-7.23, exact path following is not achieved in the presence of ocean current for neither the surface or underwater vehicle even though the controllers ensure that the controlled states converge to their respective references.

In the case of the surface ship, $u_r(t)$ reaches U_{rd} and the yaw angle error $\tilde{\psi} = \psi - \psi_d$ quickly converges to zero for all three paths (figure 7.5-7.7). However, the actual and desired trajectories do not coincide, and the Serret-Frenet path errors $x_{b/f}$ and $y_{b/f}$ do not stabilize at zero. Rather, the actual trajectories have the correct shape but are displaced slightly to the southeast. This is due to the fact that the ocean current in the simulations has a southeast direction.

The same effect can be observed on Hugin in figure 7.21-7.23: $u_r(t)$ reaches U_{rd}, the error signals $\boldsymbol{z}_1$ and $\boldsymbol{z}_2$ in the backstepping controller converge to zero, and yet there are deviations between the desired and actual path. Hence, we can conclude that the guidance laws don't calculate the reference states that would result in exact path following. As such, they need to be expanded to compensate for the ocean current.

8.3 Simulation Results of Theorem 1 and 2

Theorem 1 and 2 both presume that certain assumptions are satisfied. Theorem 1 poses several explicit conditions that are straightforward to verify. This is done in chapter 7.1.3. As for Theorem 2, the increased complexity of an underwater vehicle system makes it difficult to find similar explicit conditions, and as such a domain $\mathbb{D}$ in which Theorem 2 is valid is defined. As can be seen in figure 7.27, 7.31 and 7.35, all Hugin simulations are within $\mathbb{D}$.

The simulation results are shown in figure 7.8-7.16 for the supply ship and figure 7.24-7.35 for Hugin. The ship and Hugin both converge to and track the desired

path with the relative surge velocity U_{rd}. The Serret-Frenet path errors converge to zero in all simulations. Hence, the control objectives are achieved. The simulations show that it takes some time for the vessel to converge to the desired path. It is worth noting that path convergence coincide with the ocean current estimates settling at the correct values. This is of course to be expected since the estimated current is used in the guidance law to counteract the actual current. As such, the correctness of the current observer is extremely important to achieve the control objectives.

In all simulations controlled inputs (the thruster force and rudder angle(s)) are reasonable. A common effect is that the rudder angle(s) fluctuates during the first seconds of simulation. This is due to the step in the references to the controller (ψ_d for the supply ship and $\theta_{fc,d}$ and $\psi_{fc,d}$ for Hugin) that occurs at start-up. One way to avoid this phenomena is to run the simulation for a few seconds to let all signals initialize and stabilize before closing the loop and connecting the controllers. Furthermore, a rate limitation on the input to the controllers can be used to avoid abrupt changes in the references that will result in a unrealistic controller output. When disregarding the fluctuations in the initialization of the simulations, the rudder angles and thruster force are as expected. For instance, the rudder angle of the supply ship converges to zero when following a straight line (figure 7.9), whereas it is nearly constant when following a circluar path (figure 7.12). As the ship moves along the path, the ocean current affects the body from different directions, resulting in a slightly varying rudder angle to counteract this effect. As for the piecewise circular path, the rudder experiences some fluctuation even after the ship converges to the desired path (figure 7.15). This coincides with the transition between the straight and circular parts of the path, during which the desired way rate $\dot{\psi}_d$ experiences a leap from zero to a non-zero value. Although the rudder response to this may appear turbulent, it is important to note that the rudder is rate limited and can only change approximately 10 degrees per second at most, making the response realistic in a real-life scenario.

The plots marked $\dot{s}$ show the evolution of the update law over time, that is the velocity of the Serre-Frenet reference frame along the desired path. The control objective is to make the marine vessel in question move to and stay in the origin of this reference frame. As such, if $\dot{s}$ was identically equal to zero, the reference frame would be stationary and the ship/Hugin would reach a stand-still position. Consequently the update law is crucial to drive the reference frame forward and ensure path following. In the original update laws of Børhaug $\Big($equation (3.37) and (3.43)$\Big)$, $\dot{s}$ would stabilize at $U_c = \sqrt{U_{rd}^2 + v_r^2 + w_r^2}$ regardless of the desired path. In Theorem 1 and 2, however, $\dot{s}$ includes the term $\hat{V}_x^f$. When following a straight line, the current always affects the Serret-Frenet frame from the same angle. As such, $\hat{V}_x^f$ is constant once $\hat{V}_x$ converges to the correct value, and $\dot{s}$ stabilize at a constant value as can be seen in figure 7.9 and 7.25. When following a circle or a helix, the current affects the Serret-Frenet frame from different directions as the

path progresses. As such, $\hat{V}_x^f$ will vary similar to a cosine signal along the path and $\dot{s}$ will not stabilize at a constant value as seen in figure 7.12, 7.29 and 7.33. As for the athletics track (figure 7.15), $\dot{s}$ is constant along the straight lines of the path and varying along the circular ones. The same effect can be observed in the extended guidance law terms f and g, which are calculated based on $\hat{V}_y^f$ and $\hat{V}_z^f$.

8.4 Assumptions and Limitations

Theorem 1 and 2 are subject to several assumptions and limitations. For instance, both theorems assume that the vessel in question can be modeled in a certain way, which naturally limits the selection of marine vessels to which the theorems are applicable. The model for the surface ship in Theorem 1 is relatively general, whereas Theorem 2 assumes a 5 DOF underwater vehicle model with roll passively stabilized. This simplifies the model, but also renders it less general. However, this is a common assumptions in maneuvering control of torpedo-shaped AUVs like Hugin. Such symmetric slender body AUVs are naturally buoyant with the CG directly below CB, as can be seen by the $\boldsymbol{g}$-matrix of the model. As such, if the AUV experiences a slight roll motion, this will create a torque that drives the roll towards zero. This is illustrated in figure 8.1.

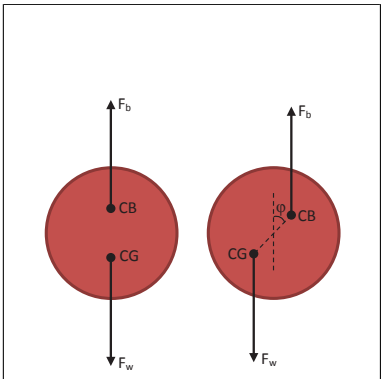

Figure 8.1: Cross-section of Hugin. When the AUV has a roll $\phi \neq 0$, the force of buoyancy and gravity results in a torque that drives the ϕ toward zero, passively stabilizing the roll.

Furthermore, Theorem 2 is restricted to a defined domain $\mathbb{D}$. In this domain, $|\theta_{fc}| < \pi/2$ and $|\theta_{fc,d}| < \arccos(k)$ for some $0 < k < 1$. The restrain on θ_{fc} is due to the well-known singularity in Euler angle representations that arises at $\theta = \pm\pi/2$. The constraint on $\theta_{fc,d}$ is more restrictive and discussed below.

Both theorems require a continuously differential path. Although this does not seem like a limitation of significance, it does exclude simple paths such as a square. In the square corners ψ_f will experience a leap of $\pm\pi/2$ radians, $\kappa = \infty$ and/or $\tau = \infty$, making the kinematics for $\dot{x}_{b/f}$, $\dot{y}_{b/f}$ and $\dot{z}_{b/f}$ also go to infinity. As such, this method is made for path following of smooth curves without any "kinks". However, it is possible to implement path following of a square by enforcing a temporary stop in the corners where the vessel gradually turns in the new desired direction by allowing the references to the controllers change slowly rather than changing them instantly.

Furthermore, the developed theorems rely on a current observer. The basis for this observer is to estimate both position and current by comparing the estimated position to the measured position. In a way, this observer is very simple and intuitive. It requires measurements/estimates of position, attitude and relative linear velocities. This information is already necessary for the guidance law, update law and controllers in both theorems, so the observer does not require any additional sensors or information beyond what is already required.

The current is assumed constant, irrotational and bounded in the intertial frame. As mentioned in the chapter 2, a constant, irrotational ocean current model is often used in marine maneuvering control problems. Theorem 1 assumes that the total current upper bounded by a known V_{max}, which is less than or equal to the desired relative surge velocity U_{rd}. This demand is not to strict since U_{rd} is chosen by the human operators. Furthermore, the ocean current must be limited relative to U_{rd} to prevent the vessel from drifting away. However, for some applications it may be desirable to have a low U_{rd}, in which case this limitation can be problematic. For instance, if an underwater vehicle such as Hugin is to be used for a pipeline inspection, a low velocity along the line to ensure proper inspection is desirable. Theorem 2 assumes that V_{max} is less than or equal to kU_{rd} for some $0 < k < 1$. As such, this is a stricter demand than that of Theorem 1. Of course, by choosing k close to 1, this condition is close to that of Theorem 1. However, as discussed above, k also limits $\theta_{fc,d}$, so by choosing a large k the valid interval for $\theta_{fc,d}$ is much smaller.

The current estimates are saturated at V_{max}. However, this does not affect the stability of the observer due to the face that the saturation is imposed after the feedback loop of the observer, see figure 8.2.

Figure 8.2: Illustration of saturation in current observer.

It is worth noting that the correctness of Theorem 1 and 2 is maintained as long as the current and current estimates are upper bounded by V_{max} and assumption **A4**/**B2** holds. As such, *the ocean current is not actually required to be constant* in order for Theorem 1 and 2 to be applicable, as long as it fulfills assumption **A4**/**B2** at all times. The current observer is known UGES and will estimate the correct current regardless of variations in this.

8.5 Simulation Results with Modeling Errors

When developing a new theorem it is necessary to first confirm its correctness under ideal circumstances. If the control objectives fail to be achieved under perfect conditions, it is certain that they will not be achieved in a real-life situation where circumstances are not optimal. As such, the main result of this thesis are Theorem 1 and 2 and the simulations of these under ideal circumstances. However, as a small test a few simulations were run with an erroneous vehicle model in the controller. Exact modeling of a marine vessel is extremely difficult, and often several simplifications are made that are not always correct in real life. Both the feedback linearization controllers and integrator backstepping controller used in Theorem 1 and 2 are known to be vulnerable to modeling errors. In the simulations, the vessel model used by the controller has the same structure as the actual vessel model, but the numeric values are incorrect. The result are shown in figure 7.36 and 7.37 and show that both the supply ship and Hugin are able to follow the desired path closely, but not completely. The path errors don't to converge to zero, but vary somewhere between 0 and 2 meters. Also, the desired relative surge velocity is not reached, and the controllers fail to drive the other controlled states to their respective references. These errors will only increase with the modeling errors in the controller. Hence, the simulations confirm that the controllers are susceptible to modeling errors. Furthermore, they are computationally expensive and include several operations of derivation, making them sensitive to measurement noise. As such, if very exact path following is required or in case of a high degree of model uncertainty, other controllers should be considered.

8.6 Improvment/Future Work

In Theorem 1 and 2, the guidance law, update law, controllers and current observers require that all states of the marine vessel are known. In the simulations, all states are assumed measured without noise, but in real-life applications this is not the case. Often only some states are measured, whereas others are simply estimated using a Kalman filter or another observer. This is done in the Navigation-block in the GNC-system described in chapter 2.8. Real-life measurements are always affected by a certain measurement noise and uncertainty.

The ultimate goal is to develop a guidance and control system that can be utilized in a real-life marine operation. Based on this, a number of measures to make the simulations more realistic are suggested as future work. If these simulations yields a satisfactory result, the next step is to implement and test the guidance and update law on a real ship/AUV.

- Replace the ideal feedback linearization and integrator backstepping controllers with more realistic PID-controllers.
- Assume only some states measured and add a Kalman-filter or another observer to estimate the remaining states.

- Add some measurement noise to the measured states to simulate realistic variations from sensor data.
- Replace/supplement the current observer with estimated current from DVL-measurements (chapter 3.4).
- Simulate with slowly varying current.

In addition, future work includes deriving explicit conditions to ensure that the closed loop system in Theorem 2 is always within the valid domain $\mathbb{D}$ and expanding the theorems to handle a time-varying desired relative surge velocity $u_{rd}(t, s)$. The latter is fairly straightforward to accomplish. Furthermore, it is desirable to prove stability of the entire cascaded system in Theorem 2 (chapter 6.2) and exponential stability of the cascaded system in Theorem 1.

Chapter 9

Conclusion

The use of marine vessels for (remote) inspection and similar missions is increasing rapidly and there are still challenges related to autonomous tracking tasks, especially for underwater vehicles. The application of AUVs are relevant within several fields of study, for instance for scientific, environmental and military use.

The goal of this thesis was to develop a guidance and control system for a marine vessel with the goal of following a general path in the presence of unknown ocean current. This has been accomplished with good results. The path following methods of Børhaug [6] described in chapter 3.7 forms the basis for this thesis, and by expanding these guidance and update laws and combining them with an ocean current observer two theorems have been developed, one applicable to underactuated surface vessels (Theorem 1) and one to underactuated underwater vehicles (Theorem 2).

The developed theorems assume that the marine vessels can be modeled in a certain way and include both a guidance law and controllers that guarantee convergence to the desired path given that certain assumptions are satisfied. In both these theorems, the desired path is parametrized as a function of the traveled distance s along the path, and a virtual Serret-Frenet reference frame propagating along the desired path with velocity $\dot{s}$ is introduced. Theorem 1 guarantee achievement of the control objectives with uniform global asymptotic stability, whereas Theorem 2 guarantee asymptotic path following within a defined domain $\mathbb{D}$. The controllers are feedback linearization and integrator backstepping controllers and utilize the vessel model to cancel nonlinearities in the vessel dynamics.

Both theorems have been verified through implementation in Simulink and simulated for several desired paths. This implementation consists of

- The marine vessel model (supply ship and Hugin).
- Controllers.

- Guidance law.
- Update law.
- Current observer.

The simulations show that the marine vessel converges to and tracks the desired path under the conditions of the Theorem 1 and 2 and confirm the correctness of the developed theorems. However, simulations also reveal that the specified controllers are sensitive to modeling errors, and due to the many operations of derivation required these controllers are sensitive to measurement noise. The ultimate goal is to develop a method that is applicable to a real-life situation. Hence, future work includes simulating more realistic conditions by adding measurement noise, state observers etc. and testing the theorems in real-life, in addition to strengthening the stability proofs.

The results of this thesis will be the basis for an article that will be submitted to the 2014 American Control Conference.

Appendix A

Formulas and Stability Theorems

A.1 Vector formulas

A cross product between two vectors can be expressed as below.

$$\begin{aligned} &\boldsymbol{\lambda} \times \boldsymbol{a} \triangleq \boldsymbol{S}(\boldsymbol{\lambda})\boldsymbol{a} \\ &\boldsymbol{S}(\boldsymbol{\lambda}) = -\boldsymbol{S}^T(\boldsymbol{\lambda}) \begin{bmatrix} 0 & -\lambda_3 & \lambda_2 \\ \lambda_3 & 0 & -\lambda_1 \\ -\lambda_2 & \lambda_1 & 0 \end{bmatrix} \end{aligned} \tag{A.1}$$

A rotation β about an axis $\boldsymbol{\lambda}$ results in a rotation matrix

$$\boldsymbol{R}_{\lambda,\beta} = \boldsymbol{I}_{3\times 3} + sin(\beta)\boldsymbol{S}(\boldsymbol{\lambda}) + [1 - cos(\beta)]\boldsymbol{S}^2(\boldsymbol{\lambda}) \tag{A.2}$$

Time differentiation of a vector $\boldsymbol{a}$ in a moving reference frame $\{b\}$ satisfies the following equation:

$$\frac{^i d}{dt}\boldsymbol{a} = \frac{^b d}{dt}\boldsymbol{a} + \boldsymbol{\omega}_{b/i} \times \boldsymbol{a} \tag{A.3}$$

A.2 Trigonometric formulas

$$\arctan(x) + \arctan(y) = \arctan\left(\frac{x+y}{1-xy}\right) \tag{A.4}$$

$$\begin{aligned}
\tan(\alpha) &= \frac{a}{b} \\
\alpha &= \arctan\left(\frac{a}{b}\right) \\
\cos(\alpha) &= \cos\left(\arctan\left(\frac{a}{b}\right)\right) \\
&= \frac{b}{\sqrt{a^2+b^2}} \\
\sin(\alpha) &= \sin\left(\arctan\left(\frac{a}{b}\right)\right) \\
&= \frac{a}{\sqrt{a^2+b^2}}
\end{aligned} \tag{A.5}$$

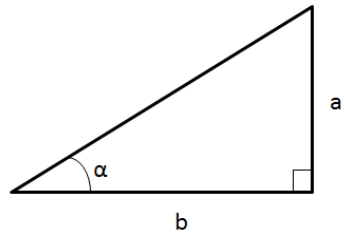

Figure A.1: Illustration of equation (A.5).

A.3 Stability theorems

A.3.1 General Stability

Definitions from [15]:
Consider the system

$$\dot{\boldsymbol{x}} = \boldsymbol{f}(t, \boldsymbol{x}). \tag{A.6}$$

$\boldsymbol{f}$ is assumed to be piecewise continuous in t and locally Lipschitz in $\boldsymbol{x}$.
The equilibrium point $\boldsymbol{x} = 0$ of the system (A.6) is

Stable if for each $\epsilon > 0$, there exists a $\delta(\epsilon, t_0 > 0)$ such that $||\boldsymbol{x}(t_0)|| < \delta \Rightarrow ||\boldsymbol{x}(t)|| < \epsilon, \forall t \geq t_0 \geq 0$

Uniformly stable if for each $\epsilon > 0$, there exists a $\delta(\epsilon > 0)$ such that $||\boldsymbol{x}(t_0)|| < \delta \Rightarrow ||\boldsymbol{x}(t)|| < \epsilon, \forall t \geq t_0 \geq 0$

Unstable if it is not stable

Asymptotically stable if it is stable and there is a positive constant $c = c(t_0)$ such that $\boldsymbol{x}(t) \to 0$ as $t \to \infty, \forall ||\boldsymbol{x}(t_0) < c||$

Uniformly asymptotically stable if it is uniformly stable and there is a positive constant c independent of t_0, such that $\boldsymbol{x}(t) \to 0$ as $t \to \infty, \forall ||\boldsymbol{x}(t_0) < c||$

Globally uniformly asymptotically stable if it is uniformly stable, $\delta(\epsilon)$ can be chosen to satisfy $\lim_{\epsilon \to \infty} \delta(\epsilon) = \infty$, and, for each pair of positive numbers η and c, there is a $T = T(\eta, c) > 0$ such that $||\boldsymbol{x}(t)|| < \eta, \forall t \geq t_0 + T(\eta, c), \forall ||\boldsymbol{x}(t_0)|| < c$

A.3.2 Hurwitz stability

Theorem 4.5 [15] : Consider the linear system

$$\dot{\boldsymbol{x}} = \boldsymbol{A}\boldsymbol{x}. \tag{A.7}$$

The equilibrium point $\boldsymbol{x}^* = 0$ is globally asymptotically (exponentially) stable if and only if all eigenvalues of $\boldsymbol{A}$ satisfy $Re(\lambda_i) < 0$.

Theorem 4.6 [15] : Consider a quadratic Lyapunov function candidate $V(\boldsymbol{x}) = \boldsymbol{x}^T \boldsymbol{P} \boldsymbol{x}$ where $\boldsymbol{P} = \boldsymbol{P}^T > 0$ is a real symmetric positive definite matrix. The derivative of V along the trajectories of the linear system in equation (A.7) is given by

$$\dot{V}(\boldsymbol{x}) = \boldsymbol{x}^T \boldsymbol{P} \dot{\boldsymbol{x}} + \dot{\boldsymbol{x}}^T \boldsymbol{P} \boldsymbol{x} = \boldsymbol{x}^T (\boldsymbol{P}\boldsymbol{A} + \boldsymbol{A}^T \boldsymbol{P}) \boldsymbol{x} = -\boldsymbol{x}^T \boldsymbol{Q} \boldsymbol{x} \tag{A.8}$$

where $\boldsymbol{Q}$ is a symmetric matrix defined by $\boldsymbol{P}\boldsymbol{A} + \boldsymbol{A}^T \boldsymbol{P} = -\boldsymbol{Q}$.

The matrix $\boldsymbol{A}$ is Hurwitz if and only if for any given positive definite symmetric matrix $\boldsymbol{Q}$ there exists a positive definite symmetric matrix $\boldsymbol{P}$ that satisfies $\boldsymbol{P}\boldsymbol{A} + \boldsymbol{A}^T \boldsymbol{P} = -\boldsymbol{Q}$. Moreover, if A is Hurwitz, P is the unique solution of $\boldsymbol{P}\boldsymbol{A} + \boldsymbol{A}^T \boldsymbol{P} = -\boldsymbol{Q}$.

A.3.3 Lyapunov stability

Stability of the system in equation (A.6) can be proven using Lyapunov's Direct method [15]. This is done by considering Lyapunov functions, often denoted V. A time-varying energy function $V(t, \boldsymbol{x})$ is said to be

Positive definite if and only if $V(t, \boldsymbol{x}) = 0$ and $V(t, \boldsymbol{x}) \geq W_1(\boldsymbol{x})$ for all $t \geq 0$ for some positive definite $W_1(\boldsymbol{x})$. Similarly, $V(t, \boldsymbol{x})$ is positive semidefinite and radially unbounded if $W_1(\boldsymbol{x})$ is positive semidefinite and radially unbounded

Decrescent if and only if $V(t, \boldsymbol{x}) = 0$ and $V(t, \boldsymbol{x}) \leq W_2(\boldsymbol{x})$ for all $t \geq 0$ for some positive definite $W_2(\boldsymbol{x})$.

Theorem 4.8 and 4.9 [15] : The equilibrium point $\boldsymbol{x}^* = 0$ is

	Stable	Uniformly stable	Uniformly asymptotically stable	GUAS
V	Positive definite	Positive definite, Decrescent	Positive definite, Decrescent	Positive definite, Decrescent, Radially unbounded
$\dot{V}$	Negative semidefinite	Negative semidefinite	Negative definite	Negative definite

Theorem 4.10 [15] : Let $\boldsymbol{x}^* = 0$ be an equilibrium point for the system in equation (A.6) and $\mathbb{D} \subset \mathbb{R}^n$ be a domain containing $\boldsymbol{x}^*$. Let $V : [0, \infty) \times \mathbb{D} \to \mathbb{R}$ be a continuously differential function such that

$$k_1||\boldsymbol{x}||^a \leq V(t,x) \leq k_2||\boldsymbol{x}||^a \tag{A.9}$$

$$\frac{\delta V}{\delta t} + \frac{\delta V}{\delta x}\boldsymbol{f}(t,\boldsymbol{x}) \leq -k_3||\boldsymbol{x}||^a \tag{A.10}$$

$\forall t \geq 0$ and $\forall \boldsymbol{x} \in \mathbb{D}$, where k_1, k_2, k_3 and a are positive constants. Then, $\boldsymbol{x}^*$ is exponentially stable. If the assumptions hold globally, then $\boldsymbol{x}^*$ is globally exponentially stable.

A.3.4 Stability of Cascades

Consider the nonlinear time-varying cascaded system

$$\begin{aligned} \dot{\boldsymbol{x}} &= \boldsymbol{f}_1(t,\boldsymbol{x}) + \boldsymbol{g}(t,\boldsymbol{x},\boldsymbol{y})\boldsymbol{y} \\ \dot{\boldsymbol{y}} &= \boldsymbol{f}_2(t,\boldsymbol{y}), \end{aligned} \tag{A.11}$$

where $\boldsymbol{f}_1$ and $\boldsymbol{f}_2$ are continuously differentiable in their arguments.

Lemma 2.2 [17] : The cascaded system in equation (A.11) is GUAS if both $\dot{\boldsymbol{x}} = \boldsymbol{f}_1(t,\boldsymbol{x})$ and $\dot{\boldsymbol{y}} = \boldsymbol{f}_2(t,\boldsymbol{y})$ are UGAS and the solutions of (A.11) are globally, uniformly bounded.

Theorem 2 [16] : The cascaded system in equation (A.11) is GUAS if the following assumptions are satisfied:

- ***A1*** - The system $\dot{\boldsymbol{x}} = \boldsymbol{f}_1(t,\boldsymbol{x})$ is GUAS with a Lyapunov function satisfying $\left\|\frac{\delta V}{\delta \boldsymbol{x}}\right\| ||\boldsymbol{x}|| \leq c_1 V(t,\boldsymbol{x}) \quad \forall ||\boldsymbol{x}|| \geq \eta$, where $c_1 > 0$ and $\eta > 0$.
- ***A2*** - The function $\boldsymbol{g}(t,\boldsymbol{x},\boldsymbol{y})$ satisfies $||\boldsymbol{g}(t,\boldsymbol{x},\boldsymbol{y})|| \leq \theta_1(||\boldsymbol{y}||) + \theta_2(||\boldsymbol{y}||)||\boldsymbol{x}||$, where $\theta_1, \theta_2 : \mathbb{R}^+ \to \mathbb{R}^+$ are continuous.
- ***A3*** - The system $\dot{\boldsymbol{y}} = \boldsymbol{f}_2(t,\boldsymbol{y})$ is GUAS and for all $t_0 \geq 0$, $\int_{t_0}^{\infty} ||\boldsymbol{y}(s,t_0,\boldsymbol{y}(t_0))||ds \leq \phi(||\boldsymbol{y}(t_0)||)$, where the function $\phi(\cdot)$ is a class $\mathcal{K}$ function.

- *Remark 1* - If the nominal system $\dot{\boldsymbol{x}} = \boldsymbol{f}_1(t, \boldsymbol{x})$ is GUAS with a quadratic Lyapunov function, $\left\| \frac{\delta V}{\delta \boldsymbol{x}} \right\| ||\boldsymbol{x}|| \leq c_1 V(t, \boldsymbol{x}) \quad \forall ||\boldsymbol{x}|| \geq \eta$ is satisfied trivially.
- *Remark 2* - If the perturbing system $\dot{\boldsymbol{y}} = \boldsymbol{f_2}(t, \boldsymbol{y})$ is UGAS and ULES (or equivalently exponentially stable within a ball of initial conditions), then $\int_{t_0}^{\infty} ||\boldsymbol{y}(s, t_0, \boldsymbol{y}(t_0))|| ds \leq \phi(||\boldsymbol{y}(t_0)||)$ is satisfied trivially.

Lemma 8 [16] : If, in addition to the assumptions in Theorem 2 [16], both $\dot{\boldsymbol{x}} = f_1(t, \boldsymbol{x})$ and $\dot{\boldsymbol{y}} = \boldsymbol{f}_2(t, \boldsymbol{y})$ are globally $\mathcal{K}$-exponentially stable, then the cascaded system in equation (A.11) is globally $\mathcal{K}$-exponentially stable.

Appendix B

Stability Proofs

B.1 Stability proof, Theorem 1

The basis for this proof is the body Serret-Frenet Kinematics:

$$\begin{aligned}
\begin{bmatrix}\dot{x}_{b/f}\\ \dot{y}_{b/f}\end{bmatrix} &= \boldsymbol{R}_b^f(\psi_{fb})\begin{bmatrix}u\\ v\end{bmatrix} - \begin{bmatrix}\dot{s}\\ 0\end{bmatrix} - \dot{s}\begin{bmatrix}0 & -\kappa\\ \kappa & 0\end{bmatrix}\begin{bmatrix}x_{b/f}\\ y_{b/f}\end{bmatrix}\\
&= \boldsymbol{R}_b^f(\psi_{fb})\left(\begin{bmatrix}u_r\\ v_r\end{bmatrix} + \boldsymbol{V}_c^b\right) - \begin{bmatrix}\dot{s}\\ 0\end{bmatrix} - \dot{s}\begin{bmatrix}0 & -\kappa\\ \kappa & 0\end{bmatrix}\begin{bmatrix}x_{b/f}\\ y_{b/f}\end{bmatrix}\\
&= \boldsymbol{R}_b^f(\psi_{fb})\left(\begin{bmatrix}u_r\\ v_r\end{bmatrix} + \boldsymbol{R}_b^i(\psi)^T\boldsymbol{V}_c\right) - \begin{bmatrix}\dot{s}\\ 0\end{bmatrix} - \dot{s}\begin{bmatrix}0 & -\kappa\\ \kappa & 0\end{bmatrix}\begin{bmatrix}x_{b/f}\\ y_{b/f}\end{bmatrix}\\
&= \boldsymbol{R}_b^f(\psi_{fb})\begin{bmatrix}u_r\\ v_r\end{bmatrix} - \begin{bmatrix}\dot{s}\\ 0\end{bmatrix} - \dot{s}\begin{bmatrix}0 & -\kappa\\ \kappa & 0\end{bmatrix}\begin{bmatrix}x_{b/f}\\ y_{b/f}\end{bmatrix} + \boldsymbol{R}_f^i(\psi_f)^T\boldsymbol{V}_c
\end{aligned} \tag{B.1}$$

The surface ship has a controller that ensures that the relative surge velocity u_r and the heading ψ tracks their references U_{rd} and ψ_d (ψ_d is given by the guidance law in equation (6.7)). The errors are defined as $\tilde{u_r} \triangleq u_r - U_{rd}$ and $\tilde{\psi} \triangleq \psi - \psi_d$. Equation (6.13) defines the kinematics of the body relative to the Serret-Frenet frame. By using equation (A.4) from the appendix, it can easily be shown that

$$\begin{aligned}
\psi_{fb} &= \psi - \psi_f\\
&= \tilde{\psi} + \psi_d - \psi_f\\
&= \tilde{\psi} + \psi_f - \arctan\left(\frac{v_r}{U_{rd}}\right) - \arctan\left(\frac{y_{b/f}+f}{\sqrt{\Delta^2 + \left(x_{b/f}\right)^2}}\right) - \psi_f\\
&= \tilde{\psi} - \arctan\left(\frac{v_r\sqrt{\Delta^2 + x_{b/f}^2} + U_{rd}(y_{b/f}+f)}{U_{rd}\sqrt{\Delta^2 + x_{b/f}^2} - v_r(y_{b/f}+f)}\right)\\
&= \tilde{\psi} - \alpha,
\end{aligned} \tag{B.2}$$

$$\begin{aligned}
\cos(\psi_{fb}) &= \cos(\tilde{\psi} - \alpha) \\
&= \cos(\tilde{\psi})\cos(\alpha) + \sin(\tilde{\psi})\sin(\alpha) \\
&= \cos(\alpha) + \cos(\alpha)\left(\cos(\tilde{\psi}) - 1\right) + \sin(\tilde{\psi})\sin(\alpha) \\
&= \cos(\alpha) + \tilde{\psi}\left[\frac{\cos(\tilde{\psi}) - 1}{\tilde{\psi}}\cos(\alpha) + \frac{\sin(\tilde{\psi})}{\tilde{\psi}}\sin(\alpha)\right],
\end{aligned} \tag{B.3}$$

$$\begin{aligned}
\sin(\psi_{fb}) &= \sin(\tilde{\psi} - \alpha) \\
&= \sin(\tilde{\psi})\cos(\alpha) - \cos(\tilde{\psi})\sin(\alpha) \\
&= -\sin(\alpha) - \sin(\alpha)\left(\cos(\tilde{\psi}) - 1\right) + \sin(\tilde{\psi})\cos(\alpha) \\
&= -\sin(\alpha) + \tilde{\psi}\left[\frac{\sin(\tilde{\psi})}{\tilde{\psi}}\cos(\alpha) - \frac{\cos(\tilde{\psi}) - 1}{\tilde{\psi}}\sin(\alpha)\right]
\end{aligned} \tag{B.4}$$

Using equation (A.5) from the appendix, the following relationship is clear:

$$\begin{aligned}
\cos(\alpha) &= \frac{U_{rd}\sqrt{\Delta^2 + x_{b/f}^2} - v_r(y_{b/f} + f)}{U_c\sqrt{\Delta^2 + x_{b/f}^2 + (y_{b/f} + f)^2}} \\
\sin(\alpha) &= \frac{v_r\sqrt{\Delta^2 + x_{b/f}^2} + U_{rd}(y_{b/f} + f)}{U_c\sqrt{\Delta^2 + x_{b/f}^2 + (y_{b/f} + f)^2}}.
\end{aligned} \tag{B.5}$$

This can be inserted into the $x_{b/f}$ and $y_{b/f}$ dynamics in equation (6.13). Defining $\tilde{V_x} \triangleq V_x - \hat{V_x}$, $\tilde{V_y} \triangleq V_y - \hat{V_y}$, $\tilde{x} \triangleq x - \hat{x}$ and $\tilde{y} \triangleq y - \hat{y}$.

$$\begin{aligned}
\dot{x}_{b/f} &= \cos(\psi_{fb})u_r - \sin(\psi_{fb})v_r - \dot{s} + \dot{s}\kappa y_{b/f} + \cos(\psi_f)V_x + \sin(\psi_f)V_y \\
&= \cos(\psi_{fb})(\tilde{u_r} + U_{rd}) - \sin(\psi_{fb})v_r - \dot{s} + \dot{s}\kappa y_{b/f} + \cos(\psi_f)V_x + \sin(\psi_f)V_y \\
&= U_{rd}\cos(\alpha) + v_r\sin(\alpha) - \dot{s} + \dot{s}\kappa y_{b/f} + \cos(\psi_f)V_x + \sin(\psi_f)V_y + \cos(\psi_{fb})\tilde{u_r} \\
&\quad + \tilde{\psi}\left[\frac{\cos(\tilde{\psi}) - 1}{\tilde{\psi}}\left(U_{rd}\cos(\alpha) + v_r\sin(\alpha)\right) + \frac{\sin(\tilde{\psi})}{\tilde{\psi}}\left(U_{rd}\sin(\alpha) - v_r\cos(\alpha)\right)\right] \\
&= U_c\frac{\sqrt{\Delta^2 + x_{b/f}^2}}{\sqrt{\Delta^2 + x_{b/f}^2 + (y_{b/f} + f)^2}} - \dot{s} + \dot{s}\kappa y_{b/f} + \cos(\psi_f)V_x + \sin(\psi_f)V_y \\
&\quad + \cos(\psi_{fb})\tilde{u_r} + \tilde{\psi}\left[\frac{\cos(\tilde{\psi}) - 1}{\tilde{\psi}}U_c\frac{\sqrt{\Delta^2 + x_{b/f}^2}}{\sqrt{\Delta^2 + x_{b/f}^2 + (y_{b/f} + f)^2}}\right. \\
&\quad \left. + \frac{\sin(\tilde{\psi})}{\tilde{\psi}}U_c\frac{y_{b/f} + f}{\sqrt{\Delta^2 + x_{b/f}^2 + (y_{b/f} + f)^2}}\right]
\end{aligned} \tag{B.6}$$

Inserting for $\dot{s}$ defined in (6.6), equation (B.6) reduces to

$$\begin{aligned}\dot{x}_{b/f} &= -U_c\frac{x_{b/f}}{\sqrt{\Delta^2+x_{b/f}^2+(y_{b/f}+f)^2}} + \dot{s}\kappa y_{b/f} + \cos(\psi_{fb})\tilde{u_r} + \cos(\psi_f)\tilde{V_x} + \sin(\psi_f)\tilde{V_y} \\ &\quad + \tilde{\psi}\underbrace{\left[\frac{\cos(\tilde{\psi})-1}{\tilde{\psi}}U_c\frac{\sqrt{\Delta^2+x_{b/f}^2}}{\sqrt{\Delta^2+x_{b/f}^2+(y_{b/f}+f)^2}} + \frac{\sin(\tilde{\psi})}{\tilde{\psi}}U_c\frac{y_{b/f}+f}{\sqrt{\Delta^2+x_{b/f}^2+(y_{b/f}+f)^2}}\right]}_{\triangleq h_1(t,U_c,\boldsymbol{\xi})}.\end{aligned} \tag{B.7}$$

$$\begin{aligned}\dot{y}_{b/f} &= \sin(\psi_{fb})u_r + \cos(\psi_{fb})v_r - \dot{s}\kappa x_{b/f} - \sin(\psi_f)V_x + \cos(\psi_f)V_y \\ &= \sin(\psi_{fb})(\tilde{u_r}+U_{rd}) + \cos(\psi_{fb})v_r - \dot{s}\kappa x_{b/f} - \sin(\psi_f)V_x + \cos(\psi_f)V_y \\ &= v_r\cos(\alpha) - U_{rd}\sin(\alpha) - \dot{s}\kappa x_{b/f} - \sin(\psi_f)V_x + \cos(\psi_f)V_y + \sin(\psi_{fb})\tilde{u_r} \\ &\quad + \tilde{\psi}\left[\frac{\cos(\tilde{\psi})-1}{\tilde{\psi}}\left(v_r\cos(\alpha)-U_{rd}\sin(\alpha)\right) + \frac{\sin(\tilde{\psi})}{\tilde{\psi}}\left(U_{rd}\cos(\alpha)+v_r\sin(\alpha)\right)\right] \\ &= -U_c\frac{y_{b/f}+f}{\sqrt{\Delta^2+x_{b/f}^2+(y_{b/f}+f)^2}} - \dot{s}\kappa x_{b/f} - \sin(\psi_f)V_x + \cos(\psi_f)V_y + \sin(\psi_{fb})\tilde{u_r} \\ &\quad + \tilde{\psi}\left[\frac{\sin(\tilde{\psi})}{\tilde{\psi}}U_c\frac{\sqrt{\Delta^2+x_{b/f}^2}}{\sqrt{\Delta^2+x_{b/f}^2+(y_{b/f}+f)^2}} - \frac{\cos(\tilde{\psi})-1}{\tilde{\psi}}U_c\frac{y_{b/f}+f}{\sqrt{\Delta^2+x_{b/f}^2+(y_{b/f}+f)^2}}\right]\end{aligned} \tag{B.8}$$

Inserting for f defined in equation (6.8), (equation B.8) reduces to

$$\begin{aligned}\dot{y}_{b/f} &= -U_c\frac{y_{b/f}}{\sqrt{\Delta^2+x_{b/f}^2+(y_{b/f}+f)^2}} - \dot{s}\kappa x_{b/f} + \sin(\psi_{fb})\tilde{u_r} - \sin(\psi_f)\tilde{V_x} + \cos(\psi_f)\tilde{V_y} \\ &\quad + \tilde{\psi}\underbrace{\left[\frac{\sin(\tilde{\psi})}{\tilde{\psi}}U_c\frac{\sqrt{\Delta^2+x_{b/f}^2}}{\sqrt{\Delta^2+x_{b/f}^2+(y_{b/f}+f)^2}} - \frac{\cos(\tilde{\psi})-1}{\tilde{\psi}}U_c\frac{y_{b/f}+f}{\sqrt{\Delta^2+x_{b/f}^2+(y_{b/f}+f)^2}}\right]}_{\triangleq h_2(t,U_c,\boldsymbol{\xi})}.\end{aligned} \tag{B.9}$$

This can be summarized as below:

$$\begin{bmatrix}\dot{x}_{b/f}\\ \dot{y}_{b/f}\end{bmatrix} = \begin{bmatrix}-U_c\frac{x_{b/f}}{\sqrt{\Delta^2+x_{b/f}^2+(y_{b/f}+f)^2}}\\ -U_c\frac{y_{b/f}}{\sqrt{\Delta^2+x_{b/f}^2+(y_{b/f}+f)^2}}\end{bmatrix} - \dot{s}\begin{bmatrix}0 & -\kappa\\ \kappa & 0\end{bmatrix}\begin{bmatrix}x_{b/f}\\ y_{b/f}\end{bmatrix} + \boldsymbol{H}(t,U_c,\boldsymbol{\xi})\boldsymbol{\xi} \tag{B.10}$$

$$\boldsymbol{H}(t,U_c,\boldsymbol{\xi})\boldsymbol{\xi} = \begin{bmatrix} \cos(\psi_{fb}) & h_1(t,U_c,\boldsymbol{\xi}) & 0 & \cos(\psi_f) & \sin(\psi_f) & 0 & 0 \\ \sin(\psi_{fb}) & h_2(t,U_c,\boldsymbol{\xi}) & 0 & -\sin(\psi_f) & \cos(\psi_f) & 0 & 0 \end{bmatrix} \begin{bmatrix} \tilde{u_r} \\ \tilde{\psi} \\ \tilde{r} \\ \tilde{V_x} \\ \tilde{V_y} \\ \tilde{x} \\ \tilde{y} \end{bmatrix} \tag{B.11}$$

The system in equation (B.10) and the dynamics of $\boldsymbol{\xi}$ (B.14) can be seen as a cascaded system where the error dynamics perturbs the nominal system in equation (B.12) through the term $\boldsymbol{H}(t,U_c,\boldsymbol{\xi})\boldsymbol{\xi}$ (appendix A.3.4).

$$\begin{bmatrix} \dot{x}_{b/f} \\ \dot{y}_{b/f} \end{bmatrix} = \begin{bmatrix} -U_c \frac{x_{b/f}}{\sqrt{\Delta^2 + x_{b/f}^2 + (y_{b/f}+f)^2}} \\ -U_c \frac{y_{b/f}}{\sqrt{\Delta^2 + x_{b/f}^2 + (y_{b/f}+f)^2}} \end{bmatrix} - \dot{s} \begin{bmatrix} 0 & -\kappa \\ \kappa & 0 \end{bmatrix} \begin{bmatrix} x_{b/f} \\ y_{b/f} \end{bmatrix} \tag{B.12}$$

Stability of the nominal system can be shown using the quadratic positive definite, decrescent and radially unbounded Lyapunov function $V = \frac{1}{2}(x_{b/f}^2 + y_{b/f}^2)$.

$$\begin{aligned} \dot{V} &= \dot{x}_{b/f} x_{b/f} + \dot{y}_{b/f} y_{b/f} \\ &= -U_c \frac{x_{b/f}^2 + y_{b/f}^2}{\sqrt{\Delta^2 + x_{b/f}^2 + (y_{b/f}+f)^2}} + \dot{s}\kappa x_{b/f} y_{b/f} - \dot{s}\kappa x_{b/f} y_{b/f} \\ &\leq -U_{rd} \frac{x_{b/f}^2 + y_{b/f}^2}{\sqrt{\Delta^2 + x_{b/f}^2 + (y_{b/f}+f)^2}} \\ &\triangleq W(x_{b/f}, y_{b/f}) < 0 \end{aligned} \tag{B.13}$$

$\dot{V}$ is negative definite and as such the nominal system is UGAS (theorem 4.8 and 4.9 in appendix A.3.3). However, it is not possible to prove ULES stability cf. Børhaug [6] due to the time-varying term f. In particular, in any ball $\mathcal{B}_r = \left\{(x_{b/f}, y_{b/f}) \in \mathbb{R}^2 : \; x_{b/f}^2 + (y_{b/f}+f)^2 \leq r^2 \right\}$, $W \leq -\lambda x_{b/f}^2 - \lambda y_{b/f}^2$ for all $0 < \lambda \leq U_{rd}/\sqrt{\Delta^2 + r^2}$. However, due to the time-varying term f, $\mathcal{B}_r$ does not contain the origin $x_{b/f} = 0$, $y_{b/f} = 0$ for all $r > 0$, only for $r > |f|$. As such, exponential stability can not be guaranteed according to theorem 4.10 in appendix A.3.3.

The error dynamics is shown in equation (B.14) and is based on the feedback linearization controllers in chapter 5.1.1 and the current and position observers in

chapter 3.4.

$$\dot{\boldsymbol{\xi}} = \begin{bmatrix} \dot{\tilde{u}}_r \\ \dot{\tilde{\psi}} \\ \dot{\tilde{r}} \\ \dot{\tilde{V}}_x \\ \dot{\tilde{V}}_y \\ \dot{\tilde{x}} \\ \dot{\tilde{y}} \end{bmatrix} = \begin{bmatrix} -(k_{u_r} + \frac{d_{11}^p}{m_{11}}) & 0 & 0 & 0 & 0 & 0 & 0 \\ 0 & 0 & 1 & 0 & 0 & 0 & 0 \\ 0 & -k_\psi & -k_r & 0 & 0 & 0 & 0 \\ 0 & 0 & 0 & 0 & 0 & -k_{x2} & 0 \\ 0 & 0 & 0 & 0 & 0 & 0 & -k_{y2} \\ 0 & 0 & 0 & 1 & 0 & -k_{x1} & 0 \\ 0 & 0 & 0 & 0 & 1 & 0 & -k_{y1} \end{bmatrix} \begin{bmatrix} \tilde{u}_r \\ \tilde{\psi} \\ \tilde{r} \\ \tilde{V}_x \\ \tilde{V}_y \\ \tilde{x} \\ \tilde{y} \end{bmatrix} \quad (B.14)$$
$$= \boldsymbol{\Lambda}\boldsymbol{\xi}$$

System (B.14) is a linear system, and $\boldsymbol{\Lambda}$ is Hurwitz. Hence, the error dynamics is UGES according to the theorem 4.5 in appendix A.3.2.

Based on this, the entire system cascaded system (B.10) and (B.14) can be proven UGAS according to theorem 2 in appendix A.3.4 if $\boldsymbol{H}(t, U_c, \boldsymbol{\xi})$ is globally bounded. Equation (B.11) shows that $\boldsymbol{H}(t, U_c, \boldsymbol{\xi})$ is bounded for bounded values of $h_1(t, U_c, \boldsymbol{\xi})$ and $h_2(t, U_c, \boldsymbol{\xi})$. These are again bounded if U_c is bounded: It is trivial to see that $\left| \frac{\sqrt{\Delta^2 + x_{b/f}^2}}{\sqrt{\Delta^2 + x_{b/f}^2 + (y_{b/f}+f)^2}} \right| \leq 1$ and $\left| \frac{y_{b/f}+f}{\sqrt{\Delta^2 + x_{b/f}^2 + (y_{b/f}+f)^2}} \right| < 1$. Furthermore, $\frac{\sin(\tilde{\psi})}{\tilde{\psi}}$ and $\frac{\cos(\tilde{\psi})-1}{\tilde{\psi}}$ have defined limits as $\tilde{\psi}$ approaches zero and are otherwise defined and bounded for all values of ψ.

The total relative speed $U_c = \sqrt{U_{rd}^2 + v_r^2}$ is clearly bounded for bounded v_r. The proof in chapter 9.A in [6] can be applied to show that v_r is in fact bounded. Originally, this proof affirm the boundedness of the sway velocity v given that certain conditions are satisfied, but it can also be applied to relative sway velocity v_r. The proof assumes $u_r(t) \in [U_{min}, U_{max}]$, $\forall t \geq t_0$. In Theorem 1, $u_{rd}(t, s) = U_{rd} = constant$. The feedback linearization controller drives $\tilde{u}_r \to 0$ exponentially, so $u_r(t) = U_{rd}$, $\forall\ t \geq t_0 \geq 0$ for some t_0. Hence, $U_{min} = U_{max} = U_{rd}$, and if assumptions **A1**-**A3** are satisfied, it can be concluded that v_r is uniformly bounded $\forall t \geq t_0$.

Consequently, all conditions of theorem 2 in appendix A.3.4 are satisfied. In particular, the nominal system is UGAS with a quadratic Lyapunov-function. The error dynamics is UGES, and the interconnection matrix $\boldsymbol{H}$ is globally bounded. Consequently, the cascaded system in equation (B.10) and (B.14) is UGAS, and $x_{b/f}$, $y_{b/f}$ and $\tilde{u}_r$ converge to zero with uniform global asymptotic stability. Thus the control objectives are satisfied.

Proving exponential stability for the cascaded system remains a topic for future work.

B.2 Stability proof, Theorem 2

The basis for this proof is the body Serret-Frenet Kinematics:

$$\begin{bmatrix} \dot{x}_{b/f} \\ \dot{y}_{b/f} \\ \dot{z}_{b/f} \end{bmatrix} = \boldsymbol{R}_b^f(\boldsymbol{\Theta}_{fb}) \begin{bmatrix} u_r \\ v_r \\ w_r \end{bmatrix} - \begin{bmatrix} \dot{s} \\ 0 \\ 0 \end{bmatrix} - \dot{s} \begin{bmatrix} 0 & -\kappa & 0 \\ \kappa & 0 & -\tau \\ 0 & \tau & 0 \end{bmatrix} \begin{bmatrix} x_{b/f} \\ y_{b/f} \\ z_{b/f} \end{bmatrix} + \boldsymbol{R}_f^i(\boldsymbol{\Theta}_{if})^T \boldsymbol{V}_c \quad \text{(B.15)}$$

Hugin has a feedback linearization controller that ensures that the relative surge velocity u_r tracks the reference U_{rd} and an integrator backstepping controller that ensures that the relative orientation of the c-frame θ_{fc} and ψ_{fc} converges to and tracks the reference $\theta_{fc,d}$ and $\psi_{fc,d}$ given by the guidance laws in equation (6.33).The errors are defined as $\tilde{u_r} \triangleq u_r - U_{rd}$, $\tilde{\theta}_{fc} \triangleq \theta_{fc} - \theta_{fc,d}$ and $\tilde{\psi_{fc}} \triangleq \psi_{fc} - \psi_{fc,d}$. Equation (6.37) defines the kinematics of the body relative to the Serret-Frenet frame. From chapter 3.7 it is known that

$$\boldsymbol{R}_b^f(\boldsymbol{\Theta}_{fb}) = \boldsymbol{R}_c^f(\boldsymbol{\Theta}_{fc}) \boldsymbol{R}_b^c(\boldsymbol{\Theta}_{cb}), \quad \text{(B.16)}$$

where $\boldsymbol{\Theta}_{fc} = [\phi_{fc}, \theta_{fc}, \psi_{fc}]^T$ is calculated from the rotation matrix in equation (3.41) and $\boldsymbol{\Theta}_{cb} = [0, \alpha_c, -\beta_c]^T$ and

$$\begin{aligned} \alpha_c &\triangleq \arctan\left(\frac{w_r}{U_{rd}}\right), \\ \beta_c &\triangleq \arctan\left(\frac{v_r}{\sqrt{U_{rd}^2 + w_r^2}}\right) \end{aligned} \quad \text{(B.17)}$$

Using equation (A.5) from the appendix, it is easy to see that

$$\begin{aligned} \sin(\alpha_c) &= \frac{w_r}{\sqrt{U_{rd}^2 + w_r^2}} \\ \cos(\alpha_c) &= \frac{U_{rd}}{\sqrt{U_{rd}^2 + w_r^2}} \\ \sin(\beta_c) &= \frac{v_r}{\sqrt{U_{rd}^2 + v_r^2 + w_r^2}} = \frac{v_r}{U_c} \\ \cos(\beta_c) &= \frac{\sqrt{U_{rd}^2 + w_r^2}}{U_c} \end{aligned} \quad \text{(B.18)}$$

As such,

$$
\begin{aligned}
\boldsymbol{R}_b^f(\boldsymbol{\Theta}_{fb})\begin{bmatrix} u_r \\ v_r \\ w_r \end{bmatrix} &= \boldsymbol{R}_b^f(\boldsymbol{\Theta}_{fb})\begin{bmatrix} U_{rd} \\ v_r \\ w_r \end{bmatrix} + \boldsymbol{R}_b^f(\boldsymbol{\Theta}_{fb})\begin{bmatrix} \tilde{u} \\ 0 \\ 0 \end{bmatrix} \\
&= \boldsymbol{R}_c^f(\boldsymbol{\Theta}_{fc})\boldsymbol{R}_b^c(\boldsymbol{\Theta}_{cb})\begin{bmatrix} U_{rd} \\ v_r \\ w_r \end{bmatrix} + \boldsymbol{R}_b^f(\boldsymbol{\Theta}_{fb})\begin{bmatrix} \tilde{u} \\ 0 \\ 0 \end{bmatrix} \\
&= \boldsymbol{R}_c^f(\boldsymbol{\Theta}_{fc})\begin{bmatrix} \cos(\alpha_c)\cos(\beta_c) & \sin(\beta_c) & \sin(\alpha_c)\cos(\beta_c) \\ -\cos(\alpha_c)\sin(\beta_c) & \cos(\beta_c) & -\sin(\alpha_c)\sin(\beta_c) \\ -\sin(\alpha_c) & 0 & \cos(\alpha_c) \end{bmatrix}\begin{bmatrix} U_{rd} \\ v_r \\ w_r \end{bmatrix} \\
&\quad + \boldsymbol{R}_b^f(\boldsymbol{\Theta}_{fb})\begin{bmatrix} \tilde{u} \\ 0 \\ 0 \end{bmatrix} \\
&= \boldsymbol{R}_c^f(\boldsymbol{\Theta}_{fc})\begin{bmatrix} \frac{U_{rd}}{\sqrt{U_{rd}^2+w_r^2}}\frac{\sqrt{U_{rd}^2+w_r^2}}{U_c} & \frac{v_r}{U_c} & \frac{w_r}{\sqrt{U_{rd}^2+w_r^2}}\frac{\sqrt{U_{rd}^2+w_r^2}}{U_c} \\ -\frac{U_{rd}}{\sqrt{U_{rd}^2+w_r^2}}\frac{v_r}{U_c} & \frac{\sqrt{U_{rd}^2+w_r^2}}{U_c} & -\frac{w_r}{\sqrt{U_{rd}^2+w_r^2}}\frac{v_r}{U_c} \\ -\frac{w_r}{\sqrt{U_{rd}^2+w_r^2}} & 0 & \frac{U_{rd}}{\sqrt{U_{rd}^2+w_r^2}} \end{bmatrix}\begin{bmatrix} U_{rd} \\ v_r \\ w_r \end{bmatrix} \\
&\quad + \boldsymbol{R}_b^f(\boldsymbol{\Theta}_{fb})\begin{bmatrix} \tilde{u} \\ 0 \\ 0 \end{bmatrix} \\
&= \boldsymbol{R}_c^f(\boldsymbol{\Theta}_{fc})\begin{bmatrix} \frac{U_{rd}^2+v_r^2+w_r^2}{U_c} \\ \frac{-U_{rd}^2v_r+(U_{rd}^2+w_r^2)v_r-w_r^2v_r}{\sqrt{U_{rd}^2+w_r^2}U_c} \\ \frac{-U_{rd}w_r+U_{rd}w_r}{\sqrt{U_{rd}^2+w_r^2}} \end{bmatrix} + \boldsymbol{R}_b^f(\boldsymbol{\Theta}_{fb})\begin{bmatrix} \tilde{u} \\ 0 \\ 0 \end{bmatrix} \\
&= \boldsymbol{R}_c^f(\boldsymbol{\Theta}_{fc})\begin{bmatrix} U_c \\ 0 \\ 0 \end{bmatrix} + \boldsymbol{R}_b^f(\boldsymbol{\Theta}_{fb})\begin{bmatrix} \tilde{u} \\ 0 \\ 0 \end{bmatrix} \\
&= \begin{bmatrix} U_c\cos(\theta_{fc})\cos(\psi_{fc}) \\ U_c\cos(\theta_{fc})\sin(\psi_{fc}) \\ -U_c\sin(\theta_{fc}) \end{bmatrix} + \begin{bmatrix} \tilde{u}_r\cos(\theta_{fb})\cos(\psi_{fb}) \\ \tilde{u}_r\cos(\theta_{fb})\sin(\psi_{fb}) \\ -\tilde{u}_r\sin(\theta_{fb}) \end{bmatrix}.
\end{aligned}
\tag{B.19}
$$

Furthermore,

$$
\begin{aligned}
\cos(\theta_{fc}) &= \cos(\theta_{fc,d}+\tilde{\theta}_{fc}) = \cos(\theta_{fc,d}) + \cos(\theta_{fc,d})\left(\cos(\tilde{\theta}_{fc})-1\right) - \sin(\theta_{fc,d})\sin(\tilde{\theta}_{fc}) \\
\sin(\theta_{fc}) &= \sin(\theta_{fc,d}+\tilde{\theta}_{fc}) = \sin(\theta_{fc,d}) + \sin(\theta_{fc,d})\left(\cos(\tilde{\theta}_{fc})-1\right) + \cos(\theta_{fc,d})\sin(\tilde{\theta}_{fc}) \\
\cos(\psi_{fc}) &= \cos(\psi_{fc,d}+\tilde{\psi}_{fc}) = \cos(\psi_{fc,d}) + \cos(\psi_{fc,d})\left(\cos(\tilde{\psi}_{fc})-1\right) - \sin(\psi_{fc,d})\sin(\tilde{\psi}_{fc}) \\
\sin(\psi_{fc}) &= \sin(\psi_{fc,d}+\tilde{\psi}_{fc}) = \sin(\psi_{fc,d}) + \sin(\psi_{fc,d})\left(\cos(\tilde{\psi}_{fc})-1\right) + \cos(\psi_{fc,d})\sin(\tilde{\psi}_{fc}).
\end{aligned}
\tag{B.20}
$$

As such,

$$\begin{aligned}
&\cos(\theta_{fc})\cos(\psi_{fc}) = \cos(\theta_{fc,d}+\tilde{\theta}_{fc})\cos(\psi_{fc,d}+\tilde{\psi}_{fc}) \\
&\quad = \cos(\theta_{fc,d})\cos(\psi_{fc,d}) - \sin(\theta_{fc,d})\sin(\tilde{\theta}_{fc})\cos(\psi_{fc,d})\cos(\tilde{\psi}_{fc}) \\
&\qquad + \sin(\theta_{fc,d})\sin(\tilde{\theta}_{fc})\sin(\psi_{fc,d})\sin(\tilde{\psi}_{fc}) + \cos(\theta_{fc,d})\cos(\psi_{fc,d})\left(\cos(\tilde{\theta}_{fc})-1\right) \\
&\qquad - \cos(\theta_{fc,d})\cos(\tilde{\theta}_{fc})\sin(\psi_{fc,d})\sin(\tilde{\psi}_{fc}) \\
&\qquad + \cos(\theta_{fc,d})\cos(\tilde{\theta}_{fc})\cos(\psi_{fc,d})\left(\cos(\tilde{\psi}_{fc})-1\right) \\
&\quad = \cos(\theta_{fc,d})\cos(\psi_{fc,d}) + \tilde{\theta}_{fc}\left[-\frac{\sin(\tilde{\theta}_{fc})}{\tilde{\theta}_{fc}}\sin(\theta_{fc,d})\cos(\psi_{fc,d})\cos(\tilde{\psi}_{fc})\right. \\
&\qquad \left. + \frac{\sin(\tilde{\theta}_{fc})}{\tilde{\theta}_{fc}}\sin(\theta_{fc,d})\sin(\psi_{fc,d})\sin(\tilde{\psi}_{fc}) + \frac{\cos(\tilde{\theta}_{fc})-1}{\tilde{\theta}_{fc}}\cos(\theta_{fc,d})\cos(\psi_{fc,d})\right] \\
&\qquad + \tilde{\psi}_{fc}\left[-\frac{\sin(\tilde{\psi}_{fc})}{\tilde{\psi}_{fc}}\cos(\theta_{fc,d})\cos(\tilde{\theta}_{fc})\sin(\psi_{fc,d})\right. \\
&\qquad \left. + \frac{\cos(\tilde{\psi}_{fc})-1}{\tilde{\psi}_{fc}}\cos(\theta_{fc,d})\cos(\tilde{\theta}_{fc})\cos(\psi_{fc,d})\right],
\end{aligned} \tag{B.21}$$

$$\begin{aligned}
&\cos(\theta_{fc})\sin(\psi_{fc}) = \cos(\theta_{fc,d}+\tilde{\theta}_{fc})\sin(\psi_{fc,d}+\tilde{\psi}_{fc}) \\
&\quad = \cos(\theta_{fc,d})\sin(\psi_{fc,d}) - \sin(\theta_{fc,d})\sin(\tilde{\theta}_{fc})\sin(\psi_{fc,d})\cos(\psi\theta_{fc}) \\
&\qquad - \sin(\theta_{fc,d})\sin(\tilde{\theta}_{fc})\cos(\psi_{fc,d})\sin(\psi\theta_{fc}) + \cos(\theta_{fc,d})\sin(\psi_{fc,d})\left(\cos(\tilde{\theta}_{fc})-1\right) \\
&\qquad + \cos(\theta_{fc,d})\cos(\tilde{\theta}_{fc})\cos(\psi_{fc,d})\sin(\psi\theta_{fc}) \\
&\qquad + \cos(\theta_{fc,d})\cos(\tilde{\theta}_{fc})\sin(\psi_{fc,d})\left(\cos(\tilde{\theta}_{fc})-1\right) \\
&\quad = \cos(\theta_{fc,d})\sin(\psi_{fc,d}) + \tilde{\theta}_{fc}\left[-\frac{\sin(\tilde{\theta}_{fc})}{\tilde{\theta}_{fc}}\sin(\theta_{fc,d})\sin(\psi_{fc,d})\cos(\tilde{\psi}_{fc})\right. \\
&\qquad \left. - \frac{\sin(\tilde{\theta}_{fc})}{\tilde{\theta}_{fc}}\sin(\theta_{fc,d})\cos(\psi_{fc,d})\sin(\psi\theta_{fc}) + \frac{\cos(\tilde{\theta}_{fc})-1}{\tilde{\theta}_{fc}}\cos(\theta_{fc,d})\sin(\psi_{fc,d})\right] \\
&\qquad + \tilde{\psi}_{fc}\left[\frac{\sin(\tilde{\psi}_{fc})}{\tilde{\psi}_{fc}}\cos(\theta_{fc,d})\cos(\tilde{\theta}_{fc})\cos(\psi_{fc,d})\right. \\
&\qquad \left. + \frac{\cos(\tilde{\psi}_{fc})-1}{\tilde{\psi}_{fc}}\cos(\theta_{fc,d})\cos(\tilde{\theta}_{fc})\sin(\psi_{fc,d})\right].
\end{aligned} \tag{B.22}$$

$$\begin{aligned}\sin(\theta_{fc}) &= \sin(\theta_{fc,d} + \tilde{\theta}_{fc}) = \sin(\theta_{fc,d}) + \sin(\theta_{fc,d})\left(\cos(\tilde{\theta}_{fc}) - 1\right) + \cos(\theta_{fc,d})\sin(\tilde{\theta}_{fc}) \\ &= \sin(\theta_{fc,d}) + \tilde{\theta}_{fc}\left[\frac{\sin(\tilde{\theta}_{fc})}{\tilde{\theta}_{fc}}\cos(\theta_{fc,d}) + \frac{\cos(\tilde{\theta}_{fc}) - 1}{\tilde{\theta}_{fc}}\sin(\theta_{fc,d})\right]\end{aligned} \tag{B.23}$$

By inserting this in equation (B.19) yields the following result:

$$\begin{aligned}\boldsymbol{R}_b^f(\boldsymbol{\Theta}_{fb})\begin{bmatrix}u_r\\v_r\\w_r\end{bmatrix} &= \begin{bmatrix}U_c\cos(\theta_{fc})\cos(\psi_{fc})\\U_c\cos(\theta_{fc})\sin(\psi_{fc})\\-U_c\sin(\theta_{fc})\end{bmatrix} + \begin{bmatrix}\tilde{u}_r\cos(\theta_{fb})\cos(\psi_{fb})\\\tilde{u}_r\cos(\theta_{fb})\sin(\psi_{fb})\\-\tilde{u}_r\sin(\theta_{fb})\end{bmatrix} \\ &= \begin{bmatrix}U_c\cos(\theta_{fc,d})\cos(\psi_{fc,d})\\U_c\cos(\theta_{fc,d})\sin(\psi_{fc,d})\\-U_c\sin(\theta_{fc,d})\end{bmatrix} + \underbrace{\begin{bmatrix}\cos(\theta_{fb})\cos(\psi_{fb}) & h_{11} & h_{12}\\\cos(\theta_{fb})\sin(\psi_{fb}) & h_{21} & h_{22}\\-\sin(\theta_{fb}) & h_{31} & h_{32}\end{bmatrix}}_{\triangleq \boldsymbol{H}_1}\underbrace{\begin{bmatrix}\tilde{u}_r\\\tilde{\theta}_{fc}\\\tilde{\psi}_{fc}\end{bmatrix}}_{\boldsymbol{\xi}_1}\end{aligned} \tag{B.24}$$

$$\begin{aligned}h_{11} &= -U_c\frac{\sin(\tilde{\theta}_{fc})}{\tilde{\theta}_{fc}}\sin(\theta_{fc,d})\cos(\psi_{fc,d})\cos(\tilde{\psi}_{fc}) + U_c\frac{\sin(\tilde{\theta}_{fc})}{\tilde{\theta}_{fc}}\sin(\theta_{fc,d})\sin(\psi_{fc,d})\sin(\tilde{\psi}_{fc}) \\ &\quad + U_c\frac{\cos(\tilde{\theta}_{fc}) - 1}{\tilde{\theta}_{fc}}\cos(\theta_{fc,d})\cos(\psi_{fc,d}) \\ h_{12} &= -U_c\frac{\sin(\tilde{\psi}_{fc})}{\tilde{\psi}_{fc}}\cos(\theta_{fc,d})\cos(\tilde{\theta}_{fc})\sin(\psi_{fc,d}) + U_c\frac{\cos(\tilde{\psi}_{fc}) - 1}{\tilde{\psi}_{fc}}\cos(\theta_{fc,d})\cos(\tilde{\theta}_{fc})\cos(\psi_{fc,d}) \\ h_{21} &= -U_c\frac{\sin(\tilde{\theta}_{fc})}{\tilde{\theta}_{fc}}\sin(\theta_{fc,d})\sin(\psi_{fc,d})\cos(\tilde{\psi}_{fc}) - U_c\frac{\sin(\tilde{\theta}_{fc})}{\tilde{\theta}_{fc}}\sin(\theta_{fc,d})\cos(\psi_{fc,d})\sin(\tilde{\psi}_{fc}) \\ &\quad + U_c\frac{\cos(\tilde{\theta}_{fc}) - 1}{\tilde{\theta}_{fc}}\cos(\theta_{fc,d})\sin(\psi_{fc,d}) \\ h_{22} &= U_c\frac{\sin(\tilde{\psi}_{fc})}{\tilde{\psi}_{fc}}\cos(\theta_{fc,d})\cos(\tilde{\theta}_{fc})\cos(\psi_{fc,d}) + U_c\frac{\cos(\tilde{\psi}_{fc}) - 1}{\tilde{\psi}_{fc}}\cos(\theta_{fc,d})\cos(\tilde{\theta}_{fc})\sin(\psi_{fc,d}) \\ h_{31} &= -U_c\frac{\sin(\tilde{\theta}_{fc})}{\tilde{\theta}_{fc}}\cos(\theta_{fc,d}) - U_c\frac{\cos(\tilde{\theta}_{fc}) - 1}{\tilde{\theta}_{fc}}\sin(\theta_{fc,d}) \\ h_{32} &= 0\end{aligned} \tag{B.25}$$

Thus, the dynamics of $x_{b/f}$, $y_{b/f}$ and $z_{b/f}$ in equation (6.37) can be rewritten.

$$\begin{aligned}\begin{bmatrix}\dot{x}_{b/f}\\\dot{y}_{b/f}\\\dot{z}_{b/f}\end{bmatrix} &= \boldsymbol{R}_b^f(\boldsymbol{\Theta}_{fb})\begin{bmatrix}u_r\\v_r\\w_r\end{bmatrix} - \begin{bmatrix}\dot{s}\\0\\0\end{bmatrix} - \dot{s}\begin{bmatrix}0 & -\kappa & 0\\\kappa & 0 & -\tau\\0 & \tau & 0\end{bmatrix}\begin{bmatrix}x_{b/f}\\y_{b/f}\\z_{b/f}\end{bmatrix} + \boldsymbol{R}_f^i(\boldsymbol{\Theta}_{if})^T\boldsymbol{V}_c \\ &= \begin{bmatrix}U_c\cos(\theta_{fc,d})\cos(\psi_{fc,d})\\U_c\cos(\theta_{fc,d})\sin(\psi_{fc,d})\\-U_c\sin(\theta_{fc,d})\end{bmatrix} + \boldsymbol{H}_1\boldsymbol{\xi}_1 - \begin{bmatrix}\dot{s}\\0\\0\end{bmatrix} - \dot{s}\begin{bmatrix}0 & -\kappa & 0\\\kappa & 0 & -\tau\\0 & \tau & 0\end{bmatrix}\begin{bmatrix}x_{b/f}\\y_{b/f}\\z_{b/f}\end{bmatrix} + \boldsymbol{V}_c^f\end{aligned} \tag{B.26}$$

The guidance laws can be seen in equation (6.33). By applying equation (A.5) from the appendix, it is easy to see that

$$\begin{aligned}
\cos(\theta_{fc,d}) &= \frac{\sqrt{\Delta^2 + y_{b/f}^2}}{\sqrt{\Delta^2 + y_{b/f}^2 + (z_{b/f} + f)^2}} \\
\sin(\theta_{fc,d}) &= \frac{z_{b/f} + f}{\sqrt{\Delta^2 + y_{b/f}^2 + (z_{b/f} + f)^2}} \\
\cos(\psi_{fc,d}) &= \frac{\sqrt{\Delta^2 + x_{b/f}^2 + z_{b/f}^2}}{\sqrt{\Delta^2 + x_{b/f}^2 + (y_{b/f} + g)^2 + z_{b/f}^2}} \\
\sin(\psi_{fc,d}) &= -\frac{y_{b/f} + g}{\sqrt{\Delta^2 + x_{b/f}^2 + (y_{b/f} + g)^2 + z_{b/f}^2}}.
\end{aligned} \tag{B.27}$$

This can be inserted into the $x_{b/f}$, $y_{b/f}$ and $z_{b/f}$ dynamics in equation (B.26). Defining $\tilde{V}_x \triangleq V_x - \hat{V}_x$, $\tilde{V}_y \triangleq V_y - \hat{V}_y$, $\tilde{V}_z \triangleq V_z - \hat{V}_z$, $\tilde{x} \triangleq x - \hat{x}$, $\tilde{y} \triangleq y - \hat{y}$ and $\tilde{z} \triangleq z - \hat{z}$.

$$\begin{aligned}
\dot{x}_{b/f} &= U_c \cos(\theta_{fc,d}) \cos(\psi_{fc,d}) + \cos(\theta_{fb}) \cos(\psi_{fb}) \tilde{u}_r + h_{11} \tilde{\theta}_{fc,d} + h_{12} \tilde{\psi}_{fc} \\
&\quad - \dot{s} + \kappa \dot{s} y_{b/f} + V_x^f \\
&= U_c \frac{\sqrt{\Delta^2 + y_{b/f}^2}}{\sqrt{\Delta^2 + y_{b/f}^2 + (z_{b/f} + f)^2}} \frac{\sqrt{\Delta^2 + x_{b/f}^2 + z_{b/f}^2}}{\sqrt{\Delta^2 + x_{b/f}^2 + (y_{b/f} + g)^2 + z_{b/f}^2}} \\
&\quad - \dot{s} + \kappa \dot{s} y_{b/f} + V_x^f + \cos(\theta_{fb}) \cos(\psi_{fb}) \tilde{u}_r + h_{11} \tilde{\theta}_{fc,d} + h_{12} \tilde{\psi}_{fc}
\end{aligned} \tag{B.28}$$

Inserting for $\dot{s}$ as defined in equation (6.32) and the current and current estimates as defined in equation (6.27) yields the following result:

$$\begin{aligned}
\dot{x}_{b/f} &= -U_c \frac{x_{b/f}}{\sqrt{\Delta^2 + x_{b/f}^2 + y_{b/f}^2 + z_{b/f}^2}} + \kappa \dot{s} y_{b/f} + V_x^f - \hat{V}_x^f + \cos(\theta_{fb}) \cos(\psi_{fb}) \tilde{u}_r \\
&\quad + h_{11} \tilde{\theta}_{fc,d} + h_{12} \tilde{\psi}_{fc} \\
&= -U_c \frac{x_{b/f}}{\sqrt{\Delta^2 + x_{b/f}^2 + y_{b/f}^2 + z_{b/f}^2}} + \kappa \dot{s} y_{b/f} + \cos(\theta_{fb}) \cos(\psi_{fb}) \tilde{u}_r + h_{11} \tilde{\theta}_{fc,d} \\
&\quad + h_{12} \tilde{\psi}_{fc} + \cos(\psi_f) \cos(\theta_f) \tilde{V}_x + \cos(\theta_f) \sin(\psi_f) \tilde{V}_y - \sin(\theta_f) \tilde{V}_z
\end{aligned} \tag{B.29}$$

$$
\begin{aligned}
\dot{y}_{b/f} &= U_c \cos(\theta_{fc,d}) \sin(\psi_{fc,d}) + \cos(\theta_{fb}) \sin(\psi_{fb}) \tilde{u}_r + h_{21} \tilde{\theta}_{fc} + h_{22} \tilde{\psi}_{fc} - \kappa \dot{s} x_{b/f} + \tau \dot{s} z_{b/f} + V_y^f \\
&= -U_c \cos(\theta_{fc,d}) \frac{y_{b/f} + g}{\sqrt{\Delta^2 + x_{b/f}^2 + (y_{b/f} + g)^2 + z_{b/f}^2}} - \kappa \dot{s} x_{b/f} + \tau \dot{s} z_{b/f} + V_y^f \\
&\quad + \cos(\theta_{fb}) \sin(\psi_{fb}) \tilde{u}_r + h_{21} \tilde{\theta}_{fc} + h_{22} \tilde{\psi}_{fc} \\
&= -U_c \frac{\sqrt{\Delta^2 + y_{b/f}^2}}{\sqrt{\Delta^2 + y_{b/f}^2 + (z_{b/f} + f)^2}} \frac{y_{b/f}}{\sqrt{\Delta^2 + x_{b/f}^2 + (y_{b/f} + g)^2 + z_{b/f}^2}} \\
&\quad - U_c \cos(\theta_{fc,d}) \frac{g}{\sqrt{\Delta^2 + x_{b/f}^2 + (y_{b/f} + g)^2 + z_{b/f}^2}} + V_y^f - \kappa \dot{s} x_{b/f} + \tau \dot{s} z_{b/f} \\
&\quad + \cos(\theta_{fb}) \sin(\psi_{fb}) \tilde{u}_r + h_{21} \tilde{\theta}_{fc} + h_{22} \tilde{\psi}_{fc}
\end{aligned}
\tag{B.30}
$$

By rewriting the second order equation that solves for g (equation (6.35)), it can easily be seen that

$$
U_c \cos(\theta_{fc,d}) \frac{g}{\sqrt{\Delta^2 + x_{b/f}^2 + (y_{b/f} + g)^2 + z_{b/f}^2}} = \hat{V}_y^f. \tag{B.31}
$$

As such, by inserting for the current and current estimates as defined in equation (6.27),

$$
\begin{aligned}
\dot{y}_{b/f} &= -U_c \frac{\sqrt{\Delta^2 + y_{b/f}^2}}{\sqrt{\Delta^2 + y_{b/f}^2 + (z_{b/f} + f)^2}} \frac{y_{b/f}}{\sqrt{\Delta^2 + x_{b/f}^2 + (y_{b/f} + g)^2 + z_{b/f}^2}} \\
&\quad - \kappa \dot{s} x_{b/f} + \tau \dot{s} z_{b/f} + V_y^f - \hat{V}_y^f + \cos(\theta_{fb}) \sin(\psi_{fb}) \tilde{u}_r + h_{21} \tilde{\theta}_{fc} + h_{22} \tilde{\psi}_{fc} \\
&= -U_c \frac{\sqrt{\Delta^2 + y_{b/f}^2}}{\sqrt{\Delta^2 + y_{b/f}^2 + (z_{b/f} + f)^2}} \frac{y_{b/f}}{\sqrt{\Delta^2 + x_{b/f}^2 + (y_{b/f} + g)^2 + z_{b/f}^2}} \\
&\quad - \kappa \dot{s} x_{b/f} + \tau \dot{s} z_{b/f} + \cos(\theta_{fb}) \sin(\psi_{fb}) \tilde{u}_r + h_{21} \tilde{\theta}_{fc} + h_{22} \tilde{\psi}_{fc} \\
&\quad + \left(\cos(\psi_f) \sin(\phi_f) \sin(\theta_f) - \cos(\phi_f) \sin(\psi_f)\right) \tilde{V}_x \\
&\quad + \left(\cos(\phi_f) \cos(\psi_f) + \sin(\phi_f) \sin(\psi_f) \sin(\theta_f)\right) \tilde{V}_y + \cos(\theta_f) \sin(\phi_f) \tilde{V}_z.
\end{aligned}
\tag{B.32}
$$

$$\begin{aligned}
\dot{z}_{b/f} &= -U_c \sin(\theta_{fc,d}) - \sin(\theta_{fb})\tilde{u}_r + h_{31}\tilde{\theta}_{fc} + h_{32}\tilde{\psi}_{fc} - \tau \dot{s} y_{b/f} + V_z^f \\
&= -U_c \frac{z_{b/f} + f}{\sqrt{\Delta^2 + y_{b/f}^2 + (z_{b/f} + f)^2}} - \tau \dot{s} y_{b/f} + V_z^f - \sin(\theta_{fb})\tilde{u}_r + h_{31}\tilde{\theta}_{fc} + h_{32}\tilde{\psi}_{fc} \\
&= -U_c \frac{z_{b/f}}{\sqrt{\Delta^2 + y_{b/f}^2 + (z_{b/f} + f)^2}} - U_c \frac{f}{\sqrt{\Delta^2 + y_{b/f}^2 + (z_{b/f} + f)^2}} - \tau \dot{s} y_{b/f} + V_z^f \\
&\quad - \sin(\theta_{fb})\tilde{u}_r + h_{31}\tilde{\theta}_{fc} + h_{32}\tilde{\psi}_{fc}
\end{aligned} \tag{B.33}$$

By rewriting the second order equation that solves for f (equation (6.34)), it can easily be seen that

$$U_c \frac{f}{\sqrt{\Delta^2 + y_{b/f}^2 + (z_{b/f} + f)^2}} = \hat{V}_z^f. \tag{B.34}$$

As such, by inserting for the current and current estimates as defined in equation (6.27),

$$\begin{aligned}
\dot{z}_{b/f} &= -U_c \frac{z_{b/f}}{\sqrt{\Delta^2 + y_{b/f}^2 + (z_{b/f} + f)^2}} - \tau \dot{s} y_{b/f} + \tilde{V}_z^f - \sin(\theta_{fb})\tilde{u}_r + h_{31}\tilde{\theta}_{fc} + h_{32}\tilde{\psi}_{fc} \\
&= -U_c \frac{z_{b/f}}{\sqrt{\Delta^2 + y_{b/f}^2 + (z_{b/f} + f)^2}} - \tau \dot{s} y_{b/f} - \sin(\theta_{fb})\tilde{u}_r + h_{31}\tilde{\theta}_{fc} + h_{32}\tilde{\psi}_{fc} \\
&\quad + (\sin(\phi_f)\sin(\psi_f) + \cos(\phi_f)\cos(\psi_f)\sin(\theta_f))\tilde{V}_x \\
&\quad + (\cos(\phi_f)\sin(\psi_f)\sin(\theta_f) - \cos(\psi_f)\sin(\phi_f))\tilde{V}_y + \cos(\phi_f)\cos(\theta_f)\tilde{V}_z.
\end{aligned} \tag{B.35}$$

This can be summarized as below:

$$\begin{aligned}
\begin{bmatrix} \dot{x}_{b/f} \\ \dot{y}_{b/f} \\ \dot{z}_{b/f} \end{bmatrix} &= \begin{bmatrix} -U_c \frac{x_{b/f}}{\sqrt{\Delta^2 + x_{b/f}^2 + y_{b/f}^2 + z_{b/f}^2}} \\ -U_c \frac{\sqrt{\Delta^2 + y_{b/f}^2}}{\sqrt{\Delta^2 + y_{b/f}^2 + (z_{b/f}+f)^2}} \frac{y_{b/f}}{\sqrt{\Delta^2 + x_{b/f}^2 + (y_{b/f}+g)^2 + z_{b/f}^2}} \\ -U_c \frac{z_{b/f}}{\sqrt{\Delta^2 + y_{b/f}^2 + (z_{b/f}+f)^2}} \end{bmatrix} \\
&\quad - \dot{s} \begin{bmatrix} 0 & -\kappa & 0 \\ \kappa & 0 & -\tau \\ 0 & \tau & 0 \end{bmatrix} \begin{bmatrix} x_{b/f} \\ y_{b/f} \\ z_{b/f} \end{bmatrix} + \boldsymbol{H}(t, U_c, \boldsymbol{\xi})\boldsymbol{\xi}
\end{aligned} \tag{B.36}$$

$$\boldsymbol{H}(t,U_c,\boldsymbol{\xi})^T = \begin{bmatrix} \cos(\theta_{fb})\cos(\psi_{fb}) & \cos(\theta_{fb})\sin(\psi_{fb}) & -\sin(\theta_{fb}) \\ h_{11} & h_{21} & h_{31} \\ h_{12} & h_{22} & h_{32} \\ 0 & 0 & 0 \\ 0 & 0 & 0 \\ \cos(\psi_f)\cos(\theta_f) & \cos(\psi_f)\sin(\phi_f)\sin(\theta_f) - \cos(\phi_f)\sin(\psi_f) & \cos(\phi_f)\cos(\psi_f)\sin(\theta_f) + \sin(\phi_f)\sin(\psi_f) \\ \cos(\theta_f)\sin(\psi_f) & \sin(\phi_f)\sin(\psi_f)\sin(\theta_f) + \cos(\phi_f)\cos(\psi_f) & \cos(\phi_f)\sin(\psi_f)\sin(\theta_f) - \cos(\psi_f)\sin(\phi_f) \\ -\sin(\theta_f) & \cos(\theta_f)\sin(\phi_f) & \cos(\phi_f)\cos(\theta_f) \\ 0 & 0 & 0 \\ 0 & 0 & 0 \\ 0 & 0 & 0 \end{bmatrix}$$

$$\boldsymbol{\xi}^T = \begin{bmatrix} \tilde{u_r} & \tilde{\theta}_{fc} & \tilde{\psi}_{fc} & \tilde{q} & \tilde{r} & \tilde{V}_x & \tilde{V}_y & \tilde{V}_z & \tilde{x} & \tilde{y} & \tilde{z} \end{bmatrix} \tag{B.37}$$

The system in equation (B.36) and the dynamics of $\boldsymbol{\xi}$ (B.40) can be seen as a cascaded system where the error dynamics perturbs the nominal system in equation (B.38) through the term $\boldsymbol{H}(t,U_c,\boldsymbol{\xi})\boldsymbol{\xi}$ (appendix A.3.4).

$$\begin{bmatrix} \dot{x}_{b/f} \\ \dot{y}_{b/f} \\ \dot{z}_{b/f} \end{bmatrix} = \begin{bmatrix} -U_c \frac{x_{b/f}}{\sqrt{\Delta^2+x_{b/f}^2+y_{b/f}^2+z_{b/f}^2}} \\ -U_c \frac{\sqrt{\Delta^2+y_{b/f}^2}}{\sqrt{\Delta^2+y_{b/f}^2+(z_{b/f}+f)^2}} \frac{y_{b/f}}{\sqrt{\Delta^2+x_{b/f}^2+(y_{b/f}+g)^2+z_{b/f}^2}} \\ -U_c \frac{z_{b/f}}{\sqrt{\Delta^2+y_{b/f}^2+(z_{b/f}+f)^2}} \end{bmatrix} - \dot{s} \begin{bmatrix} 0 & -\kappa & 0 \\ \kappa & 0 & -\tau \\ 0 & \tau & 0 \end{bmatrix} \begin{bmatrix} x_{b/f} \\ y_{b/f} \\ z_{b/f} \end{bmatrix} \tag{B.38}$$

Stability of the nominal system can be shown using the quadratic, positive definite, decrescent and radially unbounded Lyapunov function $V = \frac{1}{2}(x_{b/f}^2 + y_{b/f}^2 + z_{b/f}^2)$.

$$\begin{aligned} \dot{V} &= \dot{x}_{b/f}x_{b/f} + \dot{y}_{b/f}y_{b/f} + \dot{z}_{b/f}z_{b/f} \\ &= -U_c \frac{x_{b/f}^2}{\sqrt{\Delta^2 + x_{b/f}^2 + y_{b/f}^2 + z_{b/f}^2}} - U_c \frac{z_{b/f}^2}{\sqrt{\Delta^2 + y_{b/f}^2 + (z_{b/f}+f)^2}} \\ &\quad - U_c \frac{\sqrt{\Delta^2 + y_{b/f}^2}}{\sqrt{\Delta^2 + y_{b/f}^2 + (z_{b/f}+f)^2}} \frac{y_{b/f}^2}{\sqrt{\Delta^2 + x_{b/f}^2 + (y_{b/f}+g)^2 + z_{b/f}^2}} \\ &\leq -U_{rd} \left(\frac{x_{b/f}^2}{\sqrt{\Delta^2 + x_{b/f}^2 + y_{b/f}^2 + z_{b/f}^2}} + \frac{z_{b/f}^2}{\sqrt{\Delta^2 + y_{b/f}^2 + (z_{b/f}+f)^2}} \right. \\ &\quad \left. + \frac{\sqrt{\Delta^2 + y_{b/f}^2}}{\sqrt{\Delta^2 + y_{b/f}^2 + (z_{b/f}+f)^2}} \frac{y_{b/f}^2}{\sqrt{\Delta^2 + x_{b/f}^2 + (y_{b/f}+g)^2 + z_{b/f}^2}} \right) \\ &\triangleq W(x_{b/f}, y_{b/f}, z_{b/f}) < 0 \end{aligned} \tag{B.39}$$

$\dot{V}$ is negative definite and the nominal system is UGAS according to theorem 4.8/4.9 in appendix A.3.3.

The error dynamics is shown in equation (B.40) and is based on the feedback linearization controller and integrator backstepping controller in chapter 5.2.1 and 5.2.2 and the current and position observers in chapter 3.4.

$$\dot{\boldsymbol{\xi}} = \begin{bmatrix} \dot{\tilde{u}}_r \\ \dot{\tilde{\theta}}_{fc} \\ \dot{\tilde{\psi}}_{fc} \\ \dot{\tilde{q}} \\ \dot{\tilde{r}} \\ \dot{\tilde{V}}_x \\ \dot{\tilde{V}}_y \\ \dot{\tilde{V}}_z \\ \dot{\tilde{x}} \\ \dot{\tilde{y}} \\ \dot{\tilde{z}} \end{bmatrix} = \begin{bmatrix} \dot{\tilde{u}}_r \\ \dot{\boldsymbol{z}}_1 \\ \dot{\boldsymbol{z}}_2 \\ \dot{\tilde{V}}_x \\ \dot{\tilde{V}}_y \\ \dot{\tilde{V}}_z \\ \dot{\tilde{x}} \\ \dot{\tilde{y}} \\ \dot{\tilde{z}} \end{bmatrix} = \begin{bmatrix} -k_{u_r} & \mathbf{0} & \mathbf{0} & 0 & 0 & 0 & 0 & 0 & 0 \\ 0 & -\boldsymbol{K}_1 & \boldsymbol{A} & 0 & 0 & 0 & 0 & 0 & 0 \\ 0 & -\boldsymbol{A}^T & -\boldsymbol{K}_2 & 0 & 0 & 0 & 0 & 0 & 0 \\ 0 & \mathbf{0} & \mathbf{0} & 0 & 0 & 0 & -k_{x2} & 0 & 0 \\ 0 & \mathbf{0} & \mathbf{0} & 0 & 0 & 0 & 0 & -k_{y2} & 0 \\ 0 & \mathbf{0} & \mathbf{0} & 0 & 0 & 0 & 0 & 0 & -k_{z2} \\ 0 & \mathbf{0} & \mathbf{0} & 1 & 0 & 0 & -k_{x1} & 0 & 0 \\ 0 & \mathbf{0} & \mathbf{0} & 0 & 1 & 0 & 0 & -k_{y1} & 0 \\ 0 & \mathbf{0} & \mathbf{0} & 0 & 0 & 1 & 0 & 0 & -k_{z1} \end{bmatrix} \begin{bmatrix} \tilde{u}_r \\ \boldsymbol{z}_1 \\ \boldsymbol{z}_2 \\ \tilde{V}_x \\ \tilde{V}_y \\ \tilde{V}_z \\ \tilde{x} \\ \tilde{y} \\ \tilde{z} \end{bmatrix}$$

$$= \boldsymbol{\Lambda}\boldsymbol{\xi} \tag{B.40}$$

Equation (B.40) has an UES equilbrium point in $\boldsymbol{\xi} = 0$. This is shown using Lyapunov analysis. It is known that

$$\begin{aligned} \begin{bmatrix} \dot{\tilde{x}} \\ \dot{\tilde{V}}_x \end{bmatrix} &= \underbrace{\begin{bmatrix} -k_{x1} & 1 \\ -k_{x2} & 0 \end{bmatrix}}_{\boldsymbol{A}_x} \begin{bmatrix} \tilde{x} \\ \tilde{V}_x \end{bmatrix} \\ \begin{bmatrix} \dot{\tilde{y}} \\ \dot{\tilde{V}}_y \end{bmatrix} &= \underbrace{\begin{bmatrix} -k_{y1} & 1 \\ -k_{y2} & 0 \end{bmatrix}}_{\boldsymbol{A}_y} \begin{bmatrix} \tilde{y} \\ \tilde{V}_y \end{bmatrix} \\ \begin{bmatrix} \dot{\tilde{z}} \\ \dot{\tilde{V}}_z \end{bmatrix} &= \underbrace{\begin{bmatrix} -k_{z1} & 1 \\ -k_{z2} & 0 \end{bmatrix}}_{\boldsymbol{A}_z} \begin{bmatrix} \tilde{z} \\ \tilde{V}_z \end{bmatrix}. \end{aligned} \tag{B.41}$$

Under the constraints of Theorem 2, $k_{x1}, k_{x2}, k_{y1}, k_{y2}, k_{z1}, k_{z2} > 0$ and $\boldsymbol{A}_x$, $\boldsymbol{A}_y$ and $\boldsymbol{A}_z$ are Hurwitz. Thus, there exists three symmetric positive definite matrices $\boldsymbol{P}_x$,

$\boldsymbol{P}_y$ and $\boldsymbol{P}_z$ (theorem 4.6 in appendix A.3.2) such that

$$\begin{aligned}\boldsymbol{P}_x\boldsymbol{A}_x + \boldsymbol{A}_x^T\boldsymbol{P}_x &= -\begin{bmatrix}1 & 0\\ 0 & 1\end{bmatrix}\\ \boldsymbol{P}_y\boldsymbol{A}_y + \boldsymbol{A}_y^T\boldsymbol{P}_y &= -\begin{bmatrix}1 & 0\\ 0 & 1\end{bmatrix}\\ \boldsymbol{P}_z\boldsymbol{A}_z + \boldsymbol{A}_z^T\boldsymbol{P}_z &= -\begin{bmatrix}1 & 0\\ 0 & 1\end{bmatrix}.\end{aligned} \tag{B.42}$$

Taking the positive definite, decresent, radially unbounded Lyapunov candidate

$$V = \frac{1}{2}\tilde{u}_r^2 + \frac{1}{2}\boldsymbol{z}_1^T\boldsymbol{z}_1 + \frac{1}{2}\boldsymbol{z}_2^T\boldsymbol{z}_2 + \begin{bmatrix}\tilde{x} & \tilde{V}_x\end{bmatrix}\boldsymbol{P}_x\begin{bmatrix}\tilde{x}\\ \tilde{V}_x\end{bmatrix} + \begin{bmatrix}\tilde{y} & \tilde{V}_y\end{bmatrix}\boldsymbol{P}_y\begin{bmatrix}\tilde{y}\\ \tilde{V}_y\end{bmatrix} + \begin{bmatrix}\tilde{z} & \tilde{V}_z\end{bmatrix}\boldsymbol{P}_z\begin{bmatrix}\tilde{z}\\ \tilde{V}_z\end{bmatrix}. \tag{B.43}$$

It can easily be seen that the time-derivative of V is given as

$$\begin{aligned}\dot{V} = {} & \tilde{u}_r\dot{\tilde{u}}_r + \frac{1}{2}\dot{\boldsymbol{z}}_1^T\boldsymbol{z}_1 + \frac{1}{2}\boldsymbol{z}_1^T\dot{\boldsymbol{z}}_1 + \frac{1}{2}\dot{\boldsymbol{z}}_2^T\boldsymbol{z}_2 + \frac{1}{2}\boldsymbol{z}_2^T\dot{\boldsymbol{z}}_2 + \begin{bmatrix}\dot{\tilde{x}} & \dot{\tilde{V}}_x\end{bmatrix}\boldsymbol{P}_x\begin{bmatrix}\tilde{x}\\ \tilde{V}_x\end{bmatrix} + \begin{bmatrix}\tilde{x} & \tilde{V}_x\end{bmatrix}\boldsymbol{P}_x\begin{bmatrix}\dot{\tilde{x}}\\ \dot{\tilde{V}}_x\end{bmatrix}\\ & + \begin{bmatrix}\dot{\tilde{y}} & \dot{\tilde{V}}_y\end{bmatrix}\boldsymbol{P}_y\begin{bmatrix}\tilde{y}\\ \tilde{V}_y\end{bmatrix} + \begin{bmatrix}\tilde{y} & \tilde{V}_y\end{bmatrix}\boldsymbol{P}_y\begin{bmatrix}\dot{\tilde{y}}\\ \dot{\tilde{V}}_y\end{bmatrix} + \begin{bmatrix}\dot{\tilde{z}} & \dot{\tilde{V}}_z\end{bmatrix}\boldsymbol{P}_z\begin{bmatrix}\tilde{z}\\ \tilde{V}_z\end{bmatrix} + \begin{bmatrix}\tilde{z} & \tilde{V}_z\end{bmatrix}\boldsymbol{P}_z\begin{bmatrix}\dot{\tilde{z}}\\ \dot{\tilde{V}}_z\end{bmatrix}\\ = {} & -k_{u_r}\tilde{u}_r^2 - \boldsymbol{z}_1^T\boldsymbol{K}_1\boldsymbol{z}_1 - \boldsymbol{z}_2^T\boldsymbol{K}_2\boldsymbol{z}_2 - \tilde{x}^2 - \tilde{V}_x^2 - \tilde{y}^2 - \tilde{V}_y^2 - \tilde{z}^2 - \tilde{V}_z^2.\end{aligned} \tag{B.44}$$

$\dot{V}$ is negative definite (the controller gain $k_{u_r} > 0$ and the controller gain matrices $\boldsymbol{K}_1 = \boldsymbol{K}_1^T$ and $\boldsymbol{K}_2 = \boldsymbol{K}_2^T$ are symmetric positive definite). Hence, the equilibrium point $\boldsymbol{\xi} = \boldsymbol{0}$ is UAS (theorem 4.8/4.9 in appendix A.3.3). Furthermore, the Lyapunov function satisfies the conditions of theorem 4.10 in appendix A.3.3, so $\boldsymbol{\xi} = \boldsymbol{0}$ is UES. However, the error dynamics is *not* globally stable due to the singularity $\theta_{fc} = \pi/2$ in the matrix $\boldsymbol{A}$ (discussed in chapter 5.2.2). This singularity is not contained in the domain $\mathbb{D}$ (6.36) in which Theorem 2 is valid, so the error dynamics is UES in $\mathbb{D}$.

Theorem 2 in appendix A.3.4 regarding the stability of cascaded systems is not applicable due to the fact that the error dynamics is not UGAS. However, since $\boldsymbol{\xi} \to \boldsymbol{0}$, one can apply assumption **B3** and assume $\boldsymbol{\xi} = \boldsymbol{0}$. As such, equation (B.36) reduces to the nominal system in equation (B.38), which is known UGAS. Hence, it is possible to conclude that the control objectives are achieved asymptotically.

Proving stability of the cascaded system (B.36) and (B.40) remains a topic for future work.

Bibliography

[1] Aguiar, A. P., and Pascoal, A. Dynamic positioning and way-point tracking of underactuated auvs in the presence of ocean currents. In *Decision and Control, 2002, Proceedings of the 41st IEEE Conference on* (2002).

[2] Antonelli, G. Underwater robots, motion and force control of vehicle-manipulator systems. In *Springer Handbook of Robotics*. 2008.

[3] Balchen, J., Andresen, T., and Foss, B. *Reguleringsteknikk*. Institutt for teknisk kybernetikk, NTNU, 2004.

[4] Borhaug, E., Pavlov, A., and Pettersen, K. Straight line path following for formations of underactuated underwater vehicles. In *Decision and Control, 2007 46th IEEE Conference on* (2007), pp. 2905–2912.

[5] Borhaug, E., Pavlov, A., and Pettersen, K. Integral los control for path following of underactuated marine surface vessels in the presence of constant ocean currents. In *Decision and Control, 2008. CDC 2008. 47th IEEE Conference on* (2008), pp. 4984 –4991.

[6] Børhaug, E., and teknisk-naturvitenskapelige universitet Institutt for teknisk kybernetikk, N. *Nonlinear Control and Synchronization of Mechanical Systems*. Doktoravhandlinger ved NTNU. Norwegian University of Science and Technology, Faculty of Information Technology, Mathematics and Electrical Engineering, Department of Engineering Cybernetics, 2008.

[7] Breivik, M., and Fossen, T. Guidance laws for planar motion control. In *Decision and Control, 2008. CDC 2008. 47th IEEE Conference on* (2008), pp. 570 –577.

[8] Caharija, W., Pettersen, K., Candeloro, M., and Sorensen, A. Relative velocity control and integral los for path following of underactuated surface vessels. *IFAC Conference on Manoeuvring and Control of Marine Craft* (2012).

[9] Caharija, W., Pettersen, K., Gravdahl, J., and Borhaug, E. Integral los guidance for horizontal path following of underactuated autonomous

underwater vehicles in the presence of vertical ocean currents. *2012 American Control Conference - ACC 2012* (2012).

[10] Caharija, W., Pettersen, K., Gravdahl, J., and Borhaug, E. Integral los guidance for horizontal path following of underactuated autonomous underwater vehicles in the presence of vertical ocean currents. *2012 American Control Conference - ACC 2012* (2012).

[11] Caharija, W., Pettersen, K., Gravdahl, J., and Sorensen, A. Topics on current compensation for path following applications of underactuated underwater vehicles. *9th IFAC Workshop on Navigation, Guidance and Control of Underwater Vehicles* (2012).

[12] Fossen, T. *Handbook of Marine Craft Hydrodynamics and Motion Control.* Wiley, 2011.

[13] Fredriksen, E., and Pettersen, K. Global kappa;-exponential way-point manoeuvering of ships. In *Decision and Control, 2004. CDC. 43rd IEEE Conference on* (2004).

[14] Hagen, P. E., Midtgaard, O., and Hasvold, O. Making *AUVs* truly autonomous.

[15] Khalil, H. *Nonlinear systems.* Prentice Hall PTR, 2002.

[16] Panteley, E., and Loria, A. On global uniform asymptotic stability of nonlinear time-varying systems in cascade. *Systems and Control Letters 33*, 2 (1998).

[17] Panteley, E., and Loria, A. Brief growth rate conditions for uniform asymptotic stability of cascaded time-varying systems. *Automatica 37*, 3 (2001).

[18] Parasuraman, R., Sheridan, T., and Wickens, C. A model for types and levels of human interaction with automation. *IEEE Trans. Syst. Man Cybern. A, Syst. Humans (USA)* (2000).

[19] Snyder, J. Doppler velocity log (dvl) navigation for observation-class rovs. In *OCEANS 2010* (2010).

[20] Yuh, J., Marani, G., and Blidberg, D. R. Applications of marine robotic vehicles. *Intelligent Service Robotics* (2011).

[21] Yuh, J., and West, M. Underwater robotics. *Advanced Robotics* (2001).